Assessment of Fischer–Tropsch liquid fuels production via solar hybridized dual fluidized bed gasification of solid fuels

Peijun Guo

Thesis submitted for the degree of Doctor of Philosophy

School of Chemical Engineering

Faculty of Engineering, Computer & Mathematical Sciences

The University of Adelaide, Australia

May 2017

Table of Contents

ABSTRACT

To mitigate the emissions from the widely studied and even applied coal to FT liquid (FTL) fuels systems, two kinds of promising renewable energy, biomass and solar energy, have been proposed and assessed as a partial or total substitute for coal feed. The concept of a solar hybridized FTL fuels production system has the potential to obtain higher productivity with lower greenhouse gas emissions, when compared with a conventional system. However, less attention has been paid to the comprehensive system analysis of this topic. Hence, the aim of the present thesis is to achieve the annual performance of the solar hybridized solid fuels to FTL fuels processes with novel configurations.

A novel solar hybridized dual fluidized bed (SDFB) gasification process for FTL fuels production is proposed and investigated in the present thesis for cases with high reactivity solid fuels as the feedstock. The concept offers sensible thermal storage of the bed material and a process that delivers a constant production rate and quality of syngas despite solar variability. As a reference scenario for this concept, the proposed solar hybridized coal-to-liquids (SCTL) process is simulated for the case with lignite as the feedstock using a pseudo-dynamic model that assumes steady state operation at each time step for a one-year, hourly integrated solar insolation time series. For a solar multiple of 3 and bed material storage capacity of 16 h, the calculated annual solar share is 21.8%, assuming that the char conversion in the steam gasification process is 100%. However, the solar share is also found to be strongly dependent on the char conversion in the steam gasification process, so that the solar share is calculated to decrease to zero as the conversion is decreased to 57%.

Abstract

New configurations of the solar hybridized solid fuels (biomass and/or coal) to FTL fuels process are proposed and assessed, which are characterized with a novel SDFB gasifier with char separation, the incorporation of carbon capture and sequestration (CCS) and/or the use of FT reactor tail-gas recycle. Montana lignite and spruce wood have been chosen as the studied coal and biomass, respectively. Assessed using the pseudo-dynamic model, the annual solar share of the SCTL system can be increased from 12.2% to 20.3% by the addition of the char separation, for a char gasification conversion of 80%. To achieve well-to-wheel greenhouse gas emissions for FT liquid fuels parity with diesel derived from mineral crude oil, a biomass fraction of 58% is required for the studied non-solar coal and biomass-to-liquids system with a dual fluidized bed (DFB) gasifier. This biomass fraction can be reduced to 30% by the addition of carbon capture and sequestration and further reduced to 17% by the integration of solar energy with a solar multiple of 2.64 and a bed material storage capacity of 16 h. This reduction of the biomass fraction is very important given that biomass is typically more expensive than coal. As the biomass fraction is increased from 0% to 100%, the specific FT liquids output is decreased from 59.6% to 48.3% due to the increasing light hydrocarbons content. These two outputs (for biomass fractions of 0% and 100%, respectively) can both be increased to 71.5% and 70.9%, respectively, by integrating a tail-gas recycling configuration.

Co-gasification of biomass with coal has the potential to further reduce the GHG emission from the SCTL systems, as discussed above. The application of biomass is usually limited by some properties (e.g., high moisture, low heating value and so on), which can be improved by torrefaction, as proved by previous work. Previous work also found that torrefaction can impact the bio-char gasification reactivity. In the present thesis, to better understand the influence of torrefaction on the bio-char gasification

reactivity, further investigations were carried out on the char physicochemical characteristics that can influence the gasification reactivity, i.e., the char specific surface area, the char carbonaceous structure and the catalytic effect of inorganic matter in the char. The present experimental investigation showed that the influence of the torrefaction on the char gasification reactivity depended strongly on the biomass species and char preparation conditions. For a pyrolysis temperature of 800 ºC, the gasification reactivity of the chars from both the torrefied grape marc and the torrefied macroalgae were found to be lower than that of the chars from their corresponding raw fuels. This is mainly due to a lower specific surface area and a lower content of alkali metals (sodium and/or potassium) in the chars produced from both the torrefied grape marc and the torrefied macroalgae than for those chars produced from their corresponding raw fuels. However, the opposite influence of torrefaction was found for the macroalgae char when the pyrolysis temperature was increased to 1000 ºC. This is mainly due to a higher sodium concentration and a more amorphous carbonaceous structure for the torrefied macroalgae char than for the raw macroalgae char.

In the present thesis, the process modelling results can be used for further economic analysis of the proposed novel configurations of solar hybridized coal and/or biomass to FTL fuels system via an SDFB gasifier. In addition, according to the experimental results of this study, the investigation of the influence of torrefaction on the bio-char characteristics can help to better understand the influence of torrefaction on the bio-char gasification reactivity.

DECLARATION

I certify that this work contains no material which has been accepted for the award of any other degree or diploma in my name, in any university or other tertiary institution and, to the best of my knowledge and belief, contains no material previously published or written by another person, except where due reference has been made in the text. In addition, I certify that no part of this work will, in the future, be used in a submission in my name, for any other degree or diploma in any university or other tertiary institution without the prior approval of the University of Adelaide and where applicable, any partner institution responsible for the joint-award of this degree.

I give consent to this copy of my thesis when deposited in the University Library, being made available for loan and photocopying, subject to the provisions of the Copyright Act 1968.

The author acknowledges that copyright of published works contained within the present thesis resides with the copyright holder of those works.

I also give permission for the digital version of my thesis to be made available on the web, via the University's digital research repository, the Library Search and also through web search engines, unless permission has been granted by the University to restrict access for a period of time.

_____ _____

Peijun Guo Date

ACKNOWLEDGEMENT

The completion of the present thesis could not have been accomplished without the guidance, support, advice and contributions of many people.

I would firstly like to acknowledge the support given to me by my supervisors Professor Peter Ashman, Professor Graham (Gus) Nathan, Dr Philip van Eyk, Dr Woei Saw and Professor Ellen Stechel. I thank Peter for all of the support he gave me through the up and down times of the PhD process, and constant guidance in all things related to solid fuel gasification. I thank Gus for contributing his knowledge and experience in the area of solar hybridization. I thank Ellen for her knowledge and experience in the area of FTL fuels production. I thank Philip and Saw for all their help on both the modelling and experimental work. I would also like to thank my supervisors for all their help with my technical writing skills.

The work was supported by the Australian Solar Thermal Research Initiative (ASTRI), a project supported by the Australian Government, through the Australian Renewable Energy Agency (ARENA). The Australian Government, through ARENA, supports Australian research and development in solar photovoltaic and solar thermal technologies to help solar power become cost competitive with other energy sources. I would also like to thank the China Scholarship Council (CSC) for their generous support by providing a scholarship for my PhD study.

I thank current and former Chemical Engineering Office staff members Sue Earle, Monica Dinan, Michelle Fitton, Terry Utting and Pauline Gill for providing endless assistance relating to administrative matters for my PhD candidature. I would also like to thank the Chemical Engineering Workshop staff during the period of the

experimental campaign of this work, especially Jason Peak and Jeffrey Hiorns. I would also like to thank the supervisor of the Analytical Lab, Qiuhong Hu, for providing assistance relating to sample analysis. I would like to thank David Bruce from school of Physical Sciences for his help on the acid digestion. I would also like to thank Alison Jane Hunter for her assistance in proofreading my thesis.

I would like to thank my supervisors in my master's study, Professor Hongguang Jin and Professor Jun Sui for their knowledge and experience with thermodynamics and their support for my overseas study application.

I would like to thank my Mum, Dad, Grandmother, Mother-in-law and Father-in-law. The love and support you have given me throughout my life has led me to this definitive point, and I am extremely grateful.

Finally, I would like to thank Meimei for being the most loving, patient and understanding wife for me over this long process. I know it was a great challenge for her to quit her job and come with me to an unfamiliar country. Because of your constant, unwavering support, I have finally completed this arduous task. I am forever grateful.

我 永 远 爱 你 .

PREFACE

The present thesis is submitted as a portfolio of publications according to the "Specifications for Thesis 2017" of the University of Adelaide. The main body of the work contained in the present thesis is published within the following three journal papers:

1. **Guo, P.**, van Eyk, P. J., Saw, W. L., Ashman, P. J., Nathan, G. J., and Stechel, E. B. (2015). Performance Assessment of Fischer-Tropsch Liquid Fuels Production by Solar Hybridized Dual Fluidized Bed Gasification of Lignite. Energy & Fuels, 29(4), 2738-2751. Copyright of this paper belongs to the American Chemical Society.
2. **Guo, P.**, Saw, W. L., van Eyk, P. J., Stechel, E. B., Ashman, P. J., and Nathan, G. J. (2017) System optimization for Fischer-Tropsch liquid fuels production via solar hybridized dual fluidized bed gasification of solid fuels. Energy & Fuels, 31(2), 2033-2043. Copyright of this paper belongs to the American Chemical Society.
3. **Guo, P.**, Saw, W. L., van Eyk, P. J., Stechel, E. B., de Nys, R., Ashman, P. J., and Nathan, G. J. (2017) Gasification reactivity and physicochemical properties of the chars from raw and torrefied wood, grape marc and macroalgae. Energy & Fuels, 31(3), 2246-2259. Copyright of this paper belongs to the American Chemical Society.

Some additional aspects of this work were published in peer-reviewed conference papers:

a. **Guo, P.**, van Eyk, P. J., L., Ashman, P. J., and Nathan, G. J. (2013). Hybrid Solar Gasification of Biomass in a Dual Fluidized Bed Reactor for the Polygeneration of Liquid Fuels and Electricity. Proceedings of the Chemeca Conference, Brisbane, Australia.

b. **Guo, P.**, Saw, W. L., van Eyk, P. J., Ashman, P. J., Nathan, G. J., and Stechel, E. B. (2015). Fischer-Tropsch liquid fuel production by co-gasification of coal and biomass in a solar hybrid dual fluidized bed gasifier. Procedia, 69, 1770-1779.

CHAPTER 1

INTRODUCTION

1.1 Background

1.1.1 Fischer-Tropsch liquid fuels production

The continual depletion of crude oil reserves, energy-supply security concerns and the projected long-term demand for transport liquid fuels has provided motivation for the development of alternative fuels. The gasification of solid feedstocks (e.g., coal and/or biomass), together with the subsequent Fischer-Tropsch (FT) processing of the syngas, is considered to be one of the promising classes of technology to meet this need due to its capacity to process a variety of feedstock (e.g., coal, biomass, petroleum coke and so on), and the high quality of the FT liquid (FTL) fuels (being free of sulphur, nitrogen, and other contaminants typically found in petroleum products), and its compatibility with the requirements of current vehicles (Takeshita & Yamaji, 2008).

1.1.1.1 Fischer-Tropsch synthesis

The Fischer-Tropsch (FT) synthesis is a set of catalytic chemical reactions that convert syngas (CO and H_2) into long chain hydrocarbons. It was first developed by Franz Fischer and Hans Tropsch in Germany in 1920s. Equations 1.1 and 1.2 describe the FT reaction in its simplest form (Trimm & Adesina, 1996).

$$(2n+1)H_2 + nCO \rightarrow C_nH_{2n+2} + nH_2O \quad (1.1)$$

$$2nH_2 + nCO \rightarrow C_nH_{2n} + nH_2O \quad (1.2)$$

The FT reaction is catalyzed by both iron and cobalt at pressures ranging from 10 to 60 bar and at temperatures ranging from 200 to 300 °C (Ail & Dasappa, 2016). For cobalt catalysts, the required ratio ranges between 2.06−2.16 since the extent of the water gas shift reaction ($CO + H_2O \leftrightarrow CO_2 + H_2$) is negligible (Dry, 2004; Tavasoli, *et al.*, 2007; Ail & Dasappa, 2016). However, the water-gas shift reaction occurs

concurrently with the FT reaction when iron is used as a catalyst, thus making it possible to use syngas with an H_2/CO ratio of less than 2.1 (Ail & Dasappa, 2016).

The FT product distribution follows the Anderson–Schultz–Flory (ASF) chain length statistics as shown in Equation 1.3:

$$\alpha_{Cn} = (1-\alpha)\alpha^{(n-1)} \tag{1.3}$$

Here α_{Cn} is the mole fraction of hydrocarbons with n carbon atoms in the product from the FT reactor; α is the chain growth probability. A higher value of α will lead to a higher production (Dry, 2002) although variations may be required to account for the nature of the catalyst particles (Overett, *et al.*, 2000).

1.1.1.2 Conversion processes for FTL fuels production

Figure 1.1 presents a simplified process flow diagram for FTL fuels production. Syngas generation via gasification or reforming has been widely studied and demonstrated. Since the present thesis will focus on the solid fuels to FTL fuels production, syngas generation via reforming will not be discussed in the following sections. Nitrogen free syngas is preferred here to lower the size of the downstream reactors and to achieve better conversion of the FT synthesis process. Therefore, pure oxygen is required by the autothermal syngas generation processes (in which part of fuel is burned to provide heat for the syngas generation processes) while air is still acceptable for the allothermal ones (in which the heat required by the syngas generation processes is provided by external combustion processes, e.g., dual fluidized bed gasifier) (Hofbauer, *et al.*, 2002). Since the FT synthesis process requires clean syngas with a specific H_2 to CO molar ratio, the raw syngas should be cleaned and upgraded by removing the contaminants and acid gases (e.g., H_2S, particles, HCN, NH_3, CO_2, COS, HCl and so on) and by adjusting the H_2 to CO ratio (e.g., using a water gas shift reactor) before being sent to the FT reactor.

Then the FT liquids can be upgraded to produce the target fuels (e.g., gasoline, diesel, kerosene, etc).

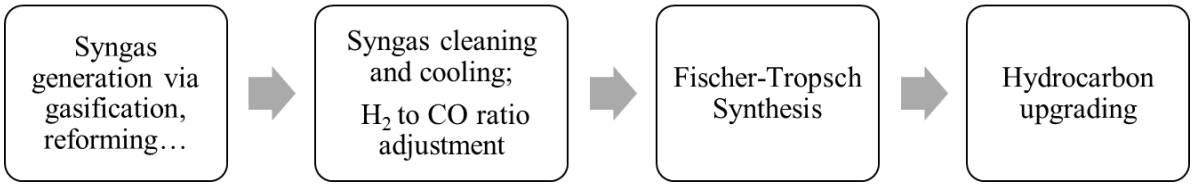

Figure 1.1 A simplified process flow diagram for FTL fuels production.

The vast reserves and relatively low cost of coal, as well as the relatively well developed coal gasification technology, have led to great international interest in the production of FTL fuels via the gasification of coal. However, the high greenhouse gas emissions from coal-to-liquids (CTL) processes are a major barrier to their implementation. Co-gasification of biomass with coal, carbon capture and sequestration (CCS) technology, as well as the concept of solar gasification, have the potential to mitigate these emissions.

1.1.1.3 Application prospect of FTL fuels

The industrial application of the FT process started in Germany and by the 1940s, there were nine plants in operation with a total capacity of about 600×10^3 t per year (Schulz, 1999; Dry, 2002). After the second world war, these plants ceased to operate due to the availability of cheaper crude oil resulting from the discovery of big oil fields, e.g. in Saudi Arabia, Alaska, the North Sea and other areas (Dry, 2002). However, a coal-based FT plant was built in Sasolburg, South Africa, during the 1950s, relying on extremely cheap domestic coal and the particular State policy. By 2007, South Africa's FT plants produced over 150×10^3 barrels of liquid fuels per day, which was more than 40% of its national liquid fuels requirements (Gibson, 2007). Over the past half century,

in consequence of the considerably varied price of the crude oil, the decisions to construct FT plants have clearly been fraught with risk.

The economic factor is not the only one which can influence the development of FT technology. Environmental demands and energy supply security concerns also provide incentives to apply the FT process. Moreover, FTL fuels are largely compatible with current vehicles and are blendable with current petroleum fuels (Tijmensen, *et al.*, 2002; Takeshita & Yamaji, 2008). Due to the syngas cleaning process, which is necessary for the FT synthesis process, FT products are free of sulphur, nitrogen, aromatics, and other contaminants typically found in petroleum products, which is especially true for FT-diesel with a very high cetane number (Takeshita & Yamaji, 2008). Beyond this, the clean FTL fuels are expected to be suitable for fuel cell vehicle applications without damaging the fuel cell catalyst (Tijmensen, *et al.*, 2002). In addition, any carbonaceous feedstock (e.g., coal, biomass, natural gas and so on) can be used to produce syngas for the FT synthesis process to produce liquid fuels which are easy to transport and store. The diverse feedstock of the FT process can strengthen the energy supply security for countries poor in oil but rich in other carbonaceous fuels. For instance, China imported around 60% of the petroleum it consumed in 2015 (IEA, 2016). Therefore, in China, the proponents of coal to liquids (CTL) technology argue that the country should take advantage of its abundant coal reserves to reduce its dependence on imported petroleum.

1.1.2 Gasification of solid fuels

In typical gasification processes of coal, biomass and other solid carbonaceous fuels, a series of physicochemical processes (drying, pyrolysis, heterogeneous and homogeneous reactions) take place in different temperature ranges. A simplified

chemical reaction sequence for the gasification of coal or biomass is shown in Figure 1.2.

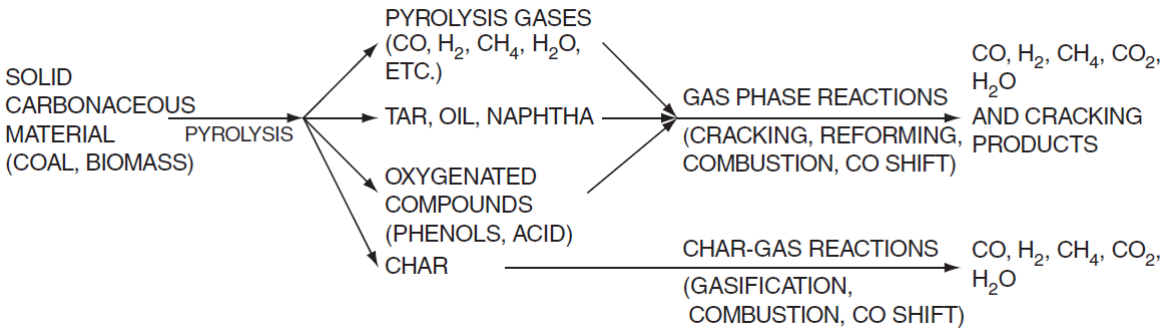

Figure 1.2 Simplified reaction sequence for gasification of coal or biomass (Higman & van der Burgt, 2003).

1.1.2.1 Drying and pyrolysis

In the drying process, moisture migrates from inside the particle to the surface and then evaporates by absorbing heat according to the following equation (Bell, *et al.*, 2011):

$$H_2O\ (l) \xrightarrow{drying} H_2O\ (g) \quad \Delta H_R = 43.99\, kJ/gmol \tag{1.4}$$

In the solid fuels (e.g., coal and biomass) gasification process, pyrolysis is a series of complex physical and chemical processes which takes place as the temperature increases to above 200 ˚C.

$$Solid\ fuel\ (s) \xrightarrow{pyrolysis} char\ (s) + Volatiles\ (g)\ \ \Delta H_R = positive, variable \tag{1.5}$$

1.1.2.2 Reaction with oxygen

In an air or oxygen blown gasifier, O_2 can react with the char and volatiles to form combustion and/or partial combustion products according to the following equations (Bell, *et al.*, 2011):

$$\text{Volatiles} + \mathrm{O_2} \rightarrow CO_2 + CO + H_2 + H_2O + H_2S + SO_2 \qquad \Delta\mathrm{H}_R = negative, variable \tag{1.6}$$

$$\mathrm{C} + \mathrm{O_2} \rightarrow \mathrm{CO_2} \quad \Delta\mathrm{H}_R = -393.98\, kJ/mol\, carbon \tag{1.7}$$

$$\mathrm{C} + 1/2\ \mathrm{O_2} \rightarrow \mathrm{CO} \quad \Delta\mathrm{H}_R = -110.65\, kJ/mol\, carbon \tag{1.8}$$

The heat generated from these reactions with oxygen can be used to drive the other endothermic gasification reactions in the gasifier.

1.1.2.3 Other gasification reactions

Two important gasification reactions, i.e., the steam gasification reaction (Equation 1.9) and Boudouard reaction (Equation 1.10), also take place in most of the gasifiers (Bell, *et al.*, 2011).

$$\mathrm{C} + \mathrm{H_2O} \rightarrow \mathrm{H_2} + \mathrm{CO} \quad \Delta\mathrm{H}_R = +131.46\, kJ/mol\, carbon \tag{1.9}$$

$$\mathrm{C} + \mathrm{CO_2} \rightarrow 2\,\mathrm{CO} \quad \Delta\mathrm{H}_R = +172.67\, kJ/mol\, carbon \tag{1.10}$$

In most of the gasifiers, the pyrolysis and heterogeneous reactions involving oxygen (Equations 1.7 and 1.8) are fast. Therefore, the slower steam gasification reaction (Equation 1.9) and the Boudouard reaction (Equation 1.10) determine the required gasifier residence time (Higman & van der Burgt, 2003).

1.1.2.4 Other gas phase reactions

Due to the high temperature in the gasifier (typically higher than 700 ˚C), the water-gas shift reaction (Equation 1.11) and steam reforming reaction (Equation 1.12) may occur spontaneously even in the absence of a catalyst (Bell, *et al.*, 2011).

$$CO + H_2O \leftrightarrow CO_2 + H_2 \quad \Delta H_R = -20.6\, kJ/mol \tag{1.11}$$

$$CH_4 + H_2O \leftrightarrow CO + 3H_2 \quad \Delta H_R = 103.1\, kJ/mol \tag{1.12}$$

1.1.3 Application of biomass and solar energy for FTL fuels production

As discussed above in Section 1.1.1.2, the CTL processes have been widely investigated and even applied due to the plentiful reserves and relatively low cost of coal. To mitigate CO_2 emissions from the CTL processes, two kinds of promising renewable energy, biomass and solar energy, have received growing attention as partial or total substitutes for the coal feed.

1.1.3.1 Application of solar energy

In the conventional gasification processes, a portion of the feedstock is combusted to provide high-temperature heat for the endothermic gasification reactions (as discussed in Section 1.1.2). To increase the syngas yield per unit of feedstock and reduce the amount of CO_2 produced from the gasification process, solar gasification has been widely investigated in the past few decades (Piatkowski, *et al.*, 2011). Solar gasification is a process in which concentrated solar thermal provides the heat to drive the endothermic reactions, which displaces the partial combustion of feedstock in the conventional gasification process. Therefore, compared with the conventional solid

fuels to FTL fuels process, the FTL fuels production system via a solar gasification process has the potential to achieve a greater FTL fuels output per unit of feedstock and lower CO_2 emissions. However, the transient nature of the solar resource would result in an intermittent syngas output from the solar gasification process, which would impact the downstream operation of the FTL fuels production process.

With sufficient energy storage, a stable flow-rate and composition of syngas to the FT reactor can potentially be obtained over a full year of operation for the FTL fuels production system via a solar gasification process. In addition, since no secondary source of thermal energy is proposed to be used to drive the gasification reactions, this type of system has the potential to achieve a significant solar share, which is a parameter defined as the fraction of the total energy flow attributed to solar energy. Solar share can be defined in two different ways: either based on energy inputs or energy outputs (Sheu, *et al.*, 2012). The solar share defined based on energy output can show the percentage of output that comes from solar. However, two types of product (electricity and liquid fuels) are usually proposed in the FTL fuels production system. Therefore, it is better to evaluate the variation of each type of product that resulted from the integration of solar energy rather than using a single parameter solar share. In the present thesis, solar share is defined based on the energy input to present the percentage of solar energy in the total energy input, thus indicating the ratio of carbonless solar energy input to the carbonaceous fuel input. However, the huge capacity for energy storage required by the system discussed above would limit its application (Kaniyal, *et al.*, 2016).

On the other hand, solar hybridized FTL fuels production systems were proposed, together with solar hybridized gasification processes, to maintain a continuous and even steady input to the FT reactor. In these systems, a secondary source of thermal energy

(e.g., the partial combustion of the feedstock, combustion of synthesis gas product and so on) is proposed to be supplied to assist the solar thermal input. Hybridization requires a much lower amount of energy storage to maintain a continuous and steady operation of the FT reactor, even if this is at the expense of reduced solar share (Kaniyal, *et al.*, 2013b; Kaniyal, *et al.*, 2016). Therefore, increasing attention has been focused on the investigation of solar hybridized FTL fuels production. However, of the recently proposed solar hybridized coal and/or biomass to FTL fuels systems, the high gasification temperature (> 1200 ˚C) (Kaniyal, *et al.*, 2013a; Kaniyal, *et al.*, 2013b), the unsteady operation of the FT synthesis process (Kaniyal, *et al.*, 2013a; Kaniyal, *et al.*, 2013b), the need for storage of syngas (Kaniyal, *et al.*, 2013a; Kaniyal, *et al.*, 2013b; Kaniyal, *et al.*, 2016) and/or the need for high temperature molten salt storage (Hathaway, *et al.*, 2014; Nickerson, *et al.*, 2015) have impeded their application.

1.1.3.2 Application of biomass

The gasification of biomass has been widely studied because the greenhouse gas emissions can potentially be reduced by substituting biomass for coal. In addition, the continual depletion of fossil fuel reserves and the increasing global population have also provided motivation for the development of the utilization of biomass as an alternative renewable energy source. In addition to the widely studied woody biomass, the utilization of agricultural and industrial residues and algal biomass has also received much attention. Agricultural and industrial residues have significant economic advantage, while the algal biomass has merits including the high areal energy yields, adaptability to a diverse range of aquatic environments and no requirement for arable land (Lawton, *et al.*, 2013; Stephens, *et al.*, 2013; Kumar, *et al.*, 2016; Neveux, *et al.*, 2016). However, the application of biomass can be limited by the typically high cost (compared with coal) and some biomass properties, e.g., the high oxygen content, high moisture content, low calorific value,

hygroscopic nature and low density, which can result in a low conversion efficiency and difficulties in collection, grinding, transportation and/or storage.

Torrefaction is a mild thermal pre-treatment technology (200−300 ºC) that has been widely studied and demonstrated to improve these properties thus making the biomass more suitable in large scale applications (e.g., fluidized bed gasification, high temperature entrained flow gasification). Various types of reactors (e.g., fluidized bed reactors, moving bed reactors, rotary drum and toroidal reactors) have been proposed and/or demonstrated for large-scale torrefaction processes (Chew & Doshi, 2011; Chen, *et al.*, 2015; Thrän, *et al.*, 2016). Even if the commercial implementation of torrefaction is currently in its early phase, its potential has been demonstrated by running pilot-scale and demonstration plants (Chew & Doshi, 2011; Thrän, *et al.*, 2016).

In addition, an influence of torrefaction on bio-char gasification reactivity has also been found (Couhert, *et al.*, 2009; Fisher, *et al.*, 2012; Weiland, *et al.*, 2014; Karlstrom, *et al.*, 2015; Li, *et al.*, 2015; Cerone, *et al.*, 2016; Ku, *et al.*, 2016; Kulkarni, *et al.*, 2016), which can influence carbon conversion during the gasification process, thus affecting the whole FTL fuels production process. To better understand the influence of torrefaction on bio-char gasification reactivity, the factors affecting reactivity (e.g., the specific surface area, the catalytic inorganic matter content and the carbonaceous structure) of the bio-chars prepared from raw and torrefied biomass should be investigated. However, little work has been undertaken on this topic.

The aims of the present thesis are to evaluate the annual performance of the solar hybridized coal and/or biomass to FTL fuels processes with novel configurations and to better understand the influence of torrefaction on the bio-char gasification reactivity. To meet the former aim, a novel solar hybridized dual fluidized bed (DFB) gasification

process is proposed for FTL fuels production as a reference scenario. Furthermore, based on this reference scenario, additional new configurations of solar hybridized FTL fuels process are also proposed, which are characterized with a novel SDFB gasifier with char separation, the incorporation of carbon capture and sequestration (CCS) and/or the use of FT reactor tail-gas recycle. All of these proposed systems are assessed by using a pseudo-dynamic model for coal and/or biomass. The latter aim is met by experimentally investigating the gasification reactivity, the specific surface area, the carbonaceous structure and the catalytic inorganic element content of both the raw and torrefied biomass chars produced under various conditions.

1.2 Scope and structure of the thesis

Chapter 2 provides a critical review of the literature relating to solar hybridized FTL fuels production and bio-char reactivity. The emphasis of this chapter is on the solar gasification processes, solar and non-solar FTL fuels production processes, factors affecting char reactivity (char characteristics), and the influence of torrefaction on the char gasification reactivity.

Chapter 3 presents the first of three journal publications, and proposes a novel solar hybridized dual fluidized bed gasification process for FTL fuels production using lignite as the feedstock. This concept offers sensible thermal storage of the bed material and a process that delivers a constant production rate and quality of syngas, despite solar variability. This solar hybridized FTL fuels production system is assessed using a pseudo-dynamic model that assumes steady state operation at each time step for a one-year, hourly integrated solar insolation time series.

Chapter 4 presents the second of three journal publications, and proposes a new configuration of the solar hybridized dual fluidized bed gasification process with char

separation for the production of FTL fuels from solid fuels of biomass and/or coal. The addition of carbon capture and sequestration and the used of FT reactor tail-gas recycle configurations is also assessed by simulating the new systems using the pseudo-dynamic model described in Chapter 3.

Chapter 5 presents the final journal publication of the present thesis, and deals with the influence of torrefaction on the gasification reactivity of the char produced at different temperatures for three types of biomass, i.e., pine wood (woody biomass), grape marc (agricultural and industrial residue) and macroalgae (algal biomass). In addition, the influence of torrefaction on the factors affecting char reactivity (i.e., the char specific surface area, the char carbonaceous structure and the catalytic inorganic element content in the char) was also investigated to further explain the variation of the char reactivity caused by the torrefaction.

Chapter 6 presents the conclusions of the work, together with the recommendations for future work in this area of research.

Finally, a list of the references cited in Chapters 1, 2 and 6 is given. All other references cited in the individual journal papers (Chapters 3-5) are presented within the relevant papers.

CHAPTER 2

LITERATURE REVIEW

2.1 Introduction

This chapter reviews the published literature related to solar hybridized FTL fuels production and bio-char reactivity. The emphasis of this chapter is on the solar and non-solar FTL fuels production processes, solar gasification processes, factors affecting char reactivity (i.e., char specific surface area, char carbonaceous structure and catalytic inorganic matter in the char), as well as the influence of torrefaction on the bio-char gasification reactivity.

2.2 Fischer-Tropsch liquid (FTL) fuels production

2.2.1 FTL fuels production via coal gasification

The commercial applications of the CTL technology were not very successful, except for the one in South Africa, as discussed in Section 1.1.1.3. Therefore, the long-term viability of CTL plants should be assessed considering the price fluctuations of crude oil and coal, policy factors and technology development. CTL was suggested as having the potential to account for around a third of global liquid fuels by 2050, without considering a climate policy (Henry Chen, *et al.*, 2011). However, the huge carbon footprint could make the viability of the CTL process quite limited in regions with a climate policy. The techno-economic analysis was performed to assess the prospect of the CTL process in China by considering different system configurations and coupling carbon capture and sequestration (CCS) technology (Zhou, *et al.*, 2013). The authors suggested that the recycled synthesis of unreacted syngas could be better than the once-through synthesis for liquid fuels production because more carbon could be incorporated into the liquid fuels through the recirculation. Moreover, although CCS technologies could lead to certain economic losses, it was also expected to be competitive if climate policies were applied. Another techno-economic analysis of CTL

was also performed to assess the feasibility of the CTL technology in China (Zhou, *et al.*, 2016). The economic analysis showed that it could be economically competitive to develop the CTL process, when the oil price was over 70 USD/bbl. Moreover, the authors also suggested that the CTL process was less thermodynamically efficient than the conventional crude oil to liquid fuels process due to the low carbon efficiency caused by the low H_2 to CO molar ratio in the crude syngas generated by coal gasification.

Depending on the types of feedstock and gasifier, as well as the operating conditions, the H_2 to CO molar ratio produced through gasification is typically about 0.7–1.1 which is lower than the optimal ratio required by the FT synthesis process (typically around 2) (Adams & Barton, 2011). Therefore, the water-gas shift reaction ($CO + H_2O \leftrightarrow CO_2 + H_2$) has been proposed to upgrade the syngas to the required H_2 to CO molar ratio. However, the heat loss from the mildly exothermic water-gas shift reaction, together with the capital and energy intensive CO_2 recovery step (CO_2 generated by using the water-gas shift reaction) can cause a negative impact on the energetic, environmental and economic performance of the system (Adams & Barton, 2011; Fout, *et al.*, 2015).

2.2.2 FTL fuels production via natural gas reforming

Compared with coal gasification, natural gas autothermal steam reforming can be used to generate syngas with a better H_2 to CO molar ratio (around 2) for the FT synthesis process, thus achieving a better energetic and environmental performance of the FTL production process, compared with the coal gasification process (Sudiro & Bertucco, 2009; Wood, *et al.*, 2012). In addition, gas to liquids (GTL) technology is also expected to play an important role in reducing the natural gas flaring associated with oil

production and monetizing the natural gas resources stranded in remote locations (Wood, *et al.*, 2012).

The life cycle greenhouse gas emissions of the natural gas to liquids process were calculated to be equivalent or less than that of the current fossil-fuel process (Baliban, *et al.*, 2013). Compared with the performance of the GTL process with steam reforming alone, the GTL process with CO_2/steam-mixed reforming has the potential to achieve a higher process efficiency and lower value in both the total CO_2 emissions and the total product cost per unit of product. (Zhang, *et al.*, 2016a). Nuclear energy was also proposed to provide the heat for natural gas reforming, thereby displacing the burning of natural gas (Salkuyeh & Adams Ii, 2013). The high-temperature helium produced in a modular helium reactor (a type of nuclear reactor in which helium is used as the coolant) was proposed to deliver the nuclear heat to natural gas reformer. For a coal and natural gas to liquids process without CCS, the calculated fossil fuel consumption can be reduced by up to 22%, while the calculated CO_2 emissions can be decreased by up to 44%, with the incorporation of carbonless nuclear energy. However, the CO_2 emitted from nuclear fuel production and nuclear waste disposal processes were not considered in their analysis.

Natural gas to FTL fuels processes will not be discussed in the following sections since they are beyond the scope of the present thesis. The present thesis will focus on the solid fuels to FTL fuels processes.

2.2.3 FTL fuels production via biomass gasification

As a type of promising renewable energy, biomass has been widely investigated as the feedstock for producing low-emission liquid fuels (Larson, 2006; Hu, *et al.*, 2012; Ail

& Dasappa, 2016). In addition, compared with the direct biomass to liquid process, FT liquid fuels have a significant environmental advantage because they are free of sulphur.

2.2.3.1 Biomass only processes

Techno-economic analysis has been widely performed to evaluate the viability of the biomass to liquids (BTL) process. The evaluation of an FTL fuels production system with 400 MW_{th} biomass input shows that a calculated overall efficiency of 45% (HHV basis) can be achieved while the system has the potential to produce FTL fuels at 16 €/GJ (the biomass price was assumed to be 3 €/GJ) (Hamelinck, *et al.*, 2004). In addition, better energetic and economic performance of the system is also expected with the increasing scale and technology improvements. In Finland, there is the potential to produce FT bio-diesel at a cost of around 18 €/GJ, including by-products income (Natarajan, *et al.*, 2014). A techno-economic analysis has also been performed for two biomass to liquids (BTL) plants based on gasification utilizing 2000 t/d (~ 390 MW) corn stover (dry basis, ~ 4.9 USD/GJ) (Swanson, *et al.*, 2010). A low temperature (870 ˚C) fluidized bed gasifier and a high temperature (1300 ˚C) entrained flow gasifier were proposed for the two plants, respectively. The analysis shows that the high temperature gasification scenario has the potential to produce gasoline with a lower cost (about 30.3−37.7 USD/GJ) than the low temperature one, although the investment costs (500−650 million dollars) are higher. The costs of the FTL liquid fuels produced from biomass can be significantly influenced by the cost of the feedstock. Even though the price of biomass is sensitive to species and time, it is generally more expensive than coal. In addition, if the BTL processes were widely applied, the feedstock cost would further increase due to the severe competition for biomass.

2.2.3.2 Co-feed of biomass and coal

Co-feed of biomass and coal to FTL fuels productions has the potential to take advantage of certain synergies between coal (high CO_2 emissions, while low cost) and biomass (low CO_2 emissions, but high cost), thus achieving certain emission targets with relative low cost (van Vliet, *et al.*, 2009; Noureldin, *et al.*, 2014). For example, Xie, *et al.* (2011) suggested that the calculated greenhouse gas emissions of the FT diesel (without CCS) could be at parity with diesel derived from mineral crude oil with a biomass fraction of 61% (with forest residue as the biomass). The application of CCS was suggested to have the potential to reduce this required biomass fraction to less than 10%. To further reduce the calculated greenhouse gas emissions to close to zero, only 55% of biomass in the feedstock (the biomass and coal mixture) is required, if CCS is applied. For a once-through coal and biomass (corn stover) to liquid process with CCS, a biomass fraction of only 9% (higher heating value basis) was required to achieve the calculated net life cycle greenhouse gas emissions for the FTL fuels parity with the liquid fuels derived from crude oil (the electricity co-product greenhouse gas credit is assumed to be 138 kg CO_2 equivalent / MWh) (Larson, *et al.*, 2010). For this system, there is the potential to produce FTL fuels at a cost of 12.2 USD/GJ. In addition, the calculated greenhouse emissions for the FTL fuels could be decreased to zero as the biomass fraction was increased to 37.4%. However, the calculated cost of the FTL fuels can be increased to 18.7 USD/GJ. van Vliet, *et al.* (2009) also suggested that the proposed FTL plant with CCS technology had the potential to produce liquid fuels with zero well-to-wheel emissions if 54% biomass was proposed to be co-gasified with coal. Furthermore, negative well-to-wheel emissions could be achieved by increasing the biomass fraction to a value higher than 54%.

Parasitic electricity consumption and challenges in CO_2 storage limit the application of CCS technology. Therefore, more investigation on the CO_2 storage approaches needs to be performed. But this will not be discussed further in the present thesis since it is beyond the scope of this study. In addition, the application of biomass is limited by its relatively high cost and some biomass properties, as discussed in Section 1.1.3.2. Therefore, more renewable energy sources (e.g., solar) are also needed to further improve the energetic and environmental performance of the FT liquid fuels production processes.

2.3 Solar gasification

A solar hybridized FTL fuels production system, via a solar gasification process has the potential to obtain a greater FTL fuels output per unit of feedstock and lower CO_2 emissions. Solar gasification reactors have been widely studied since the 1980s and can broadly be classified as directly or indirectly irradiated reactors. In the directly irradiated reactors, the solid fuels are directly exposed to concentrated solar irradiation, while the heat is transferred to the reaction zone via an opaque wall or other medium in the indirectly irradiated reactors (Piatkowski, *et al.*, 2011). Compared with the indirect reactors, the direct ones offer the advantage of a more efficient heat transfer, which enables a higher reaction temperature (Piatkowski, *et al.*, 2011; Nathan, *et al.*, 2017). Nevertheless, to introduce the irradiation to the reaction site, a directly irradiated reactor requires an aperture through which the convective losses should be minimized. For this reason, a quartz glass window was successfully employed in lab-scale reactors for short-term operation (Kodama, *et al.*, 2002; Z'Graggen, *et al.*, 2006; Z'Graggen, *et al.*, 2007; Piatkowski, *et al.*, 2011; Gokon, *et al.*, 2012). However, both the reliability and the scalability of the window become big challenges under high pressures and severe

gas environments, especially for long-term application. On the other hand, interest is growing in investigating the indirectly irradiated reactors, which can eliminate the window, although the exergetic losses caused by the temperature difference between the wall and the reaction site need to be minimized (Piatkowski, *et al.*, 2011; Nathan, *et al.*, 2017). Nevertheless, the challenges to the application of solar gasification are still linked to the methods and materials which are used to transfer the concentrated solar thermal to the reaction site reliably and efficiently.

2.3.1 Directly irradiated solar gasifiers

2.3.1.1 Packed-bed gasifier

Solar gasification reactors have been widely studied since the 1980s, with directly irradiated packed bed solar gasifiers for both coal and biomass among the first types to be assessed (Gregg, *et al.*, 1980; Taylor, *et al.*, 1983). Simulated solar irradiation was introduced to the gasification zone through a window from the side (Gregg, *et al.*, 1980) and top (Gregg, *et al.*, 1980). Even though directly irradiated packed bed solar gasifiers are relatively simple, robust (for a wide range of feedstock) and cost effective, their performance is limited by the build-up of ash (especially for feedstock with a significant ash content), which then inhibits the irradiation heat to be transferred to the unreacted fuel (Kaniyal, *et al.*, 2016). However, effective design to remove ash continuously has not be investigated yet. In addition, the limitations of heat and mass transfer through the bed and the window can impede the large-scale application of this type of gasifier.

2.3.1.2 Fluidized bed gasifier

Compared with packed bed gasifiers, fluidized bed gasifiers have a greater potential to be applied on a large scale due to their improved heat and mass transfer through the bed.

Taylor, *et al.* (1983) proposed one of the first designs of solar fluidized bed gasifiers. The fluidized bed was located in a quartz tube through which the solar irradiation was introduced onto the top of the bed. The bed zone was surrounded by a ceramic reflector-insulator to reduce the heat loss. Murray and Fletcher (1994) designed another type of quartz tube fluidized bed gasifier which was located in a cavity. Simulated solar irradiation was introduced to the side of the bed. A similar design was also proposed by Kodama, *et al.* (2002) for coal gasification with CO_2. However, quartz tube reactors are not reliable for large-scale applications (Puig-Arnavat, *et al.*, 2013). Kodama, *et al.* (2010) studied the CO_2 gasification of coal in a top windowed stainless steel fluidized bed gasifier prototype designed for beam-down optics. Based on this concept, an internally circulating fluidized bed gasifier was also proposed and used to investigate CO_2 gasification of coal coke (Kodama, *et al.*, 2008; Gokon, *et al.*, 2012). Compared with the design of the fluidized bed gasifier without internal circulation, this design allows for a homogeneous and higher temperature (middle and bottom layer) inside the bed. Further demonstrations on the steam gasification of coal coke with and without quartz sand were also investigated in this type of gasifier by operating in batch mode (Gokon, *et al.*, 2014; Gokon, *et al.*, 2015). As suggested by the authors, this type of gasifier could be operated in continuous mode if a continuous feeding system and steady irradiation are available. However, for this type of gasifier, the window could be contaminated by the elutriated particles and dust, thus reducing its reliability, especially for large-scale applications.

2.3.1.3 Vortex-flow gasifier

As shown in Figure 2.1, a solar vortex-flow gasifier has been demonstrated in 5 kW scale to achieve good conversion of carbonaceous feedstock into syngas due to the high temperature (> 1000 ˚C) and relative long residence time resulting from the swirling

flow in the gasifier (Z'Graggen, *et al.*, 2006; Z'Graggen, *et al.*, 2007; Z'Graggen, *et al.*, 2008). Inside the reactor, a steam-particle stream progressed towards the rear along a helical path, while the concentrated solar radiation was used to directly irradiate it. The aperture, through which the solar radiation was introduced into the reactor, was equipped with a diverging frustum for mounting the window where the radiation intensity is about 10 times lower and the dust deposition can be reduced. In addition, the window was protected from overheating and particle contamination by an aerodynamic curtain which would result in parasitic energy consumption. The upscaling of the 5 kW prototype vortex-flow gasifier to pilot-scale (300 kW to 500 kW) was investigated (Z'Graggen & Steinfeld, 2008; Vidal, *et al.*, 2010). The experience of the pilot-scale plant operation would provide input to the pre-design of a larger scale commercial plant in the future. However, the vortex-flow gasifiers are restricted by the fine particle size requirement. Therefore, it could not be suitable for biomass gasification applications because the energy required for the grinding of biomass is very high in order to produce fine biomass particles (Mani, *et al.*, 2004). In addition, the large-scale application of the vortex-flow gasifiers could be limited by the size of the window. The diameter of the window is already over 1 m for the pilot-scale (300 kW) application (Z'Graggen & Steinfeld, 2008).

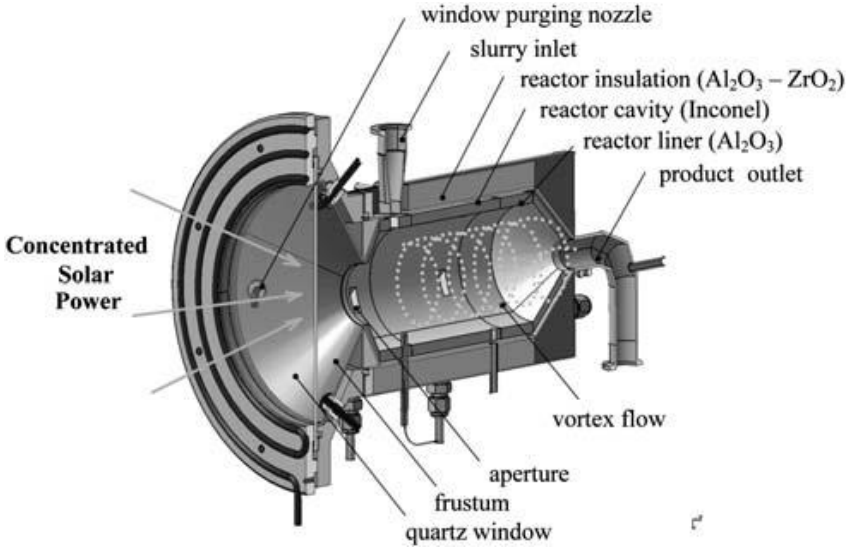

Figure 2.1 Scheme of the directly irradiated vortex-flow solar reactor configuration (Z'Graggen, *et al.*, 2006; Z'Graggen, *et al.*, 2007; Z'Graggen, *et al.*, 2008).

2.3.2 Indirectly irradiated solar gasifiers

2.3.2.1 Packed-bed gasifier

A 5 kW indirectly irradiated packed-bed gasifier was designed and tested (Piatkowski & Steinfeld, 2008; Piatkowski, *et al.*, 2009). This gasifier consists of two cavities in series, separated by a radiant emitter plate (SiC-coated graphite plate). The beam-down incident solar radiation was introduced into the upper cavity through a window to heat up the radiant emitter plate, which then radiated the reactants in the lower cavity to drive the reactions. Therefore, the contact between the particles and the quartz window can be avoided by this plate. This type of gasifier was scaled up to 150 kW_{th} and successfully used for the solar gasification of six different types of carbonaceous waste materials (industrial sludge, fluff, tire chips, dried sewage sludge, low-rank coal, and sugar cane bagasse). The authors also suggested that this solar reactor concept was scalable to a commercial application (MW_{th}) and can generally tolerate bulk carbonaceous feedstock of any shape and size without prior processing. Similar to the

directly irradiated packed-bed gasifier, the large-scale application of this type of indirectly irradiated packed-bed gasifier could be limited by the poor heat and mass transfer through the bed and by the build-up of ash on the surface (especially for feedstock with a significant ash content) (Kaniyal, *et al.*, 2016).

2.3.2.2 Tubular gasifier

Solar reactors consisting of opaque tubular absorber(s) have also been used for gasification (Melchior, *et al.*, 2009; Lichty, *et al.*, 2010). The solar irradiation was introduced onto the tubular absorber(s) in a cavity through an aperture. The carbonaceous particles were transported through the hot zones of the tubes where the gasification reactions occur. A window is not necessary in this type of reactor if the material of the tubes can be stable in air at operational temperatures. In addition, this type of gasifier has the potential for large-scale application due to both the elimination of the window and the good heat and mass transfer inside the tube. However, large temperature differentials (potentially over 300 ˚C) were observed between tube locations, which could lead to different performances from each tube. In addition, to achieve high carbon conversion, fine particles and high temperatures (> 1000 ˚C) are required for this type of solar gasifier. The high temperatures could lead to high energy losses, while the fine particles requirement would limit the biomass application in this type of gasifier because the level of energy required for grinding biomass is very high to produce fine biomass particles (Mani, *et al.*, 2004). A two zone solar reactor based on the combined drop-tube and fixed bed concepts was proposed and designed to retain the merit of the efficient radiative heat transfer inherent in drop tube reactors while overcoming their particle size and residence time restrictions (Kruesi, *et al.*, 2013; Kruesi, *et al.*, 2014). The drop tube zone located in the upper part of the gasifier was for fast pyrolysis while the trickle bed (in a porous structure) was for the char gasification,

which was much slower compared with the pyrolysis. A series of 20-minute steam gasification experiments with bagasse particles was conducted in both the drop tube and the two zone solar reactors at a 1.5 kW_{th} solar radiative power input. The results showed that both the CH_4 and the C_2 hydrocarbons were more efficiently decomposed in the two zone gasifier. Moreover, the bagasse feedstock was energetically upgraded by 5%. However, the operation of this type of gasifier could be limited by clogging of the porous structure, especially for high temperature and long-term operations.

2.3.2.3 Molten-salt pool gasifiers

Adinberg, *et al.* (2004) experimentally investigated the fast pyrolysis of cellulose particles in a molten salt medium at temperatures of 800−915 ˚C, using an electrically heated lab-scale reactor. A high heating rate of up to 100 ˚C/s was demonstrated for cellulose particles in the molten carbonates of sodium and potassium. At 850 ˚C, the conversion of biomass to gas was about 94 wt% for the fast pyrolysis in the molten salt medium, while it was only about 72% for the case in an inert gas medium without using the molten salt. A reactor concept was then developed for the utilization of concentrated solar thermal energy. This reactor, consisting of a set of vertical tubes to absorb solar radiation, exploited free convection of the molten salt to deliver the thermal energy to the reaction/thermal-storage medium. Biomass gasification in high temperature molten salt (mixture of lithium, sodium, and potassium carbonate) has also been investigated (Hathaway, *et al.*, 2011). The results showed that, compared with an inert environment, the molten salt increased the rate of pyrolysis by 74% and increased the gasification rates by more than an order of magnitude, while promoting a product gas composition nearer to thermodynamic equilibrium predictions. Further analysis indicated that the increase in the pyrolysis rate was mainly caused by the heat transfer enhancement, while a catalytic effect of the molten salt was found during the char gasification process.

A techno-economic analysis was performed for the solar biomass gasification in molten salt with various molten salt heat capacities and nominal syngas yield rates (Hathaway, *et al.*, 2014). Comparing the cost of the syngas with the natural gas price, the authors suggested that this concept did not compete in United States at that time. However, this analysis did not include the potential greenhouse gas savings and consequent economic benefits. The authors recommended that pro-renewable policies (e.g., a tax rate reduction, a bond yield and duration reduction, and a production credit) and changes in natural gas economics would be necessary to make it competitive.

However, the unstable chemical properties of molten salt at high temperatures (> 800 ˚C) could limit the application of molten-salt pool gasifiers (Ma, *et al.*, 2014). The ash accumulation in the molten-salt has the potential to impact the operation of this type of gasifier, especially for high ash feedstock applications. Therefore, ash separation would be a challenge in this type of gasifier.

As discussed in Sections 2.3.1 and 2.3.2, large-scale application of solar gasifiers is still in its early phase. Current proposed solar gasifiers are constrained by the issues about window reliability, reactor scalability, heat and mass transfer, feedstock size tolerance, heat medium stability and so on .Hence, it is desirable to seek alternative solar gasification concepts with the potential to address the challenges raised above.

2.3.3 Solar hybridized dual fluidized bed gasifier

Solid particles are considered to be well suited for use as a solar thermal heat carrier and storage medium due to their potentially lower cost and higher operating temperature (~ 1000 ˚C), compared with molten-salt (Kolb, *et al.*, 2006; Ma, *et al.*, 2014). A dual fluidized bed gasifier has the potential to use solid particles to transfer the concentrated solar thermal to the gasification zones. Therefore, in this section, the

merits and viability of the solar hybridized dual fluidized bed gasification concept are discussed.

2.3.3.1 Conventional dual fluidized bed gasifier

The dual fluidized bed gasifier, a type of allothermal gasifier, has been widely studied and demonstrated around the world (Feldman, *et al.*, 1988; Hofbauer, *et al.*, 2002; Hofbauer, *et al.*, 2003; Sudiro, *et al.*, 2008; Aigner, *et al.*, 2011; Abdelouahed, *et al.*, 2012; Sauciuc, *et al.*, 2012; Kern, *et al.*, 2013a, 2013b; Kern, *et al.*, 2013c; Saw & Pang, 2013). In contrast with autothermal gasifiers, in which part of the fuel is oxidized by oxygen to provide heat for the endothermic gasification reactions, DFB gasifiers separate the combustion and gasification reactions. Figure 2.2 presents the concept of a DFB gasifier (Guo, *et al.*, 2015). The feedstock is gasified with steam in the gasification reactor to produce syngas. The heat required by the gasification process is transferred from the combustion reactor via the hot bed material. The warm bed material and residue char from the gasification reactor are then sent to the combustion reactor in which the char is burned with air to heat the bed material. Additional feedstock is required in the combustion reactor if the char is not sufficient.

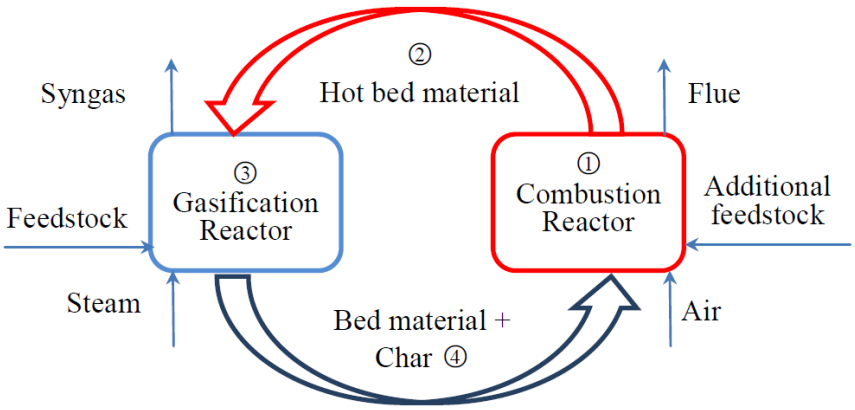

Figure 2.2 Concept of dual fluidized bed gasifier (Guo, *et al.*, 2015).

Gasification of low rank coal, biomass or their blends has already been well demonstrated in the DFB gasifier (Aigner, *et al.*, 2011; Schmid, *et al.*, 2012; Kern, *et al.*, 2013a, 2013b; Kern, *et al.*, 2013c; Saw & Pang, 2013). In addition, the DFB gasifier has also been successfully utilized to produce syngas for a pilot-scale FTL fuels production process without applying the downstream H_2/CO ratio adjustment (Kim, *et al.*, 2016). An average H_2/CO ratio of 1.67 was obtained from the DFB gasifier, which satisfied the requirements of the iron-based FT catalysts used in the FT reactor.

2.3.3.2 Potential to integrate solar energy

In a DFB gasifier, the bed material can potentially be heated via concentrated solar thermal energy rather than via combusting additional feedstock in the combustion reactor. Figure 2.2 also identifies four alternative locations into which the concentrated solar thermal energy can potentially be introduced into a DFB gasification system, namely into the combustion reactor (location 1), into the hot bed material leaving the combustion reactor (location 2), into the gasification reactor (location 3), and into the bed material and char leaving the gasification reactor (location 4) (Guo, *et al.*, 2015). Among these locations, location 2 will be considered in the present thesis due to its potential merits, as explored below. For this concept, concentrated solar energy is only proposed to heat the inert bed material. Therefore, it could be unnecessary to seal the particle solar receiver from the outside environment if the particles can survive in the outside environment at the operational temperature. Moreover, since solar energy can potentially be integrated into an additional solar receiver to heat the solid particles, no significant modification would be required to the demonstrated conventional DFB gasifier. In addition, the steady state operation of the gasification reactor can be achieved by maintaining the steady particle input to the gasification reactor. In this new concept, a solar hybridized dual fluidized bed gasifier, the heat required when solar is

not available can be provided in the short term by the sensible heat stored in the hot solid particles or by the supplementary feedstock combustion in the combustion reactor when the storage of hot solid particles runs out. To maximize the solar input into the system, the combustion in the combustion reactor needs to be minimized. Therefore, the improvement of char gasification conversion could be important to reduce char combustion thus increasing the solar input, even though this could also increase the additional feedstock input into the combustion reactor when solar is not available. However, this solar hybridized dual fluidized bed gasification concept has not yet been investigated.

2.3.3.3 Particle receiver

In the solar hybridized dual fluidized bed gasification concept discussed above, the solar particle receiver is a key component in which the particles are proposed to be heated using concentrated solar thermal radiation. Inert solid particles can potentially be a relatively inexpensive alternative medium to transfer the high-temperature (~ 1000 ˚C) concentrated solar thermal to the gasification zone or to store the solar thermal heat as sensible heat (Bertocchi, *et al.*, 2004; Tan & Chen, 2010; Röger, *et al.*, 2011; Ho, *et al.*, 2014; Ho & Iverson, 2014; Xiao, *et al.*, 2014). Due to the inert properties of the solid particles, solar radiation can be absorbed directly in air without the need for sealing, as discussed above, in Section 2.3.3.2. In addition, the selection of high-temperature inert particles can offer the potential to heat the particles to, and store the particles at, very high temperatures (~ 1000 ˚C). The concept of a falling particle receiver has been intensively studied for the last few decades (Hruby, 1986; Tan & Chen, 2010; Röger, *et al.*, 2011; Ho, *et al.*, 2014; Ho & Iverson, 2014; Ho, In Press), although only a few sets of on-sun tests of a simple falling particle receiver have been performed (Siegel, *et al.*, 2010; C.K. Ho, *et al.*, 2015; C.K. Ho, *et al.*, 2016). Those initial on-sun tests only

obtained 50% thermal efficiency, a maximum particle temperature increase of about 250 ˚C and a peak particle output temperature (near the centre of the receiver) of about 720 ˚C. More recently, on-sun tests of a 1 MW_{th} continuously recirculating particle receiver have been performed and have obtained bulk particle outlet temperatures reaching over 700 °C, and thermal efficiencies from ~ 50% to 80%. A spiral solar particle receiver with a conical cover was also investigated using a solar simulator (Xiao, *et al.*, 2014). Their experimental results showed that the particle temperature reached 650 ˚C and the thermal efficiency was about 60%. Experimental tests have been performed for a fluidized-bed receiver in which simulated solar irradiation was introduced from the top, while compressed air was used to fluidize the bed from the bottom (Flamant, *et al.*, 1980). For a mean flux density of ~500 kW/m^2, the measured equilibrium temperatures of the particles were about 927 ˚C for silica sand and over 1127 ˚C for silicon carbide. However, thermal efficiencies were only reported between 20 and 40%.

Better solar particle receiver design is still desired to reduce thermal losses, to increase the output temperature of particles and to increase the feasibility of large-scale application, while particles with better radiative properties and durability are still desired for high temperature operation and storage. If these challenges could be overcome, the particle receiver could be a promising technology for high-temperature (~ 1000 ˚C) utilization of concentrated solar thermal energy, thus increasing the feasibility of the concept of solar hybridized dual fluidized bed gasification. However, detailed investigation on the particle receiver is beyond the scope of the present thesis.

2.4 Solar hybridized FTL fuels production process

The gasification of solid feedstock, together with the subsequent FT processing of syngas, is considered to be one of the promising technologies to meet the long-term demand for reliable sources of transport liquid fuels, as discussed in Section 2.2. Recently, solar hybridized FTL fuels production has received much interest in the literature because of its potential to achieve greater FTL fuels production per unit of feedstock and lower CO_2 emissions, compared with the conventional non-solar FTL fuels production processes (Kaniyal, *et al.*, 2013a; Kaniyal, *et al.*, 2013b; Hathaway, *et al.*, 2014). However, the continuous and steady state operation desired by the FTL fuels production process and the transient nature of the solar resource lead to a challenge associated with the process integration.

Sudiro and Bertucco (2007) proposed and assessed a solar hybridized FTL fuels production process combining steam gasification of coal and steam reforming of natural gas in a solar reactor. The calculated specific output per unit of feedstock (LHV of product/LHV of feedstock) of this solar hybrid process was about 95%, which was about 67% higher than that of a non-solar coal to liquid process. However, the assessment of this study is based on an averaged daily solar radiation and solar hour. Therefore, a more comprehensive assessment accounting for the seasonal, diurnal, and cloud-related variability of the solar resource was desired for the solar hybridized FTL fuels production system.

Kaniyal, *et al.* (2013b) assessed a solar hybridized CTL system using a pseudo-dynamic model that assumes pseudo-steady state operation at each time-step, for a one-year, hourly integrated, solar insolation time series. A solar hybridized, oxygen blown, atmospheric pressure vortex-flow gasifier was proposed in this solar hybridized system,

together with pressurized storage of upgraded syngas and oxygen. According to their results, with the integration of this pressured syngas storage unit, the variation in throughput of each unit of this solar system could be maintained within normal operational ranges despite the fluctuation in the transient solar input. In addition, due to the introduction of solar energy, a calculated annually averaged improvement of 21% to the total energetic output and a reduction of 30% in the mine-to-tank greenhouse gas emissions could be obtained.

Further calculations were also performed to analyse the sensitivity of this solar hybridized CTL system's performance to variations in gasification reactor pressure, to turn-downs in the solid fuel feed rate, and to the proportion of biomass co-gasified with coal (Kaniyal, *et al.*, 2013a). The calculation results showed that with a 53 wt% biomass co-gasification fraction in the solar gasifier, a mine-to-tank greenhouse gas emissions parity with diesel production from crude oil could be obtained. However, for a non-solar CTL system, this calculated biomass fraction was about 65%. This reduction is very important because of some current issues of biomass applications including the steady and sustainable supply, cost, gasifier design and so on.

In addition, the economic feasibility of this solar hybridized CTL system was also analysed for the plants built in 2020 (Saw, *et al.*, 2015). The results showed that the total permanent investment cost (the economic data was reported in AUD) was around \$467−\$493 million for the solar hybridized CTL system producing 1500 barrel per day of FT liquids, depending on the solar site, while it was around \$377−\$384 million for its corresponding non-solar system. In addition, the levelised cost of fuel for the solar hybridized CTL plant was around \$46−\$49/GJ_{LHV} while it was about \$40−\$41/GJ_{LHV} for the corresponding non-solar plant. However, for this concept, the oxygen and syngas storage would limit its application. Moreover, the requirement for a window in

the solar vortex-flow gasifier would reduce its reliability (especially for large-scale and long-term application) while the required fine particle size of feedstock would limit its application on the biomass gasification (as discussed in Section 2.3.1.3).

Kaniyal, *et al.* (2016) analysed the storage capacity required to maintain continuous system operation of the stand-alone (solar energy is proposed to be the only thermal resource and energy storage is proposed to maintain the continuous and steady operation of the system) solar CTL system with a 150 kW_{th} packed-bed solar gasifier. The calculation results showed that, for an assumed heliostat field collection area of 1000 m^2, at least 64 days of storage was required to maintain a stable flow-rate and composition of syngas to the FT reactor over a full year of operation. This value could be reduced to 35 days by increasing the heliostat field collection area from 1000 to 1500 m^2. However, the authors also suggested that the use of the packed-bed solar gasifier for FTL fuels production is unlikely to be viable without substantial changes to the design and operation of the reactor and/or downstream process.

Davidson and co-workers have proposed an alternative solar hybrid allothermal gasifier in which the gasification of biomass is performed in a ternary eutectic blend of alkali carbonate molten salts (Hathaway, *et al.*, 2014). High quality syngas (i.e., with low N_2 content) can be produced in this type of gasifier for the FTL production system without the need for an air separation unit (ASU), even if it needs to be operated under conventional non-solar conditions, when solar is not available. The heat of combustion is transferred indirectly to the gasification zones. This system also offers the advantages of a lower reactor temperature of around 927 °C, high conversion rates due to the catalytic influence of the salts, and good potential for integration with thermal energy storage through the use of the salt. However, this gasification technology is less well established. Moreover, the unstable chemical properties of the molten salt at high

temperatures (~ 927 ˚C) could also limit the application of this concept (Gil, *et al.*, 2010; Ma, *et al.*, 2014). In addition, the ash accumulation in the molten-salt has the potential to impact on the operation of this type of gasifier, especially for high ash feedstock applications, as discussed in Section 2.3.2.3.

The viability of the stand-alone solar FTL fuel production system would be limited by the huge amount of syngas storage (expensive) required to maintain the continuous system, as discussed above. On the other hand, the solar hybridized autothermal gasifier requires a cost and energy intensive ASU for pure oxygen during periods of low solar irradiation to maintain the continuous operation of the FTL fuels production system. In addition, the intermittent solar input leads to the intermittent operation of the ASU and the need for syngas storage (even though it is much smaller than the required syngas storage for the stand-alone system) to accommodate the unsteady syngas output, and both of these could add significantly to the costs. In addition, even though the molten-salt allothermal gasifiers can produce high quality syngas without the need for an ASU (air is acceptable for the external combustion) when solar is not available, the high temperature (~ 927 ˚C) operation of molten-salt together with the potential ash accumulation in the molten salt could limit its application in the solar hybridized FTL fuels production process.

As another type of allothermal gasifier, DFB gasification (discussed in Section 2.3.3.2) has the potential to offer the use of relatively inexpensive inert solid particles as the medium for high temperature (~ 1000 ˚C) sensible heat storage (Ma, *et al.*, 2014). Little relevant work on this concept of high temperature particle storage has been reported yet, hence more work on this concept still needs to be performed in the future. Detailed investigation of high temperature sensible heat storage using solid particles is beyond the scope of the present thesis. Moreover, the concept of solar hybridized DFB

gasification also has the potential to provide a steady syngas output for the downstream process of the FTL plant, by maintaining the steady particle input to the gasification reactor (discussed in Section 2.3.3.2). However, this concept of solar hybridized DFB gasification has not been investigated for the FTL production process yet.

2.5 Gasification reactivity and characteristics of torrefied biomass char

2.5.1 Gasification of torrefied biomass

2.5.1.1 Overview of torrefied biomass gasification

Recently, more attention has been focused on the gasification of torrefied biomass due to its merits (e.g., lower O/C, lower moisture content, better grindability and so on) discussed in Section 1.1.3.2 (Prins, *et al.*, 2006; Dudyński, *et al.*, 2015). However, a lower carbon conversion for the torrefied biomass gasification was found, compared with the corresponding raw biomass gasification (Couhert, *et al.*, 2009; Kwapinska, *et al.*, 2015; Kulkarni, *et al.*, 2016). One potential reason for this lower carbon conversion could be the higher char yield (the solid yield from the pyrolysis process) for the torrefied biomass compared with the corresponding raw biomass (Zheng, *et al.*, 2013; Li, *et al.*, 2014a). This higher char yield is mainly a result of both the volatile release and the cross linking and carbonization of cellulose during the torrefaction process (Elyounssi, *et al.*, 2012; Zheng, *et al.*, 2013). In addition, the lower gasification reactivity of the torrefied biomass char compared with the corresponding raw biomass char can also result in lower carbon conversion for the torrefied biomass gasification compared with the corresponding raw biomass gasification.

2.5.1.2 Char gasification reactivity of the torrefied biomass

Both the combustion and gasification reactivities of the torrefied willow char were found to be lower than those of the raw willow char (Fisher, *et al.*, 2012). The chars were produced at 850 and 1000 ˚C at low (33 ˚C/min) and at 900 ˚C at high (> 30,000 ˚C/min) heating rates. In addition, the difference in char combustion reactivity between the raw and torrefied willow chars (the low heating rate) was found to decrease as the pyrolysis temperature was increased from 850 to 1000 ˚C. Moreover, the differences in both the combustion and gasification reactivities were found to increase with the heating rate (the charring condition).

Li, *et al.* (2015) investigated the effect of torrefaction on the conversion behaviour of the forest residue char. Both the raw and torrefied forest residue chars were prepared in a drop tube reactor at 1200 ˚C with a heating rate greater than 10^4 ˚C/s. The authors employed a tracer method to study the conversion of carbon, oxygen, and hydrogen in forest residue char and torrefied forest residue char, after oxidation and gasification reactions in the drop tube reactor. The reactivity of the torrefied forest residue char was found to be lower than that of the raw forest residue char. The authors also found that the volume-mean size of the torrefied forest residue char particles is considerably larger than that of the raw forest residue char. This could be partially attributed to more intensive fragmentation of the raw forest residue char particles during the pyrolysis process, resulting from the higher volatile content. In addition, the oxygen to carbon ratio (O/C ratio) in the torrefied forest residue char was found to be higher than that in the raw forest residue char. Both the lower O/C ratio and larger char particle size could result in lower reactivity for the torrefied forest residue char, compared with the raw forest residue char.

Karlstrom, *et al.* (2015) studied the gasification reactivities of the single char particles which were prepared in situ from the pellets of the raw and torrefied pine shell, olive stones and straw. The initial diameters of the pellets were 8 mm, while the heights were ~ 3 mm. The initial carbon amounts of the char particles and the carbon conversion of the char particles were both estimated from the measured CO concentration during the char gasification process. It was found that the char reactivity of the torrefied olive stones was lower than that of the raw olive stones. However, the torrefied straw char was found to have higher gasification reactivity than the raw straw char, while both the raw and torrefied pine shell chars had similar gasification reactivities.

According to the literature, the influence of torrefaction on the bio-char reactivity strongly depends on the biomass species and pyrolysis conditions. However, little work has been done to further explore the reason why torrefaction can influence the bio-char reactivity.

2.5.2 Char characteristics

Char reactivity strongly depends on the char characteristics, i.e., the char specific surface area (SSA), char carbonaceous structure and the catalytic effect of the inorganic matter. Therefore, the investigation of the influence of torrefaction on the char characteristics would help to better understand the influence of torrefaction on the char gasification reactivity.

2.5.2.1 Char specific surface area

The BET surface areas (obtained by employing N_2 adsorption) of both the raw and torrefied (290 ˚C and 30 mins) willow chars produced in a CDS 2000 Pyrorobe at 1000 ˚C and 1000 ˚C/s were analysed and compared with each other (Jones, *et al.*, 2012). It was found that the torrefied willow char had a higher BET surface area than

the raw willow char. However, when the same raw and torrefied (290 ˚C and 30 mins) willow samples were pyrolyzed in a drop tube furnace at 1100 ˚C, the torrefied willow char was found to have a lower BET surface area than the raw willow char (McNamee, *et al.*, 2015). The BET surface area of both raw and torrefied rice husk chars prepared at 550 ˚C were investigated (Zhang, *et al.*, 2016b). The torrefied rice husk char was found to have a lower BET surface area than the raw rice husk char. Therefore, the influence of torrefaction on the BET surface area of char is strongly dependent on the torrefaction and pyrolysis conditions, as well as the biomass species. However, the method of N_2 adsorption at 77 K for BET surface area measurement is not very suitable for use to evaluate the microporosity (< 0.7 nm) due to the existence of diffusional problems. In addition, the specific surface areas of micro-pores in both raw and torrefied biomass chars need to be studied, since the surface area of the micro-pores could make up a significant or even a majority part of the char materials (Kajitani, *et al.*, 2002). Therefore, a suitable method is required to characterize the surface area of micro-pores in char.

To overcome the diffusion problem in the micro-pores for the N_2 adsorption at 77 K, the method of CO_2 adsorption at 273 K has been investigated (Toda, *et al.*, 1971; Wahby, *et al.*, 2012). Due to the larger kinetic energy of the gas molecules resulting from the higher adsorption temperature (in contrast with N_2 adsorption at 77 K), the CO_2 molecules can enter narrow pores (< 0.7 nm) without the significant diffusional problems mentioned above. In that sense, CO_2 adsorption allows one to obtain the surface area of the micro-pores (Lozano-Castelló, *et al.*, 2004). Therefore, the investigation of the influence of torrefaction on the surface area of micro-pores achieved by CO_2 adsorption at 273 K is very important. However, little relevant work has been reported.

2.5.2.2 Carbonaceous structure of char

Raman spectroscopy has been extensively used to characterise the structure of carbonaceous materials since Tuinstra and Koenig, in 1970, first correlated Raman bands to structural parameters measured from XRD for polycrystalline graphite (Tuinstra & Koenig, 1970; Li, *et al.*, 2006). Due to its sensitivity to both the crystalline and amorphous structures, Raman spectroscopy has also been widely used to characterize the coal and biomass char structure, which can be correlated to the char reactivity (Senneca, *et al.*, 1998; Lu, *et al.*, 2002; Sheng, 2007; Zaida, *et al.*, 2007; Okumura, *et al.*, 2009; Asadullah, *et al.*, 2010; Tay & Li, 2010; Wang, *et al.*, 2014; Vallejos-Burgos, *et al.*, 2016). Generally, the char samples exhibit two strong peaks at the D-band (1300−1400 cm^{-1}) and G-band (1550−1600 cm^{-1}), as shown in Figure 2.3. Traditionally, the D-band is associated with the disordered structure while the G-band is associated with the graphite E_{2g}^2 band. Due to a high proportion of amorphous structures in the char samples, the D- and G-bands are usually broad and overlapped thus hiding more structural information in the 'overlap' (Li, *et al.*, 2006).

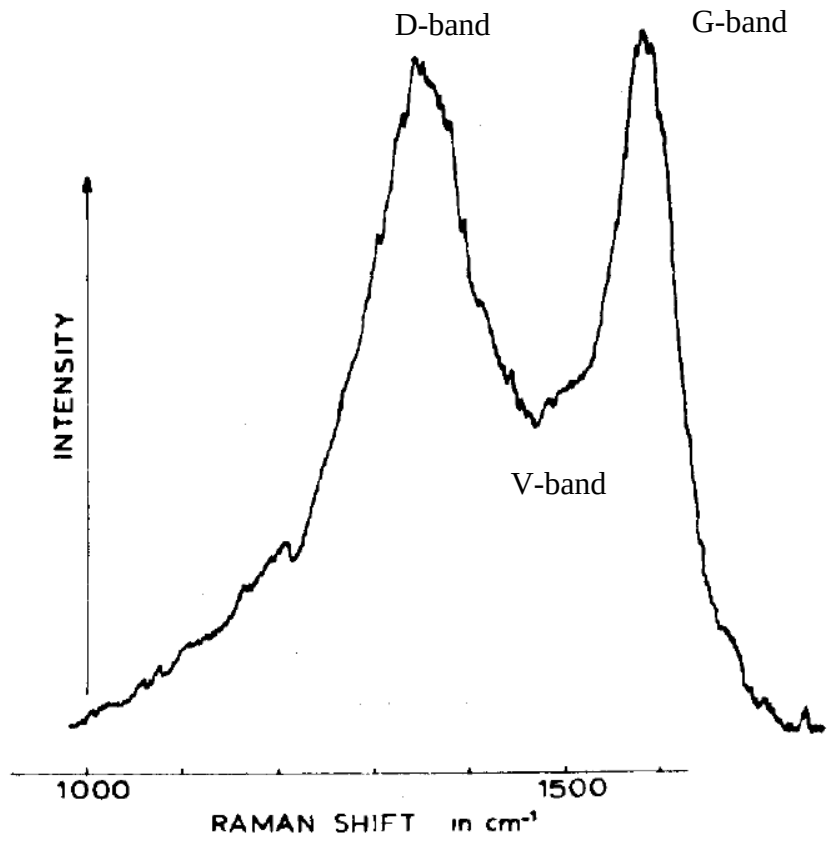

Figure 2.3 Raman shift of activated charcoal (Tuinstra & Koenig, 1970).

To explore the detailed information hidden in the overlapped D- and G-bands for the highly disordered carbon materials, the Raman spectra has been deconvolved using some specific bands in the studied range of Raman shift. Five specific bands, i.e., the G-, D1-, D2-, D3- and D4-bands, were used to deconvolve the Raman spectra of lignite char (Sheng, 2007; Zhu & Sheng, 2010). The G-band (~ 1580 cm^{-1}) was associated with the graphite E_{2g}^2 band, as discussed above. In addition, the D1-band (~ 1350 cm^{-1}) and D2-band (~ 1620 cm^{-1}) were associated with graphene layer defects while the D3-band (~ 1530 cm^{-1}) and D4-band (~ 1150 cm^{-1}) were suggested to originate from a poorly organized structure (such as amorphous carbon). Good linear correlation was found between the area ratio of the D1-band to the G-band and the reactivity for the lignite char prepared at a lower temperature (< 800 ˚C). In addition, for the lignite char

prepared at a higher temperature (> 800 ˚C), good linear correlation was found between the reactivity and the ratio of the G-band area to the integrated area under the whole Raman spectra (800−2000 cm^{-1}). The authors also suggested that the variation of catalytic activity for the inorganic matter was another important factor influencing the combustion reactivity of the char, especially the char prepared at lower temperatures (< 800 ˚C).

Li, *et al.* (2006) employed ten bands to fit the Raman spectra curve (achieved by using a 1064 cm^{-1} excitation laser) of the char while only six of them were main bands (i.e., G-, G_R-,V_L-,V_R-, D- and S-bands) for all the char samples prepared from Victorian brown coal. The authors suggested that the G-band (~ 1590 cm^{-1}) here could be mainly associated with the aromatic ring rather than with the graphite E_{2g}^2 band since no convincing signs for the presence of graphite crystallite structure in their studied chars were observed, according the XRD spectra. In addition, the D-band (~ 1300 cm^{-1}) was suggested as representing medium-to-large sized (≥ 6) aromatic ring systems. Moreover, the G_R-, V_L- and V_R-bands at 1540 cm^{-1}, 1465 cm^{-1} and 1380 cm^{-1}, respectively, may represent the aromatic ring system typically found in amorphous carbon materials. Furthermore, the S-band at 1185 cm^{-1} can represent the sp^2-sp^3 (hybrid orbitals) carbonaceous structures in the studied low rank coal chars. The total area of the Raman spectra (800−1800 cm^{-1}) was found to increase with an increasing pyrolysis temperature, mainly due to the loss of O-containing functional groups and variations in the relative concentrations of small and large aromatic ring systems. In addition, the ratio of the D-band area to the total area of the G_R-, V_L- and V_R-bands was found to increase with an increasing pyrolysis temperature, especially from 500 to 800 ˚C, for the studied chars. The increase in this ratio ($A_D/A_{(Gr+Vl+Vr)}$) indicates an increase in the ratio of large to small aromatic ring systems. Wang, *et al.* (2014) have investigated the influence of

the chemical structure determined using Raman spectroscopy on the intrinsic reactivity of a lignite char and a bituminous coal char. The authors suggested that the proportion of the smaller aromatic ring structures (indicated by the area ratio of $A_D/A_{(Gr+Vl+Vr)}$ discussed above) is an important factor influencing the intrinsic reactivity of the bituminous chars. However, for the lignite chars, the variation in the proportion of smaller aromatic ring structures could not be related to the variation in the intrinsic reactivity very well. Therefore, the authors suggested that there were other factors significantly influencing the intrinsic reactivity of the lignite chars.

Okumura, *et al.* (2009) employed the intensity ratio of the V-band (lies at the valley with a shift of about 1500 cm^{-1}, as shown in Figure 2.3) to the G-band (I_V/I_G) to indicate the degree of amorphousness of the wood char. With the increasing of the intensity ratio of I_V/I_G, the degree of amorphousness of the wood char was suggested to increase, thus leading to an increase in the char reactivity.

The carbonaceous structure analysed by using Raman spectroscopy has been found to be an important factor which can affect the char reactivity significantly. However, little work has been reported on the influence of torrefaction on the biomass char carbonaceous structure characterized by using Raman spectroscopy.

2.5.2.3 Catalytic effect of inorganic compounds

The variation in the char carbonaceous structure could not correlate to the char reactivity very well in some cases, especially for the chars prepared from biomass and the low rank coal with high ash, as discussed above (Sheng, 2007; Zhu & Sheng, 2010; Wang*, et al.*, 2014). Therefore, the catalytic effect of inorganic matter was suggested as playing a key role in influencing the char reactivity. Alkali (K and Na), alkaline earth (Ca and Mg), and transition (Fe) metals are widely found in both biomass and coal, and

are found to have a significant catalytic effect on the char gasification reactions (McKee, 1983; Suzuki, *et al.*, 1992; Brown, *et al.*, 2000; Li, *et al.*, 2000; Struis, *et al.*, 2002; Huang, *et al.*, 2009; Suzuki, *et al.*, 2011; Lahijani, *et al.*, 2013). To investigate the effect of these metals on the char reactivity, the contents of these metals in the chars were changed via acid-washing (metals removing from raw fuel or char) (Samaras, *et al.*, 1996; Kajita, *et al.*, 2010; Duman, *et al.*, 2014) or metal catalyst loading (metals adding to raw fuel or char) (Huang, *et al.*, 2009; Lahijani, *et al.*, 2013; Popa, *et al.*, 2013; Li, *et al.*, 2014b; Ding, *et al.*, 2015; Perander, *et al.*, 2015).

It is well known that inorganic matter can undergo transformation and release during thermal conversion (e.g., pyrolysis and gasification) processes, thus influencing the char gasification reactivity. During the heat treatment of the mixture of ash-free coal and K_2CO_3 in N_2 atmosphere, K_2CO_3 can react with carbon in the ash-free coal, with the release of CO at temperatures ranging from 700 to 950 ˚C (Kopyscinski, *et al.*, 2014). Due to the reduction of K_2CO_3, a more active potassium-carbon intermediate was formed on the char surface, resulting in higher char gasification reactivity. However, potassium started to release from the carbon surface at temperatures above 800 ˚C, thus reducing the char reactivity. On the other hand, the presence of CO_2 can inhibit the reduction of K_2CO_3, resulting in lower char gasification reactivity.

Na loaded into the Loy Yang brown coal substrate as sodium carboxylates was found to undergo significant transformation and release during steam gasification at 800 and 900 ˚C (Li & Li, 2006). The authors suggested that the volatilisation of Na at the initial stage of gasification/devolatilization was attributed to the volatile-char interactions, similar to those in the absence of steam. However, the release of Na at the later stages of gasification could be attributed to the physical entrainment of Na-containing species (e.g., Na_2CO_3 or Na_2O). All these losses of Na could influence the char gasification

reactivity significantly. The Na loaded into the Loy Yang brown coal substrate as NaCl was found to have very different catalytic effect on the char reactivity from the Na loaded as sodium carboxylates (Quyn, *et al.*, 2003). The authors suggested that the retention of Cl in the char prepared from NaCl-loaded coal could significantly influence the char reactivity. Cl can be at least partly released (as HCl) during low temperature pyrolysis (e.g., 500 ˚C) thus allowing the sodium to be catalytically active in the char. However, Cl in the chars prepared at high temperatures tended to combine with Na in the char to form NaCl which is less catalytically active. The transformation and release of the inorganic matter (especially Na, K, Ca and Mg) were found to strongly depend on the chemical/physical forms of the carbonaceous materials, as well as the thermal treatment conditions, e.g. the heating rate for the pyrolysis, pyrolysis and gasification temperatures, total pressure and partial pressure of reaction gas (Li, *et al.*, 2000; Quyn, *et al.*, 2003; Bayarsaikhan, *et al.*, 2005; Keown, *et al.*, 2005; Lane, *et al.*, 2015; Mi, *et al.*, 2015). In addition, the monovalent species (Na and K) were found to be usually volatilised to a much larger extent than the divalent species (Ca, Mg and Fe) (Li, *et al.*, 2000). However, little work on the transformation and release of inorganic matter (especially Na and K) during the pyrolysis and gasification processes has been reported for torrefied biomass.

To date, little study has been reported on the char carbonaceous structure and catalytic effect of inorganic matter for torrefied biomass chars. In addition, the specific surface area of the micro-pores in the torrefied biomass char still needs to be studied, since the surface area of micro-pores could make up a significant or even a majority part of the char materials.

2.6 Implications for current study

According to the literature review presented above, substantial contributions have been made on the solid fuels to FTL fuels process to improve their economic, energetic and environmental performance. The coal to FTL fuels processes have been widely studied and even applied due to the relatively low cost and plentiful reserves of coal. However, the CO_2 emissions of the coal to FTL fuels processes impede their application. Both the concentrated solar thermal energy and biomass were proposed to partially or totally substitute coal for the gasification process, thus reducing the greenhouse gas emissions from the FTL fuels production process. In addition, the integration of concentrated solar thermal energy also has the potential to increase the output per unit of feedstock by saving feedstock in the gasification process.

On the other hand, the continuous and steady operation desired by the FTL fuels production process and the transient nature of the solar resource lead to a challenge associated with process integration. Energy storage and hybridization are proposed to address this challenge. However, of the recently proposed solar hybridized coal and/or biomass to FT liquid fuels systems, the need for the storage of syngas, the need for expensive air separation, the need for pure oxygen storage or the need for high temperature molten salt storage have impeded their application. Therefore, new solar hybridization concepts need to be proposed for the solid fuels to FTL fuels process to address these issues by providing continuous and steady syngas flow and energy storage system with good techno-economic feasibility.

In addition, the utilization of biomass in the gasification process is limited by some biomass properties, e.g. high oxygen content, high moisture content, low calorific value, hygroscopic nature and low density, which can result in low conversion efficiency and

difficulties in collection, grinding, transportation and storage. As a mild thermal pre-treatment (200−300 ˚C) technology, torrefaction has been proven to address these issues. In addition, it has been found that torrefaction can affect the char reactivity which will further influence the design and operation of the gasification process. This effect strongly depends on the operating conditions and biomass species. To better understand the influence of torrefaction on char reactivity, investigation needs to be undertaken on the effects of torrefaction on the char characteristics which have been proven to have a significant effect on the char reactivity. However, little work has been report on this.

2.7 Objectives of the present study

The aims of the present thesis are to evaluate the annual performance of the solar hybridized coal and/or biomass to FTL fuels processes with novel configurations and to better understand the influence of torrefaction on the bio-char gasification reactivity.

To achieve the aims, the following detailed objectives need to be obtained in the present thesis:

1. To assess the annual averaged performance improvement of the proposed novel solar hybridized FTL fuels production process via SDFB gasification of lignite compared with an equivalent non-solar FTL fuels production process.
2. To evaluate the sensitivity of annual performance of the proposed solar hybridized lignite to FTL fuels system to the solar multiple, the storage capacity, the char gasification conversion, and the quality of the solar resource.
3. To assess the influence of the proposed new approaches (i.e., the addition of char separation, the co-gasification of biomass with coal, the incorporation of carbon capture with sequestration and the use of FT reactor tail-gas recycle) on

the performance of the solar hybridized FTL fuels production system via an SDFB gasifier.

4. To provide the difference in gasification reactivity between the raw and torrefied biomass chars and the sensitivity of this difference to pyrolysis temperature (800−1100 ˚C) and biomass species (wood, grape marc and macroalgae).
5. To better understand the influence of torrefaction on the char gasification reactivity via investigating the char characteristics (i.e., specific surface areas, carbonaceous structures and contents of the catalytic inorganic matter).

CHAPTER 3

PERFORMANCE ASSESSMENT OF FISCHER−TROPSCH LIQUID FUELS PRODUCTION BY SOLAR HYBRIDIZED DUAL FLUIDIZED BED GASIFICATION OF LIGNITE

Peijun Guo[*,†,‡], Philip J. van Eyk[†,‡], Woei L. Saw[†,‡], Peter J. Ashman[†,‡],

Graham J. Nathan[†,§] and Ellen B. Stechel[¤]

[†]*Centre for Energy Technology,* [‡]*School of Chemical Engineering and* [§]*School of Mechanical Engineering, The University of Adelaide, SA 5005, Australia*
[¤]*Light Works, Arizona State University, Tempe, AZ, USA*

Energy & Fuels 29 (2015) 2738-2751

Statement of Authorship

Title of Paper	Performance Assessment of Fischer–Tropsch Liquid Fuels Production by Solar Hybridized Dual Fluidized Bed Gasification of Lignite
Publication Status	☑ Published ☐ Accepted for Publication ☐ Submitted for Publication ☐ Unpublished and Unsubmitted work written in manuscript style
Publication Details	Guo, P., van Eyk, P. J., Saw, W. L., Ashman, P. J., Nathan, G. J., and Stechel, E. B. (2015). Performance Assessment of Fischer–Tropsch Liquid Fuels Production by Solar Hybridized Dual Fluidized Bed Gasification of Lignite. Energy & Fuels, 29(4), 2738-2751.

Principal Author

Name of Principal Author (Candidate)	Peijun Guo
Contribution to the Paper	Performed the system modelling, interpreted results, wrote manuscript and acted as corresponding author.
Overall percentage (%)	60%
Certification:	This paper reports on original research I conducted during the period of my Higher Degree by Research candidature and is not subject to any obligations or contractual agreements with a third party that would constrain its inclusion in this thesis. I am the primary author of this paper.
Signature	Date: 6/10/2016

Co-Author Contributions

By signing the Statement of Authorship, each author certifies that:

i. the candidate's stated contribution to the publication is accurate (as detailed above);

ii. permission is granted for the candidate in include the publication in the thesis; and

iii. the sum of all co-author contributions is equal to 100% less the candidate's stated contribution.

Name of Co-Author	Philip J. van Eyk
Contribution to the Paper	Supervised development of work, helped in data interpretation and manuscript evaluation.
Signature	Date: 6/10/2016
Name of Co-Author	Woei L. Saw
Contribution to the Paper	Supervised development of work, helped in data interpretation and manuscript evaluation.
Signature	Date: 6/10/2016
Name of Co-Author	Peter J. Ashman
Contribution to the Paper	Supervised development of work, helped in data interpretation and manuscript evaluation.
Signature	Date: 7/10/16
Name of Co-Author	Graham J. Nathan
Contribution to the Paper	Supervised development of work, helped in data interpretation and manuscript evaluation.
Signature	Date: 6/10/2016
Name of Co-Author	Ellen B. Stechel
Contribution to the Paper	Supervised development of work, helped in data interpretation and manuscript evaluation.
Signature	Date: 6/10/2016

energy&fuels

Article

pubs.acs.org/EF

Performance Assessment of Fischer–Tropsch Liquid Fuels Production by Solar Hybridized Dual Fluidized Bed Gasification of Lignite

Peijun Guo,*[,†,‡] Philip J. van Eyk,[†,‡] Woei L. Saw,[†,‡] Peter J. Ashman,[†,‡] Graham J. Nathan,[†,§] and Ellen B. Stechel[∥]

[†]Centre for Energy Technology, [‡]School of Chemical Engineering and [§]School of Mechanical Engineering, The University of Adelaide, Adelaide, South Australia 5005, Australia

[∥]Light Works, Arizona State University, Tempe, Arizona, United States

ABSTRACT: A novel solar hybridized dual fluidized bed (DFB) gasification process for Fischer–Tropsch liquid (FTL) fuels production is proposed and investigated here for the case with lignite as the fuel, although it is also applicable to biomass. The concept offers sensible thermal storage of bed material, the use of inert particles in the solar receiver to avoid the need for sealing, and a process that delivers a constant production rate and quality of syngas despite solar variability. This solar hybridized coal-to-liquids (SCTL) process is simulated using a pseudodynamic model that assumes steady state operation at each time step for a one-year, hourly integrated solar insolation time series. The annual energetic and environmental performance of this SCTL process is investigated as a function of the solar multiple (i.e., the heliostat field area relative to that required to meet the demand of the DFB gasifier at the point of peak solar thermal output), bed material storage capacity, the assumed char conversion in the bubbling fluidized bed gasifier (BFBG), and the solar resource. This revealed that solar energy can be stored in the bed material to increase both the solar share and output while decreasing the CO_2 emissions, with a commensurate increase in the heliostat field area. For a solar multiple of 3 and bed material storage capacity of 16 h, the annual solar share is 21.8% and the annually averaged utilization factor of the heliostat field is 40.8%, assuming that the char conversion in the BFBG is 100%. However, the solar share is also found to be strongly dependent on the char conversion in the BFBG, so that the solar share decreases to zero as the conversion is decreased to 57%. The sensitivity of the SCTL performance to the quality of the solar resource is also reported.

1. INTRODUCTION

The development of alternative fuels is driven by the limited availability of crude oil, energy-supply security concerns, and the projected long-term demand for transport liquid fuels.[1] The gasification of solid feedstocks together with the subsequent Fischer–Tropsch (FT) processing of the syngas is considered to be one of the promising classes of technology to meet this need due to its capacity to process a variety of feedstocks (e.g., coal, biomass, and petroleum coke), the high quality of the FT product (being free of sulfur, nitrogen, and other contaminants typically found in petroleum products), and its compatibility with the requirements of current vehicles.[2] The plentiful reserves of coal and their low cost has also led to increased international interest in the production of FT liquid (FTL) fuels via gasification of coal.[3−6] However, the high greenhouse gas (GHG) emissions from coal-to-liquids (CTL) processes are a major barrier to their implementation with the mine-to-tank (MTT) GHG emissions from such systems being typically more than 100% higher than diesel production from tar sands while more than 200% higher than diesel production from conventional mineral crude.[7−9] To mitigate these emissions, both carbon capture and storage (CCS) and the cogasification of biomass with coal are being widely studied.[3,10−12] However, the CO_2 compression required by CCS will impose a parasitic impact on process productivity. The steady and sustainable supply of biomass limits the applicability of biomass blending, especially for large scale utilization, and biomass is also a more expensive feedstock.[3,12] In this context, interest is growing in a further potential option to reduce the CO_2 emissions of CTL processing through the introduction of concentrated solar thermal (CST) into the gasification process.[8,13−15] Nevertheless, this topic has received relatively little attention so that there is significant potential to improve on the concepts proposed previously. Hence, the overall objective of the current investigation is to assess the performance of a novel configuration of solar fuel to liquid process that has not been previously been reported.

Solar gasification is a process in which CST provides the heat to drive the endothermic gasification reactions, which displaces the partial combustion of the feedstock in conventional nonsolar gasification. Hence, solar gasification has the potential both to reduce the CO_2 emissions from the gasification process and to increase the raw syngas output from the gasifier per unit of feedstock.[14] Solar gasification reactors have been widely studied over the past 30 years,[16] with directly irradiated packed bed solar gasifiers for both coal and biomass among the first types to be assessed.[17,18] The more recent of these reactors employ a SiC-coated graphite plate between the window and

Received: January 3, 2015
Revised: March 18, 2015
Published: March 23, 2015

DOI: 10.1021/acs.energyfuels.5b00007
Energy Fuels 2015, 29, 2738−2751

reaction zone to avoid direct contact between the reactants and the window, at the expense of a lower heat transfer rate.[19,20] Packed bed gasifiers are relatively simple, robust, and cost-effective because they can tolerate a wide range of feedstock sizes and forms and do not require excess steam flows. Nevertheless, for feedstock with a significant ash content, their performance is limited by the buildup of ash on the top of the bed that inhibits heat and mass transfer through the bed and, in turn, the reaction rate and syngas productivity.[14] Entrained flow gasifiers perform well in heat and mass transfer, which increases significantly the syngas throughput, but imposes a strict requirement on the feedstock particle size due to the short residence time within the reactor. As a third alternative, fluidized bed gasifiers offer the potential to resolve some of the heat and mass transfer limitations of the packed bed configurations and particle size sensitivity of entrained flow gasifiers. However, those employing direct irradiation to the bed, such as transparent glass tubes[18,21,22] and top windowed devices,[23,24] are also limited by contamination of the glass tube or window, while those with indirect irradiation are limited by poor heat transfer. Moreover, the single reactor solar hybridized gasifier also requires an air separation unit (ASU) for pure oxygen during periods of low solar irradiation to maintain the continuous operation of the whole FTL plant. However, the unsteady solar input leads to the unsteady operation of the ASU and the need for syngas storage to accommodate the unsteady syngas output, both of which add significantly to costs. Hence, it is desirable to seek alternative concepts with potential to address these challenges for the solar hybridized coal-to-liquids (SCTL) process.

While many hybrid systems have been proposed for power generation,[25] much less attention has been paid to hybrid options for solar fuels production. Sudiro and Bertucco[15] investigated a solar hybridized coal-to-liquids (SCTL) process together with a process for solar natural gas reforming using a directly irradiated, pressurized reactor. They reported an output that is 67% higher per unit of feedstock than the conventional CTL case, together with CO_2 emissions per kilogram of liquid fuel that are comparable with that from a natural-gas-to-liquid process. However, the temperature and pressure in this directly irradiated solar gasifier are limited by the use of a window.[26−28] Kaniyal et al.[8] assessed with a pseudodynamic model an SCTL system with an atmospheric pressure vortex flow gasifier, together with the storage of pressurized syngas and O_2. The model assumed steady state operation at each time step of a one-year, hourly integrated solar insolation time series. They calculated the annual energetic output to increase by 21% and the annual MTT GHG emissions to decrease by 30% for the SCTL system relative to the equivalent conventional reference system. The integration of concentrated solar radiation into a coal plus natural gas-to-liquids process or into a coal plus biomass-to-liquids process was also estimated to improve the energetic productivity and CO_2 emissions of the whole process significantly.[13] However, this system requires gasification at temperatures of around 1200 °C, together with the need to store both O_2 and syngas. In addition, the gasifier they proposed also used a window. Davidson and co-workers have proposed an alternative solar hybrid allo-thermal gasifier in which the gasification of biomass is performed in a ternary eutectic blend of alkali carbonate molten salts.[29,30] High quality syngas (i.e., with low N_2 content) can be produced in conventional allo-thermal gasifiers without the need for an ASU because the heat of combustion is transferred indirectly to the gasification process. This system also offers the advantages of a lower reactor temperature of around 927 °C, of high conversion due to the catalytic influence of the salts, and of good potential for integration with thermal energy storage through the use of the salt. However, this gasification technology is less well established than is the dual bed technology proposed for hybridization here, while the operating temperature of the reactors in the two technologies are comparable. In addition, the storage of molten salt at these temperatures is yet to be demonstrated,[31−33] while sensible storage of solid bed material at high temperatures is further advanced,[34] although its potential merit is yet be assessed in such a hybrid system.

Solid particles are considered to be well suited for use as a solar thermal heat carrier and storage medium due to their potentially low cost and high operating temperature (>1000 °C).[34] In the present study, a dual fluidized bed (DFB) gasifier, another type of allo-thermal gasifier, is proposed to be hybridized with CST. In this system, the solid bed material is proposed to be used as heat carrier to transfer the heat required by the gasification process from the combustion process and/or the solar receiver. Hence, the solar hybridized DFB (SDFB) gasifier offers the potential to store the solar thermal heat in the bed material as sensible heat in an additional storage tank. Furthermore, a steady syngas output can be achieved by maintaining the constant temperature of the hot bed material to the gasification process through adjusting the additional fuel input to the combustion process according to the solar radiation variation. Lab and pilot scale conventional DFB gasifiers have demonstrated the production of a raw syngas with a H_2/CO ratio near the desired 2:1, as is required in the FT process, from coal gasification.[31,32,35,36] However, no previous investigation has been reported of a hybrid system between CST and a DFB gasifier.

To address the issues raised above, the first aim of the present paper is to compare the annual performance of an SCTL system including a SDFB gasifier with an equivalent nonsolar CTL process in a way that accounts for solar variability using long-term historical measurements of direct normal irradiation (DNI). The second aim is to assess the sensitivity of annual performance of the presently studied SCTL system to the solar multiple, the storage capacity, the char conversion in the bubbling fluidized bed gasifier (BFBG), and the quality of the solar resource.

2. METHODOLOGY

2.1. SDFB Gasification and SCTL Process Description. Figure 1 displays a schematic diagram of a DFB gasification system.[32,35,36] The solid fuel is fed to a bubbling fluidized bed gasifier (BFBG), where it is reacted with steam (the fluidizing agent for the BFBG) to produce syngas, a gaseous mixture comprising predominantly H_2 and CO. The heat required by the endothermic gasification reactions is provided by hot bed material transferred from a fast fluidized bed combustor (FFBC[37]), in which the cooled bed material from the BFBG is both heated and transported back to the BFBG by high velocity flue gases via a cyclone. The residual char within the bed material from BFBG is burned with air (the fluidizing agent for the FFBC) in the FFBC. Additional fuel is required in the FFBC when the residual char is insufficient to provide the necessary heat for the gasification process and overcome the heat losses.

Figure 1 also identifies four alternative locations into which the CST can potentially be introduced into a DFB gasification system, namely into the FFBC (location 1), into the hot bed material leaving the FFBC (location 2), into the BFBG (location 3), and into the bed material and char leaving the BFBG (location 4). The present study

DOI: 10.1021/acs.energyfuels.5b00007
Energy Fuels 2015, 29, 2738−2751

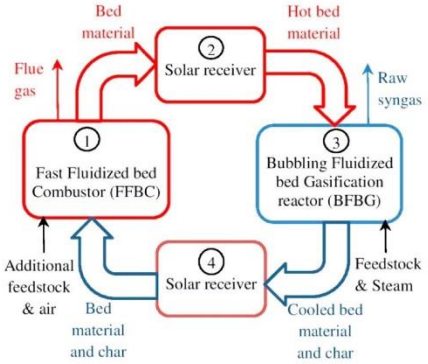

Figure 1. Diagram of the solar dual fluidized bed (DFB) gasification concept, together with four alternative locations (1, 2, 3, 4) into which the concentrated solar thermal (CST) energy can be introduced.

considers only location 2, in which the bed material from the FFBC is transported to the solar receiver on a solar tower and is directly heated by CST. This option is chosen because it requires little change to the DFB gasification system and because the heating of inert solid particles in a solar particle receiver is easier to achieve than the heating of reacting particles, which makes it the most likely to be realized in the near future.[16,38,39] Since the residual char is to be burned in the FFBC, the solar share of the SDFB gasification can be expected to increase with the conversion of solid feedstock to gas in the BFBG. Hence, low rank fuels, such as wood, bagasse, and brown coal (or lignite) are preferable to higher rank fuels, such as black coal, due to their high volatile content and char reactivity. In our study, lignite is chosen as the feedstock.

Figure 2 presents a simplified flowsheet of the proposed SCTL process. The SDFB gasifier was proposed to generate the raw syngas from the feedstock and the steam. A tar reformer was proposed to reform the tars in the raw syngas before sending the cleaned syngas for cooling and compression. A sour water−gas shift reactor (WGSR) was

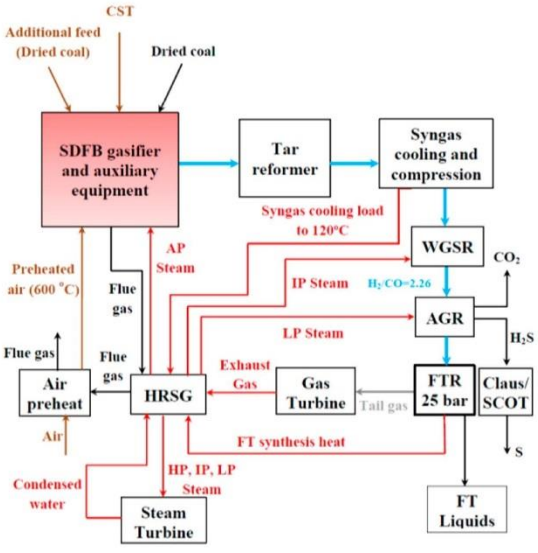

Figure 2. Simplified flowsheet of the proposed solar hybridized coal-to-liquids (SCTL) process with the proposed solar hybridized dual fluidized bed (SDFB) gasifier.

proposed to adjust the H_2:CO ratio of the pressurized syngas to a ratio of 2.26 to achieve a high conversion of CO in the FT reactor (FTR). An acid gas remover (AGR) was proposed for use downstream from the WGSR to remove both H_2S and CO_2 from the syngas before sending to the FTR. A gas turbine (GT) was proposed to utilize the tail gas from the FTR to generate electricity. A heat-recovery steam generator (HRSG) was proposed to recover heat and generate steam both for electricity generation (via the steam turbine) and to provide process steam.

Figure 3 presents the flowsheet describing the proposed SDFB gasifier and auxiliary equipment units. The bed material is used to

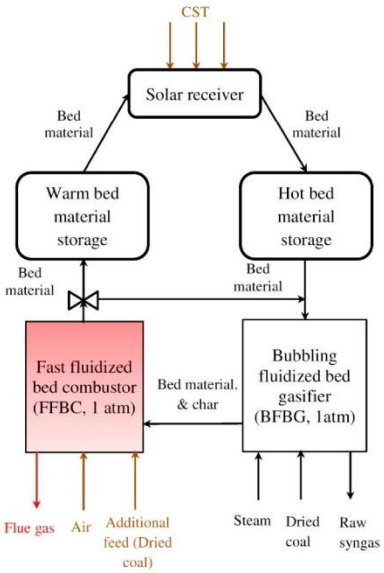

Figure 3. Flowsheet of the proposed SDFB gasifier with an integrated solar receiver and sensible heat storages.

transfer heat from the FFBC and/or solar receiver to the BFBG. Olivine sand was chosen for this because it has been widely used in lab/pilot/demonstration scale DFB gasifiers to achieve low tar content in the raw syngas and to promote the water−gas shift reaction in the gasifier toward the equilibrium state.[35,40,41] The solar receiver was modeled based on the directly irradiated, tower-mounted, falling particle cavity receiver concept because it is the system that has been best developed to date.[39] Intensive studies have been carried out on falling particle receivers since the 1980s, including one set of on-sun tests of a simple falling particle receiver at power levels up to 2.5 MW_{th}. In contrast, the investigations of other particle receivers are mostly lab scale.[38,39] Both the temperature and flow rate of the bed material to the BFBG were maintained at constant values to achieve steady production of syngas to the downstream processes. The warm and hot bed material storage units and the additional feed to the FFBC were proposed to accommodate some of the transience of the solar radiation.

Figure 4 presents the operational strategy for the SDFB system in the form of a logic control diagram. Here, the symbol Φ is defined to be the ratio of net useful solar energy absorbed by the bed material assuming that no solar spillage occurs ($\dot{Q}_{net,sol,no\text{-}spill}$), relative to the heat required by the DFB gasifier ($\dot{Q}_{DFB}$, constant) as shown in eqs 1 and 2.

$$\Phi = \max\left(\frac{\dot{Q}_{net,sol,no\text{-}spill}}{\dot{Q}_{DFB}}, 0\right) \quad (1)$$

DOI: 10.1021/acs.energyfuels.5b00007
Energy Fuels 2015, 29, 2738−2751

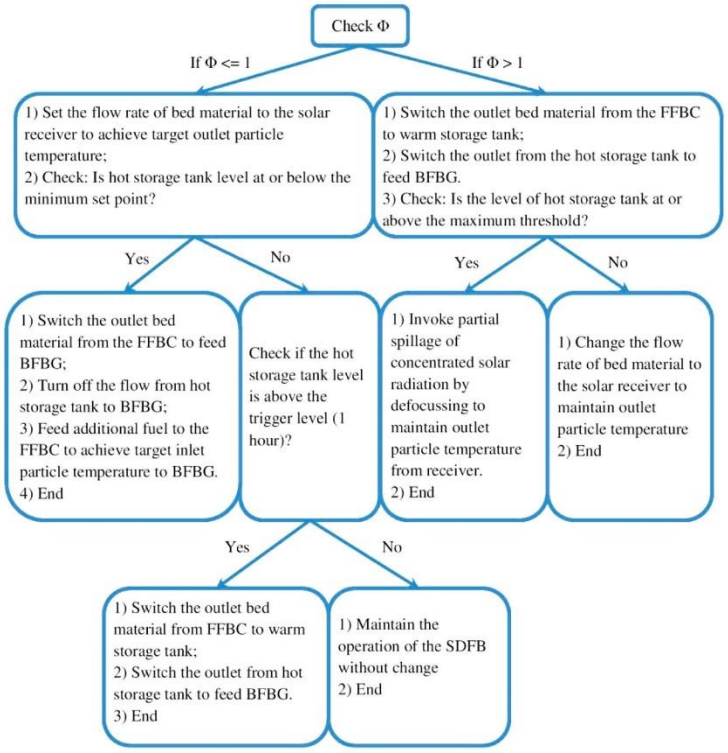

Figure 4. Logic control diagram for the SDFB gasification process used to accommodate the variation in solar radiation.

$$\dot{Q}_{\text{net,sol,no-spill}} = (I_{\text{DN}}A_{\text{coll}}\eta_{\text{opt}} - \sigma T_{\text{rec}}^4 A_{\text{aper}} - \eta_{\text{o,l,rec}} I_{\text{DN}}A_{\text{coll}}\eta_{\text{opt}})\eta_{\text{stg}} = I_{\text{DN}}A_{\text{coll}}\left(1 - \frac{\sigma T_{\text{rec}}^4}{\eta_{\text{opt}} C I_{\text{DN}}} - \eta_{\text{o,l,rec}}\right)\eta_{\text{stg}}\eta_{\text{opt}} \quad (2)$$

The value of Φ is defined to be 0 for Φ < 0, which occurs when the solar thermal input to the receiver from the heliostats is lower than the heat losses from the receiver. The effective absorptance and emittance of the solar cavity receiver are both assumed to be unity,[14] A_{coll} is the heliostat collector area, A_{aper} is the aperture area of the solar receiver, I_{DN} is the direct normal solar insolation, σ is the Stefan−Boltzmann constant (5.6705×10^{-8} W/(m^{2}K^4)), T_{rec} is the temperature of the solar receiver, C is the assumed concentration ratio ($C = A_{\text{coll}}/A_{\text{aper}} = 2000$), $\eta_{\text{o,l,rec}}$ is the proportion of other heat losses including conduction and convection losses from the receiver other than reradiation ($\sigma T_{\text{rec}}^4 A_{\text{aper}}$) and optical losses and was assumed to be 10%,[39,42] η_{stg} is the thermal efficiency of the storage unit and was assumed to be 95%,[34] and η_{opt} is the optical efficiency of the solar system which includes the solar receiver and heliostat field, defined in eq 3:[8,43,44]

$$\eta_{\text{opt}} = \eta_{\text{ref,coll}}\eta_{\text{sb}}\eta_{\text{itc}}\eta_{\text{aa}}\eta_{\text{ref,CPC}}\eta_{\text{cos}} \quad (3)$$

where $\eta_{\text{ref,coll}}$ is the heliostat collector reflection efficiency, assumed to be 88%,[45] η_{sb} is the shadowing and blocking efficiency of the heliostat field, assumed to be 93.3%,[45] η_{itc} is the interception efficiency, assumed to be 99.2%,[45] η_{aa} is the atmospheric attenuation, assumed to be 95%,[45] and $\eta_{\text{ref,CPC}}$ is the reflection efficiency of the compound parabolic concentrator (CPC), assumed to be 95%.[46] In addition, η_{cos} is the cosine efficiency of the heliostat field, which is calculated as a function of solar time for one particular position as representative of the entire field.[47,48] Because η_{cos} depends more strongly on the time and site than on A_{coll}, it was further assumed to be independent of A_{coll}. On this basis, the values assumed for the other efficiencies in eqs 3 and 4 do not influence the solar multiple (SM), which is defined as the ratio of the heliostat field area relative to that required to meet the demand of the DFB gasifier at the point of peak solar thermal output.

$$\text{SM} = \frac{A_{\text{coll}}}{A_{\text{coll}}^{\text{DFB}}} = \frac{(\dot{Q}_{\text{net,sol,no-spill}})_{\text{ann,peak}} \Big/ \left((\eta_{\text{opt}}I_{\text{DN}})_{\text{ann,peak}}\left(1 - \frac{\sigma T_{\text{rec}}^4}{(\eta_{\text{opt}}I_{\text{DN}})_{\text{peak}}C} - \eta_{\text{o,l,rec}}\right)\eta_{\text{stg}}\right)}{\dot{Q}_{\text{DFB}} \Big/ \left((\eta_{\text{opt}}I_{\text{DN}})_{\text{ann,peak}}\left(1 - \frac{\sigma T_{\text{rec}}^4}{(\eta_{\text{opt}}I_{\text{DN}})_{\text{peak}}C} - \eta_{\text{o,l,rec}}\right)\eta_{\text{stg}}\right)} = \frac{(\dot{Q}_{\text{net,sol,no-spill}})_{\text{ann,peak}}}{\dot{Q}_{\text{DFB}}} \quad (4)$$

DOI: 10.1021/acs.energyfuels.5b00007
Energy Fuels 2015, 29, 2738−2751

Here, A_{coll}^{DFB} is the required heliostat field area which can generate net annual peak solar thermal heat equal to the heat required by the DFB gasifier.

Figure 4 also shows the proposed control strategy in which the heliostats are to be defocused to spill excess energy when the thermal storage facility is full. Therefore, eq 5 can be used to define the net useful solar energy absorbed by the bed material ($\dot{Q}_{net,sol}$) at each time step.

$$\dot{Q}_{net,sol} = \dot{Q}_{net,sol,no\text{-}spill} \times U_{coll} \quad (5)$$

Here, U_{coll} is the utilization factor of the heliostat collector, as defined in eq 6.

$$U_{coll} = \begin{cases} 1 & \text{if } 0 < \Phi \le 1 \\ 1 & \text{if } \Phi > 1 \text{ and hot storage unit is not full} \\ \dfrac{\dot{Q}_{DFB}}{\dot{Q}_{net,sol,no\text{-}spill}} & \text{if } \Phi > 1 \text{ and hot storage unit is full} \\ 0 & \text{if } \Phi = 0 \end{cases} \quad (6)$$

2.2. Process Model. *2.2.1. SCTL Process Model Unit Designs.* The SCTL process is assumed to be operated at a steady-state for each 1 h time step in a one-year time series. A model for this steady-state operation was developed in Aspen Plus V7.1 for each time step using the submodels and parameters described below. Thermodynamic properties for components other than steam were estimated using the Peng–Robinson equation of state with Boston–Mathias modification (PR-BM), whereas STEAM TA was used for the steam properties.

Gasifier Model. The DFB gasifier model was validated using Rhenish lignite from Germany as the feedstock because the experimental data of Kern et al.[35] is available with this fuel for a DFB gasifier. The properties of this fuel are shown in Table 1, together

Table 1. Proximate and Ultimate Analysis of Rhenish Lignite[35] and Montana Lignite[56]

proximate analysis (wt %)	Rhenish lignite	Montana lignite
fixed carbon	35.8	46.4
volatile matter	42.2	36.9
moisture	18.6	6.8
ash	3.4	9.9
ultimate analysis (wt % dry)	Rhenish lignite	Montana lignite
C	65.5	63.6
H	3.8	4.1
O	25.2	19.5
N	0.8	2
Cl	0.1	0
S	0.4	1.3
ash	4.2	10.6

with the properties of Montana lignite, from the northern part of the United States of America, which was chosen as the feedstock with which to assess the SCTL system because the experimental data of its properties are both available and suitable for the gasifier model. The solar DNI data were taken for Farmington, New Mexico, United States of America because this site combines a good solar source, good access to water as is necessary for the gasification, and a reasonable proximity to the main lignite mines in the northern parts of the United States of America. The other key parameters employed for the validation of the gasifier are shown in Table 2, also chosen to match the operating conditions reported by Kern et al.[35] Table 3 presents the parameters of the DFB gasifier chosen to assess the performance of the proposed SCTL system. The steam to carbon ratio (ψ_{S-C}) was fixed at 1.6 (kg/kg), which is between the two values used in the experiments, while the combustion reactor temperature (T_{FFBC}) was set to 950 °C to

Table 2. Parameters Chosen for the Validation of the DFB Gasifier Model to Match Previous Experimental Data[35]

parameter	value	parameter	value
ψ_{S-C} (kg/kg)	1.3/2.1	carbon conversion in BFBG	66%/62%
P_{FFBC} (atm)	1	P_{BFBG} (atm)	1
T_{FFBC} (°C)	920	T_{BFBG} (°C)	850

Table 3. Parameters Chosen with Which to Assess the Performance of the Proposed SCTL System with the DFB Gasifier

parameter	value	parameter	value
ψ_{S-C} (kg/kg)	1.6	char conversion in BFBG	57%~100%
P_{FFBC} (atm)	1	P_{BFBG} (atm)	1
T_{FFBC} (°C)	950	T_{BFBG} (°C)	850

achieve a moderate rate of bed material circulation and size of bed material storage. The Montana lignite was assumed to be dried to 2% (weight basis) moisture, and the pyrolysis process in the BFBG was assumed to be instantaneous. The extent of the gasification reactions was modeled by the char conversion within the BFBG rather than by carbon conversion, since the latter includes the conversion of carbon in both the pyrolysis and char gasification processes. The influence of conversion efficiency was then assessed by a sensitivity analysis.

To simplify the model, the DFB gasifier was separated into three zones as shown in Figure 5: a coal pyrolysis and char gasification zone, a secondary reaction zone, and a combustion zone.[49] The other assumptions and specifications of the model were as follows:

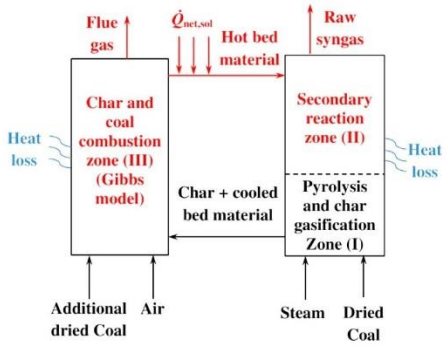

Figure 5. Simplified scheme of the model for the DFB gasifier.

i. No char or bed material was elutriated from either of the fluidized beds (FFBC and BFBG).

ii. Total heat loss from the walls was assumed to be 2% of the higher heating value (HHV) of the total input fuel to the DFB gasifier when operated under nonsolar conditions.[32] This heat loss was assumed not to change with the introduction of solar energy.

iii. The temperatures of the raw syngas, the residual char and the bed material from the BFBG were all assumed to be the same as that of the BFBG (T_{BFBG}), which is specified in Table 3. Similarly, the temperatures of the output flue gas and the hot bed material from the FFBC were assumed to be the same as the T_{FFBC}, which is specified in Table 3.

iv. The simulation of the pyrolysis process was based on the experimentally determined correlations reported by Goyal and Rehmat.[50] The pyrolysis products include gas (CO_2, CO, CH_4, H_2O, H_2, H_2S, HCL, N_2, NH_3, C_2H_4, C_2H_6, and C_3H_6), char ($C_{x1}H_{y1}O_{z1}N_{a1}S_{b1}Cl_{c1}$ (ash free basis)), and tar ($C_{x2}H_{y2}O_{z2}N_{a2}S_{b2}Cl_{c2}$).

v. The char gasification process was modeled according to eq 7, using the char conversion as a variable as described above:

DOI: 10.1021/acs.energyfuels.5b00007
Energy Fuels 2015, 29, 2738–2751

$$C_{x1}H_{y1}O_{z1}N_{a1}S_{b1}Cl_{c1} + (x1 - z1)H_2O \rightarrow x1CO + \left(x1 - z1 + \frac{y1 - 3a1 - 2b1 - c1}{2}\right)H_2 + a1NH_3 + b1H_2S + c1HCl \quad (7)$$

vi. The secondary reaction zone was assumed to comprise only the tar reforming reaction (eq 8) and the water−gas shift reaction (eq 9). Although the dry reforming of tar can also occur here, the calculated production of syngas from this zone will not change because of the assumption that the water−gas shift reaction reaches equilibrium.[35] The tar reforming conversion was assumed to be 90%,[41] while the methane reforming reaction was not considered because of the relative low values assumed for both the temperature (around 850 °C) and pressure (atmospheric pressure) in the BFBG.

$$C_{x2}H_{y2}O_{z2}N_{a2}S_{b2}Cl_{c2} + (x2 - z2)H_2O \rightarrow x2CO + \left(x2 - z2 + \frac{y2 - 3a2 - 2b2 - c2}{2}\right)H_2 + a2NH_3 + b2H_2S + c2HCl \quad (8)$$

$$CO + H_2O \leftrightarrow CO_2 + H_2 \quad (9)$$

vii. The RYield and RGibbs reactor modules of Aspen Plus were used to model the combustion of char and coal in the combustion zone. The RYield reactor was used to estimate the decomposition of the coal and char into their separate elements (H, N, O, S, solid carbon, ash, and water as moisture). The RGibbs reactor was then used to model the combustion reactions by minimizing the Gibbs free energy to determine the equilibrium composition of the outlet. The air to the combustion zone was assumed to be preheated to 600 °C by the hot flue gas. With the introduction of solar energy, despite reducing the flow rate of coal to the FFBC, the flow rate of air was assumed to be fixed to maintain the fluidization in the FFBC and the solid circulation rate of the system.

Tar Reformer. The catalytic tar reformer was modeled by assuming that tar, CH_4, and C_2H_4 in the raw syngas convert to CO and H_2, while NH_3 converts to N_2 and H_2 according to eq 8 and eqs 10−12 with assumed conversions of 90%, 20%, 50%, and 70%, respectively.[51] The water−gas shift reaction was also assumed to reach equilibrium in the tar reformer.

$$CH_4 + H_2O \rightarrow CO + 3H_2 \quad (10)$$

$$C_2H_4 + 2H_2O \rightarrow 2CO + 4H_2 \quad (11)$$

$$2NH_3 \rightarrow N_2 + 3H_2 \quad (12)$$

Wet Scrubber. The wet scrubber was proposed to cool the syngas to 150 °C and was assumed to completely remove the remaining tar, NH_3, and moisture.

Syngas Compression. The four-staged intercooled compressor was proposed to compress the cleaned syngas to 25 bar with an assumed isentropic efficiency of 83%.

Water Gas Shift Reactor (WGSR). The WGSR was proposed to maintain a constant H_2/CO ratio in the syngas across the operating range. The equilibrium reactor (REquil) in Aspen Plus was used to model the sour WGSR with an assumed temperature of 200 °C as shown in eq 9.

Acid Gas Remover (AGR). The AGR was modeled using a Rectisol AGR reactor with the assumption that 99.9% of the CO_2 and 100% of the H_2S are removed. Its consumption of electricity and low pressure steam were assumed to be 137 MJ_e/t (CO_2) and 90 MJ_{th}/t (CO_2), respectively.[3] The energy consumption required for the removal of H_2S was assumed to be the same as that for the CO_2 removal, which has little impact on the final predictions due to the insignificant amount of H_2S in the shifted syngas relative to that of CO_2. The products from the AGR were thus assumed to be a pure CO_2 stream and a sulfur rich stream.

Claus and Claus Off-gas Treatment Plant. An air-blown Claus plant was chosen for sulfur recovery from the sulfur rich stream, in which the H_2S is oxidized to elemental sulfur. The tail-gas was proposed to be cleaned up with a Shell Claus Off-gas Treatment (SCOT) plant, in which the steam raised by H_2S oxidation was assumed to be equal to that required to maintain S molten and to regenerate the SCOT plant.[52] No steam was assumed to be produced from the sulfur recovery unit.

Fischer−Tropsch Reactor (FTR). The FTR was modeled to convert syngas to paraffinic hydrocarbons with eq 13 at 240 °C and 25 bar. The conversion of CO in the cobalt catalytic FT reactions was assumed to be 90% efficient.[8] The product distribution was assumed to follow that of Anderson−Schulz−Flory as shown in eq 14,[53] while the chain growth probability α was assumed to be 0.95 to achieve a low content of light alkenes in the FT product.[3,8] The RStoic reactor was used to model the FT synthesis process in Aspen Plus, and FORTRAN code was used to determine the CO conversion for each synthesis reaction. The light gases (C_{1-4} and unreacted syngas) from the cooled FT product were assumed to be separated and sent to the gas turbine to generate electricity.

$$nCO + (2n + 1)H_2 \rightarrow C_nH_{2n+2} + nH_2O \quad (13)$$

$$\alpha_{C_n} = (1 - \alpha)\alpha^{(n-1)} \quad (14)$$

Here, α_{C_n} is the mole fraction of hydrocarbons with n carbon atoms in the product from the FTR.

Gas Turbine (GT). The gas turbine combustor was assumed to be adiabatic and modeled at 25 bar using the RGibbs reactor in Aspen Plus. The turbine was assumed to have an inlet temperature (TIT) of 1295 °C and to comprise a four-stage intercooled (to 25 °C) compression to 26 bar with an isentropic efficiency of 83%. The expander of the gas turbine also was assumed to have an isentropic efficiency of 83%.

HRSG System and Steam Turbine. The HRSG was proposed for the streams from the hot flue gas leaving the FFBC, the raw syngas from the BFBG, the gas turbine exhaust, and the heat generated by FTR. The recovered heat was modeled in four fractions based on saturation temperature: 400−920 °C, 320−400 °C, 240−320 °C, and 120−240 °C. The first fraction was proposed to be used to generate high pressure (HP) steam for the HP stage of the steam turbine, reheat, and overheat steam. The second fraction was proposed to be used to generate steam for the intermediate pressure (IP) steam turbine and the WGSR as well as to preheat the boiler feedwater to 320 °C. The third fraction was proposed to be used to generate steam for the low pressure (LP) turbine, the Rectisol process in the AGR reactor, and also to preheat the boiler feedwater to 240 °C. The final fraction was proposed to be used to generate atmospheric pressure (AP) steam for the DFB gasifier and to preheat the boiler feedwater to 120 °C. If the heat of the fourth fraction is insufficient to generate the AP steam for the DFB gasifier, the heat from the third fraction was proposed to be used to fill the gap.

The steam turbine was assumed to be a three-stage reheated turbine. The inlet temperature and pressure to the HP turbine were modeled to be 550 °C and 125 bar, respectively. The IP steam (42 bar) from the HP turbine was modeled to be reheated to 550 °C and then to pass through the IP turbine together with the IP steam generated from the HRSG system. The inlet temperature and pressure to the LP turbine were modeled to be 400 °C and 12.5 bar, respectively, while the outlet pressure was assumed to be 0.05 bar. The isentropic efficiency was assumed to be 85% for the HP turbine, 93% for the IP turbine, and 89% for the LP turbine.[3,8] The water pumps were assumed to have an isentropic efficiency of 92.5%, and a mechanical efficiency of 97%.[3]

2.2.2. Pseudodynamic Model. A pseudodynamic model (i.e., for which operation is assumed to be steady-state at each 1 h time-step in a one-year time series of historical DNI data) was implemented for a time series of historical solar DNI based on the method reported by Kaniyal et al.,[8] by following the logical control diagram shown in Figure 4. The response time for the switching between these

DOI: 10.1021/acs.energyfuels.5b00007
Energy Fuels 2015, 29, 2738−2751

conditions was assumed to be infinitely fast. The time series of the solar resource used in the present study was for the summer-to-summer period: June 1st, 2004 to May 31st, 2005 at Farmington (as described above in Gasifier Model section), in northern New Mexico, United States of America, whose latitude is 37° N.[54] This solar resource is a convenient reference for the present work to study the influence of solar multiple, the storage capacity, and the char conversion in the BFBG on the SCTL system performance rather than a specific design and evaluation for a particular site. Therefore, it is sufficient to use the solar data of a specific time period rather than to use the typical meteorological year (TMY) data. Moreover, the effect of the type of solar resource on the performance of the SCTL system was assessed by comparing performance with solar data from another site in the U.S. and two in Australia, namely Dickinson (U.S.A., 2004/2005), Woomera (Australia, 2012/2013), and Mildura (Australia, 2012/2013).[54,55] These three sites are all close to low rank coal reserves. Table 4 displays the annual peak DNI-cosine and average daily DNI-cosine for each of the four sites in the selected period. Under the other assumptions listed above, the cosine efficiency η_{cos} is the only variable factor that influences the optical efficiency (see eq 3) according to the site and time. Therefore, the product of DNI and the cosine efficiency ($I_{DN}\eta_{cos}$) is used to calculate performance at each time step for each solar resource.

Table 4. Parameters of the Solar Resources for the Sites Chosen in the Present Study

	Farmington, NM, USA, 2004/2005	Dickinson, ND, USA, 2004/2005	Woomera, SA, AUS, 2012/2013	Mildura, NSW, AUS, 2012/2013
annual peak DNI-cosine ($(I_{DN}\eta_{cos})_{peak}$ W/m^2)	1057	977	1034	1024
average daily DNI-cosine ($\overline{I_{DN}\eta_{cos}}$, kWh/m^2/day)	6.5	4.1	6.2	5.7

2.3. System Performance Analysis. The performance of an SCTL system was assessed for a range of bed material storage capacities (SC), eq 15, solar multiples (SM), eq 4, and char conversions in the BFBG ($X_{char,BFBG}$). The char composition on an ash free basis ($C_{x1}H_{y1}O_{z1}N_{a1}S_{b1}Cl_{c1}$) was assumed to remain constant during the char gasification process.

$$SC = \frac{m_{tank}}{\dot{m}_{BM,BFBG}} \tag{15}$$

Here, m_{tank} is the mass capacity of the storage unit and $\dot{m}_{BM,BFBG}$ is the mass flow rate of hot bed material to the BFBG.

To evaluate the annual performance of the SCTL system, the following metrics were used:

(1) Annual solar share,[25] SS_{ann}:

$$SS_{ann} = \frac{(Q_{net,sol})_{ann}}{(Q_{net,sol})_{ann} + (Q_{coal,HHV})_{ann}} \tag{16}$$

(2) Annual percentage change in specific FTL output of the SCTL system per unit coal relative to the nonsolar CTL system, $\Delta Q_{s,FTL,ann}$:

$$\Delta Q_{s,FTL,ann} = [((Q_{FTL,HHV})_{ann}/(Q_{coal,HHV})_{ann})_{SCTL} - ((Q_{FTL,HHV})_{ann}/(Q_{coal,HHV})_{ann})_{CTL}] / [((Q_{FTL,HHV})_{ann}/(Q_{coal,HHV})_{ann})_{CTL}] \times 100\% \tag{17}$$

(3) Annual percentage change in specific total energetic output of the SCTL system per unit of coal relative to the nonsolar CTL system, $\Delta En_{s,ann}$:

$$\Delta En_{s,ann} = \frac{\left(\frac{((Q_{FTL,HHV})_{ann} + (W_{net})_{ann})}{(Q_{coal,HHV})_{ann}}\right)_{SCTL} - \left(\frac{((Q_{FTL,HHV})_{ann} + (W_{net})_{ann})}{(Q_{coal,HHV})_{ann}}\right)_{CTL}}{\left(\frac{((Q_{FTL,HHV})_{ann} + (W_{net})_{ann})}{(Q_{coal,HHV})_{ann}}\right)_{CTL}} \times 100\% \tag{18}$$

(4) Annual MTT CO_2 emission per unit output, $E_{CO_2,ann}$:

$$E_{CO_2,ann} = \frac{(m_{CO_2})_{ann}}{(Q_{FTL,HHV})_{ann} + (W_{net})_{ann}} = \frac{(m_{CO_2})_{ann}}{(Q_{coal,HHV})_{ann}} / \frac{(Q_{FTL,HHV})_{ann} + (W_{net})_{ann}}{(Q_{coal,HHV})_{ann}} \tag{19}$$

(5) Annual MTT CO_2 emission reduction relative to the nonsolar CTL system, $\Delta E_{CO_2,ann}$:

$$\Delta E_{CO_2,ann} = \frac{(E_{CO_2,ann})_{CTL} - (E_{CO_2,ann})_{SCTL}}{(E_{CO_2,ann})_{CTL}} \tag{20}$$

(6) Annually averaged utilization factor of the heliostat collector, $\overline{U_{coll,ann}}$ and the FFBC ($\overline{U_{FFBC,ann}}$) calculated by taking the mean of the utilization factor for each time step as defined in eq 6 (U_{coll}) and eq 21 (U_{FFBC}):

$$U_{FFBC} = \frac{\dot{Q}_{fuel,FFBC}}{\dot{Q}_{fuel,FFBC,max}} \tag{21}$$

Here, $(W_{net})_{ann}$ is the annual net electricity output from the system, $(m_{CO_2})_{ann}$ is the annual mass-based MTT CO_2 emission, $(Q_{FTL,HHV})_{ann}$ is the HHV of the annual FTL output, $(Q_{coal,HHV})_{ann}$ is the HHV of the annual input of coal to the DFB gasifier, $\dot{Q}_{fuel,FFBC}$ is the HHV of the fuel (both coal and char) combusted in the FFBC, and $\dot{Q}_{fuel,FFBC,max}$ is the maximum HHV of the fuel combusted in the FFBC.

3. RESULTS AND DISCUSSION

3.1. Model Validation for DFB Gasifier Model. Figure 6 compares the outputs from the model with the measurements of Kern et al.,[35] for the conditions shown in Table 2. The agreement between the model and experimental data is within ±15% for all main gaseous products other than CH_4, whose composition in the raw syngas is relatively low (<5 vol % dry basis). On this basis, the model is sufficiently reliable to undertake a first-order assessment of the proposed SDFB system.

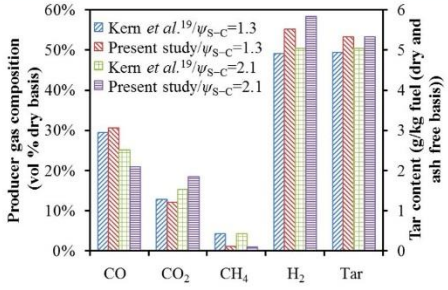

Figure 6. Comparison of the predicted values of raw syngas at the outlet from the conventional DFB gasifier with the measurements of Kern et al.[35] Conditions are shown in Table 2

DOI: 10.1021/acs.energyfuels.5b00007
Energy Fuels 2015, 29, 2738−2751

3.2. System Operational Performance. *3.2.1. Minimum Hot Bed Material Storage Capacity to Avoid Solar Spillage.* Figure 7 presents the minimum hot bed material storage capacity required to avoid solar spillage ($SC_{no\text{-}spill}$) as a function of the solar multiple (SM). It can be seen that $SC_{no\text{-}spill}$ is sensitive to the variation in SM, especially for high values of SM. For SM $\leq$ 1, the storage capacity is zero, which is not shown in Figure 7 because the axis is presented on a log scale. As SM is increased to 2.6, the value of $SC_{no\text{-}spill}$ is increased to 16 h. However, with further increases in SM to 4.0, the value of $SC_{no\text{-}spill}$ increases sharply to over 900 h. The nonlinear relationship is due mostly to the seasonal variability of the solar resource. The stored sensible heat can be consumed completely when the sun is not available for SM < 2.6. However, for SM > 2.6, the stored sensible heat is not consumed entirely at night, notably during the peak summer period. Therefore, $SC_{no\text{-}spill}$ increases sharply with SM due to the accumulation of stored sensible heat which can be consumed during the winter period. Given the anticipated high cost of storage and the large heat losses associated with very large sensible storage units,[34] it is unlikely to be economically desirable to approach the $SC_{no\text{-}spill}$ for cases where the SM exceeds the threshold. However, further investigation on techno-economic feasibility is required in the future to optimize the entire SCTL system. For the remainder of the present assessment, the values of SC = 8 and 16 h were chosen as representative values for further assessment.

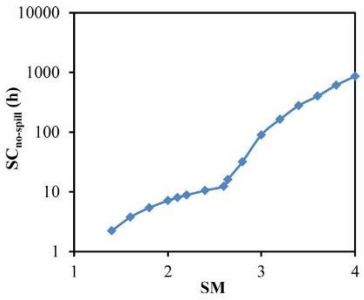

Figure 7. Minimum hot bed material storage capacity required to avoid solar spillage ($SC_{no\text{-}spill}$) as a function of the solar multiple (SM).

3.2.2. Time Resolved System Operation. Figure 8 presents the pseudodynamic response of the SCTL system for two six-day (144 h) hourly integrated solar insolation time series that are representative of winter and summer conditions for the case SM = 2.4, SC = 8 h, and $X_{char,BFBG}$ = 85%. These two short-term time series, together with the design parameters (SM, SC, and $X_{char,BFBG}$) of the SCTL system, are chosen to illustration how the SCTL system responds to variations in the solar resource and to further verify that the pseudodynamic model is reasonable. The statistical analysis, reported below, is undertaken for a time series of 12 months of data. In addition, a sensitivity study of the design parameters is presented below. The first panel in each of Figure 8A and B presents the variation in solar ratio Φ as a function of time for the summer and winter periods, respectively, of Farmington, U.S.A. The hot bed material storage level, solar spillage ($1 - U_{coll}$), and the SCTL system's conventional CTL normalized additional coal mass flow rate to the FFBC ($(\dot{m}_{add})_{SCTL}/(\dot{m}_{add})_{CTL}$) are shown in the second panel of Figure 8A and B. The third panel presents the FTL and electricity output of the SCTL system normalized by that of the conventional system ($(Q_{FTL})_{SCTL}/(Q_{FTL})_{CTL}$ and $(W_{net})_{SCTL}/(W_{net})_{SCTL}$).

It can be seen from Figure 8 that the system maintains a constant output of FTL products despite the variability of the solar resource for both time series (lowest panel), which is the

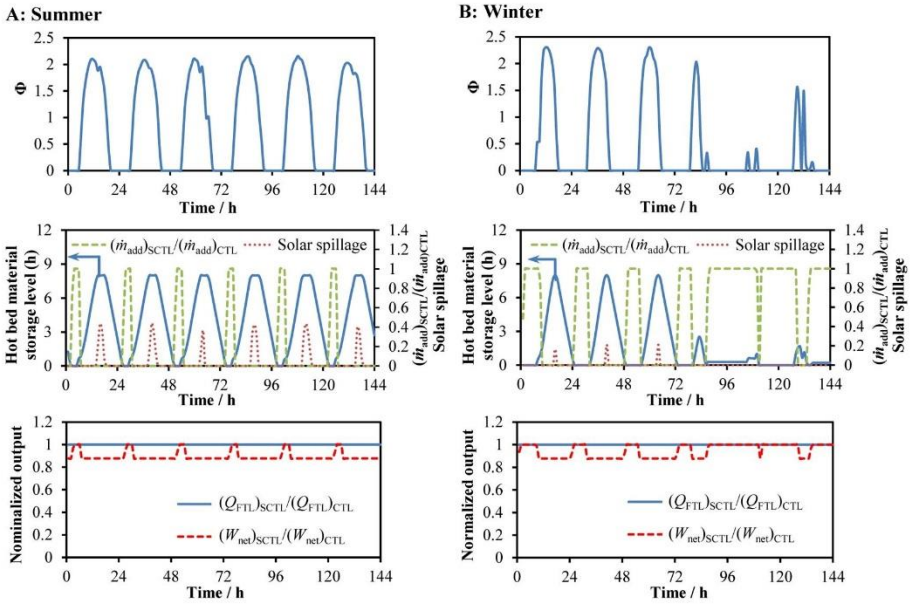

Figure 8. Pseudodynamic response of the SCTL system for two six-day (144-h) hourly averaged solar insolation time series, which are representative of winter and summer conditions in Farmington for the case SM = 2.4, SC = 8 h, and $X_{char,BFBG}$ = 85%.

DOI: 10.1021/acs.energyfuels.5b00007
Energy Fuels 2015, 29, 2738–2751

key design target for this system. However, the electricity output decreases with the introduction of solar energy, which is caused by the variation of the heat recovered from the flue gas of the FFBC with the variation in the mass flow rate of the additional fuel. It can also be seen that the storage level of the hot bed material varies with trends that are consistent with the expectation from the logic control method described in Figure 4, as do the solar spillage and the mass flow rate of the additional fuel to the FFBC.

3.3. Effect of Solar Multiple and Storage Capacity on the Performance of SCTL System. Figures 9−14 present the annually averaged performance of the present SCTL system, calculated with the pseudodynamic model, as a function of SM for the various hot bed material storage capacities (SC = 8 h, 16 h and $SC_{no\text{-}spill}$) and for an assumed char conversion in the BFBG ($X_{char,BFBG}$) of 100%. Even though this is higher than the 50% to 60% conversions that have been reported for lignite gasification in lab-scale and pilot-scale DFB gasifiers,[32,35,36] conversion can be expected to increase both with scale and with further development of the reactor design. Under these circumstances, complete conversion is considered to be appropriate as a baseline case with which to study the impact of SM and SC on the SCTL system and to highlight the best potential performance of the SCTL system with a SDFB gasifier. A sensitivity study on the $X_{char,BFBG}$ is also presented below.

3.3.1. Analysis of Capital Utilization. Utilization Factor of Heliostat Collector. Figure 9 presents the annually averaged

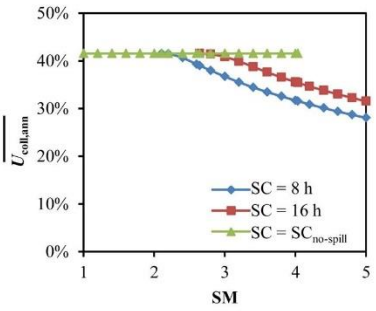

Figure 9. Annually averaged heliostat collector utilization factor ($\overline{U_{coll,ann}}$) as a function of solar multiple (SM) for different bed material storage capacities (SC).

utilization factor of the heliostat collector ($\overline{U_{coll,ann}}$) as a function of SM for different values of SC. It can be seen that for both sizes of storage capacities (8 and 16 h), there exists a threshold of SM below which no solar spillage occurs because the SC ≥ $SC_{no\text{-}spill}$. The maximum value of the $\overline{U_{coll,ann}}$ is 41.6% when no spillage occurs. A high utilization of the heliostat field is expected to be desirable, since this is typically a significant component of the capital expenditure of the plant. This threshold occurs at SM = 2.1 and 2.6 for SC = 8 and 16 h, respectively. Nevertheless, the highly nonlinear nature of the function for $SC_{no\text{-}spill}$ (Figure 7) means that it may be economically beneficial to operate with a small amount of spillage. For SM = 3 and SC = 16 h, $\overline{U_{coll,ann}}$ is 40.8%. However, SC = 16 h is 82.1% smaller capacity relative to $SC_{no\text{-}spill}$.

Utilization Factor of Combustion Reactor. Figure 10 presents the dependence of the annually averaged utilization

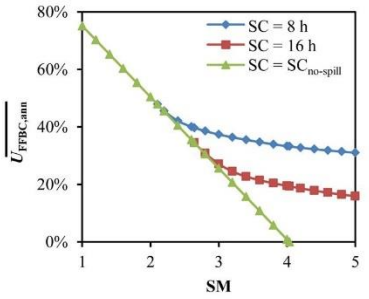

Figure 10. Annually averaged utilization factor of the combustion reactor ($\overline{U_{FFBC,ann}}$) as a function of the solar multiple (SM) for different bed material storage capacities (SC).

factor of the FFBC ($\overline{U_{FFBC,ann}}$) on SM for different values of SC. It can be seen that the $\overline{U_{FFBC,ann}}$ decreases with an increase in SM. This is to be expected because a larger heliostat field will result in a greater fraction of the energy being provided by solar energy and less by combustion. It can also be seen that the increase in SC further reduces $\overline{U_{FFBC,ann}}$ for the case in which SC ≤ $SC_{no\text{-}spill}$. This is because a larger storage capacity allows greater use to be made of the heliostat field and further increases the solar share, or reduces the amount of fuel required in the FFBC to meet the load. It can also be seen that it is hypothetically possible to provide all of the heat of reaction from solar energy, i.e., the $\overline{U_{FFBC,ann}}$ = 0. This occurs when SC = $SC_{no\text{-}spill}$ and SM = 4. However, as has already been noted with regard to Figure 7, this case requires an inordinate amount of storage, corresponding to more than 900 h.

3.3.2. Solar Share. Figure 11 presents the annual solar share (SS_{ann}) of the SCTL system as a function of SM for different

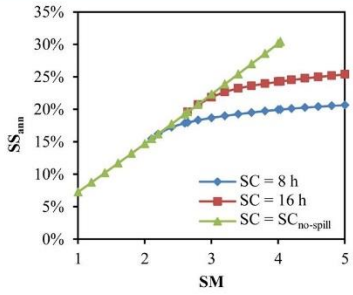

Figure 11. Annual solar share (SS_{ann}) of the SCTL system as a function of solar multiple (SM) for different bed material storage capacities (SC).

values of SC.). For SC = $SC_{no\text{-}spill}$, the value of SS_{ann} increases with SM from 8% to a maximum value of 30.4%. This value of solar thermal input corresponds to the thermal requirements of the process, with the remaining 69.6% of the energy content coming from the fuel. Moreover, the influence of SC on SS_{ann} is consistent with what has been noted from Figure 7. That is, an increase in SC for a fixed SM allows an increase in SS_{ann} through an increase in $\overline{U_{coll,ann}}$. For SM = 3 and SC = 16 h, SS_{ann} is 21.8%, which is only 2.1% lower than the 22.3% for SC = $SC_{no\text{-}spill}$.

DOI: 10.1021/acs.energyfuels.5b00007
Energy Fuels 2015, 29, 2738−2751

3.3.3. FTL Output and Specific Total Energetic Output of the SCTL System. Figure 12 presents the dependence on SM,

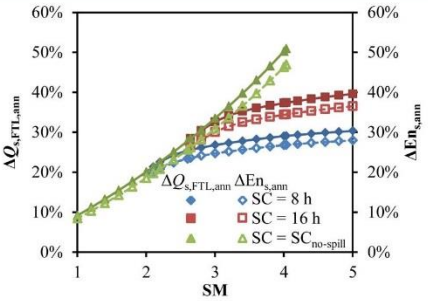

Figure 12. Percentage change in annual specific FTL output, $\Delta Q_{s,FTL,ann}$ (solid line), and specific total energetic output, $\Delta En_{s,ann}$ (dash line), of the SCTL system relative to a nonsolar CTL system as a function of solar multiple, SM, for different bed material storage, SC.

for different cases of SC, of the percentage change in both annual specific FTL output and the specific total energetic output of the SCTL system relative to their nonsolar CTL counterparts ($\Delta Q_{s,FTL,ann}$ and $\Delta En_{s,ann}$). This shows that increasing SM results in a significant increase in both $\Delta Q_{s,FTL,ann}$ and $\Delta En_{s,ann}$ due to the increase in solar share shown in Figure 11. It can also be seen that the values of $\Delta Q_{s,FTL,ann}$ lie above the corresponding values of $\Delta En_{s,ann}$ due to the decrease in the electricity output caused by the introduction of solar energy as described above in Figure 8 (third panel). For SC = $SC_{no-spill}$, the values of $\Delta Q_{s,FTL,ann}$ and $\Delta En_{s,ann}$ increase to their maximum values of 50.9% and 46.9%, respectively, as SM is increased to 4. For SM = 3 and SC = 16 h, $\Delta Q_{s,FTL,ann}$ and $\Delta En_{s,ann}$ are 32.6% and 30%, respectively, while for SC = $SC_{no-spill}$ their values are 33.5% and 30.9%, respectively.

3.3.4. CO_2 Emissions. Figure 13 presents the dependence on SM, for different values of SC, of both the annual MTT CO_2

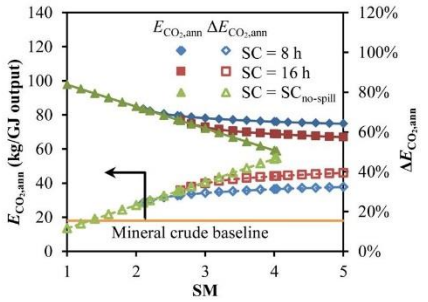

Figure 13. Annual MTT CO_2 emissions, $E_{CO_2,ann}$ (solid line), and annual reduction of MTT CO_2 emissions, $\Delta E_{CO_2,ann}$ (dash line), of the SCTL system relative to nonsolar CTL system as a function of solar multiple (SM) for different bed material storage capacities (SC).

emissions ($E_{CO_2,ann}$) and the annual reduction in MTT CO_2 from the SCTL system relative to the nonsolar CTL counterpart ($\Delta E_{CO_2,ann}$). Importantly, it can be seen that this SCTL system is calculated to offer up to 39.4% reduction in CO_2 emission relative to the conventional system with 16 h of storage, even though this case requires a very large heliostat field with SM = 5, which results in low $\overline{U_{coll,ann}}$ (as shown in Figure 9). For reference, the theoretical limit is a 46.9% reduction, which requires more than 900 h of storage. Furthermore, significant gains are also possible with smaller fields and more realistic storage capacities. For example, with SM = 3 and SC = 16 h, $\Delta E_{CO_2,ann}$ and $E_{CO_2,ann}$ are 34.1% and 72.8 kg/GJ, respectively. The above trends can be explained by the dependence of $\Delta Q_{s,FTL,ann}$ and $\Delta En_{s,ann}$ on SM. A higher value of $\Delta Q_{s,FTL,ann}$ corresponds to a lower value of CO_2 emitted per unit coal because more carbon is stored in the FTL. Similarly, a higher $\Delta En_{s,ann}$ also corresponds to a lower $E_{CO_2,ann}$ as shown in eqs 18 and 19. Nevertheless, the $E_{CO_2,ann}$ remains higher than the well-to-tank emissions for conventional mineral crude (18 kg/GJ diesel[7]). Hence, other CO_2 reduction options such as cogasification of coal and biomass and/or the CCS system will be needed to achieve an environmental benefit over mineral crude.

3.4. Performance of SCTL System with Different Char Conversion in the BFBG and Solar Resources. Figures 14

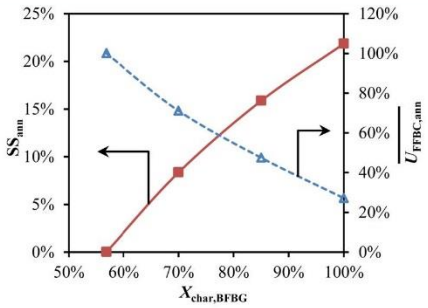

Figure 14. Annual solar share (SS_{ann}) and combustion reactor utilization ($\overline{U_{FFBC,ann}}$) as a function of char conversion in the BFBG ($X_{char,BFBG}$) at SM = 3 and SC = 16 h.

and 15 present the influence of char conversion within the BFBG ($X_{char,BFBG}$) on SS_{ann} and $\overline{U_{FFBC,ann}}$, while Figure 16 presents the influence of various solar resources. All of these

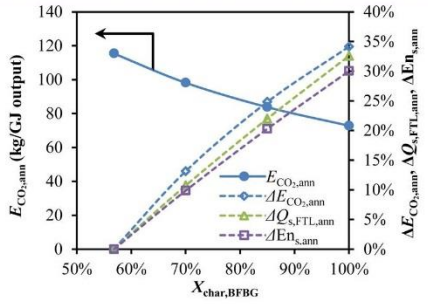

Figure 15. Influence of char conversion in the BFBG ($X_{char,BFBG}$) on annual CO_2 emission ($E_{CO_2,ann}$), percentage reduction in CO_2 emission ($\Delta E_{CO_2,ann}$), percentage improvement in FTL ($\Delta Q_{s,FTL,ann}$), and percentage improvement in total energetic output per unit feedstock ($\Delta En_{s,ann}$) relative to the nonsolar CTL system. Calculations are performed at SM = 3 and SC = 16 h.

DOI: 10.1021/acs.energyfuels.5b00007
Energy Fuels 2015, 29, 2738–2751

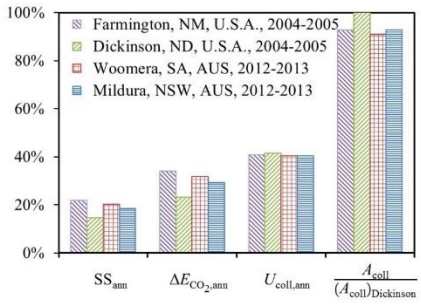

Figure 16. Annual solar share (SS_{ann}), annual percentage CO_2 emission reduction ($\Delta E_{CO_2,ann}$) relative to the nonsolar CTL system, the annually averaged utilization factor of the heliostat collector ($\overline{U_{coll,ann}}$), and the dimensionless heliostat field area ($A_{coll}/(A_{coll})_{Dickinson}$) as a function of the solar resources (SM = 3, SC = 16 h, and $X_{char,BFBG}$ = 100%).

assessments are undertaken for values of SM = 3 and SC = 16 h, which achieve a relatively good heliostat utilization factor and good improvement in the energetic and environmental performance for a relatively small storage size (Figures 9–13). Table 5 presents the influence of solar resource on the required SM and SC to realize maximum solar operation.

Table 5. Required Solar Multiple and Bed Material Storage Capacity to Realize Maximum Solar Operation for Various Solar Resources

	Farmington, NM, USA, 2004/2005	Dickinson, ND, USA, 2004/2005	Woomera, SA, AUS, 2012/2013	Mildura, NSW, AUS, 2012/2013
required SM	4	6	4.2	4.6
required SC (h)	908	1039	1010	1353

3.4.1. Effect of Char Conversion in the BFBG. Figure 14 shows that $X_{char,BFBG}$ has a significant influence on both SS_{ann} and $\overline{U_{FFBC,ann}}$. As $X_{char,BFBG}$ is decreased from 100% to 57%, the value of SS_{ann} decreases from 21.8% to 0, while the value of $\overline{U_{FFBC,ann}}$ increases from 27.2% to 100%. This is because a lower value of $X_{char,BFBG}$ results in a lower requirement for chemical energy in the BFBG and more heat of combustion being provided by char combustion in the FFBC. For the same reasons, a decrease in the value of $X_{char,BFBG}$ leads to a higher combustion reactor utilization factor.

Figure 15 presents the dependence on $X_{char,BFBG}$ of $E_{CO_2,ann}$, $\Delta E_{CO_2,ann}$, $\Delta Q_{s,FTL,ann}$, and $\Delta En_{s,ann}$ for the SCTL system. It can be seen that, as the value of $X_{char,BFBG}$ is decreased, the values of both $\Delta Q_{s,FTL,ann}$ and $\Delta En_{s,ann}$ decrease significantly. This can be explained by the trends shown in Figure 14, because a lower solar share results in more feedstock combustion (to provide heat for gasification reactions), leaving less fuel for syngas production per unit feedstock. A lower $\Delta Q_{s,FTL,ann}$ implies that a lower quantity of carbon per unit feedstock is stored in the FTL and a higher quantity of carbon per unit feedstock is emitted. Therefore, decreasing $X_{char,BFBG}$ increases $E_{CO_2,ann}$ significantly (thus decreasing the $\Delta E_{CO_2,ann}$), following eq 19.

3.4.2. Sensitivity to the Solar Resource. Table 5 presents the required SM and SC to realize maximum solar operation without the use of supplementary fuel to the FFBC for various solar resources. As expected, the lower daily average DNI-cosine results in a higher required SM (refer to Table 4 for average and peak DNI-cosine). However, the required SC does not have a direct relationship with the parameters provided in Table 4. Figure 16 presents the sensitivity of SS_{ann}, $\Delta E_{CO_2,ann}$, $\overline{U_{coll,ann}}$, and dimensionless heliostat field area ($A_{coll}/(A_{coll})_{Dickinson}$) to solar resource. It can be seen that the value of $\overline{U_{coll,ann}}$ is relatively insensitive to the solar resource. However, the values of SS_{ann} and $\Delta E_{CO_2,ann}$ are more sensitive, both varying by approximately ±22% about their mean values. The low sensitivity of $\overline{U_{coll,ann}}$ to the location implies that the energetic and environmental performance of the SCTL system depends mostly on the values of both A_{coll} and the DNI-cosine according to eqs 1–5 and 16. Hence, as shown in Figure 16, Dickinson has the lowest SS_{ann} and $\Delta E_{CO_2,ann}$ because of the lowest average DNI-cosine, even though it has the largest heliostat collector area.

4. CONCLUSION

The annual energetic and environmental performance of the SCTL system with a SDFB gasifier is analyzed as a function of solar multiple (SM), bed material storage capacity (SC), char conversion in the BFBG ($X_{char,BFBG}$), and the quality of solar resource. For the case of the minimum hot bed material storage capacity to avoid solar spillage ($SC_{no\text{-}spill}$) and $X_{char,BFBG}$ = 100%, it is found that the annual solar share (SS_{ann}), utilization factor of heliostat collector ($\overline{U_{coll,ann}}$), the percentage change in annual specific FTL output ($\Delta Q_{s,FTL,ann}$), and annual reduction of CO_2 emission ($\Delta E_{CO_2,ann}$) relative to their nonsolar CTL counterparts are increased to maximum values of 30.4%, 41.6%, 50.9%, and 46.9%, respectively, as SM is increased to 4. However, the huge required storage capacity (over 900 h) impedes the feasibility of this case. Nevertheless, significant gains are also possible with more realistic SC even though some spillage results. For SM = 3 and SC = 16 h, SS_{ann}, $\overline{U_{coll,ann}}$, $\Delta Q_{s,FTL,ann}$, and $\Delta E_{CO_2,ann}$ are calculated to be 21.8%, 40.8%, 32.6%, and 34.1%, respectively. For the case of the presently assessed lignite fuel, the net MTT CO_2 emissions exceed the value of mineral crude. Nevertheless, this disadvantage can potentially be avoided or reduced by the use of low-net-carbon feedstocks, such as biomass and waste.

Other important findings are that the performance of the SCTL system is very sensitive to $X_{char,BFBG}$. The solar share is reduced to zero as the $X_{char,BFBG}$ reduces to 57%. Hence, a good design of the BFBG and the selection of a high reactivity feedstock are essential to achieving good performance of the SCTL system. Similarly, the type of solar resource has a significant impact on the performance of the SCTL system. Both the energetic and environmental performance of the SCTL system increases with the quality of the solar resource.

■ AUTHOR INFORMATION

Corresponding Author

*Phone: +61406887246. E-mail: peijun.guo@adelaide.edu.au.

Notes

The authors declare no competing financial interest.

DOI: 10.1021/acs.energyfuels.5b00007
Energy Fuels 2015, 29, 2738–2751

■ ACKNOWLEDGMENTS

P.G. would like to thank the generous support of the Chinese Scholarship Council (CSC) who provides the scholarship for his Ph.D. study. P.J.v.E would like to acknowledge the support of the Australian Solar Institute (ASI) for providing a postdoctoral fellowship. The Australian Government, through the ASI, supported Australian research and development in solar photovoltaic and solar thermal technologies to help solar power become cost competitive with other energy sources. G.J.N. wishes to thank the Australian Research Council (ARC) for the Discovery Outstanding Researcher Award used to support this work. The authors also acknowledge the Australian Solar Thermal Research Initiative (ASTRI), a project supported by the Australian Government, through the Australian Renewable Energy Agency (ARENA). The paper has also been strengthened by addressing the insightful comments of the anonymous reviewers of the paper, for which the authors are also very grateful.

■ NOMENCLATURE

A = area (m^2)
AP = atmospheric pressure
AGR = acid gas remover
ASU = air separation unit
BFBG = bubbling fluidized bed gasifier
C = concentration ratio
CPC = compound parabolic concentrator
CTL = coal-to-liquids
DFB = dual fluidized bed
DNI = direct normal insolation
E = emission per unit output (kg/GJ)
En = total energetic output (J)
FFBC = fast fluidized bed combustor
FT = Fischer−Tropsch
FTL = Fischer−Tropsch liquids
FTR = Fischer−Tropsch reactor
GHG = greenhouse gas
HHV = higher heating value (J/kg)
HP = high pressure
HRSG = heat recovery and steam generation
I = solar insolation (W/m^2)
IP = intermediate pressure
LP = low pressure
m = mass capacity (kg)
$\dot{m}$ = mass flow rate (kg/s)
MTT = mine-to-tank
Q = heating value of fuel, heat flow (J)
$\dot{Q}$ = heat flow rate (W)
SC = storage capacity (h)
SCOT = Shell Claus off-gas treatment
SCTL = solar hybridized coal-to-liquids
SDFB = solar hybridized dual fluidized bed
SM = the ratio of the heliostat field area relative to that required to meet the demand of the DFB gasifier at the point of peak solar thermal output
SS = solar share
U = utilization factor
W = electricity output (J)
WGSR = water−gas shift reactor
X = conversion of reactant

Greek Letters

η = efficiency, heat loss proportion
Φ = ratio of net useful solar energy absorbed by the bed material if the heliostat collector is operated under optimal angle to the heat required by the DFB gasifier if no additional feed is used
ψ_{S-C} = steam to carbon ratio (kg/kg)

Subscripts

aa = atmospheric attenuation
add = additional fuel
ann = annual
aper = aperture of the solar receiver
BM = bed material
coll = heliostat collector
DN = direct normal
itc = interception
l = loss
no-spill = no spillage
o = other
opt = optical
rec = receiver
ref = reflection
s = specific (output per unit feedstock)
sb = shadowing and blocking
sol = solar
stg = storage unit

■ REFERENCES

(1) *World Energy Outlook 2014*; International Energy Agency: Paris, 2014.
(2) Takeshita, T.; Yamaji, K. Important roles of Fischer−Tropsch synfuels in the global energy future. *Energy Policy* **2008**, *36* (8), 2773−2784.
(3) Meerman, J. C.; Ramírez, A.; Turkenburg, W. C.; Faaij, A. P. C. Performance of simulated flexible integrated gasification polygeneration facilities. Part A:A technical-energetic assessment. *Renewable Sustainable Energy Rev.* **2011**, *15* (6), 2563−2587.
(4) Sudiro, M.; Bertucco, A. Production of synthetic gasoline and diesel fuel by alternative processes using natural gas and coal: Process simulation and optimization. *Energy* **2009**, *34* (12), 2206−2214.
(5) Chen, Y.; Adams, T.; Barton, P. Optimal Design and Operation of Flexible Energy Polygeneration Systems. *Ind. Eng. Chem. Res.* **2011**, *50* (8), 4553−4566.
(6) Adams, T.; Barton, P. Combining coal gasification and natural gas reforming for efficient polygeneration. *Fuel Process. Technol.* **2011**, *92* (3), 639−655.
(7) Gerdes, K. J.; Skone, T. J. *An Evaluation of the Extraction, Transport and Refining of Imported Crude Oils and the Impact on Life Cycle Greenhouse Gas Emissions*; NETL: Washington, DC, 2009; p 42.
(8) Kaniyal, A. A.; van Eyk, P. J.; Nathan, G. J.; Ashman, P. J.; Pincus, J. J. Polygeneration of Liquid Fuels and Electricity by the Atmospheric Pressure Hybrid Solar Gasification of Coal. *Energy Fuels* **2013**, *27* (6), 3538−3555.
(9) Lattanzio, R. K. *Canadian Oil Sands: Life-Cycle Assessments of Greenhouse Gas Emissions*; Congressional Research Service: Pittsburgh, PA, 2012; p 31.
(10) Larson, E. D.; Fiorese, G.; Liu, G.; Williams, R. H.; Kreutz, T. G.; Consonni, S. Co-production of synfuels and electricity from coal plus biomass with zero net carbon emissions: an Illinois case study. *Greenhouse Gas Control Technol., Proc. Int. Conf., 9th* **2009**, *1* (1), 4371−4378.
(11) Larson, E. D.; Fiorese, G.; Liu, G. J.; Williams, R. H.; Kreutz, T. G.; Consonni, S. Co-production of decarbonized synfuels and electricity from coal plus biomass with CO_2 capture and storage: an Illinois case study. *Energy Environ. Sci.* **2010**, *3* (1), 28−42.
(12) Liu, G. J.; Larson, E. D.; Williams, R. H.; Kreutz, T. G.; Guo, X. B. Making Fischer−Tropsch Fuels and Electricity from Coal and

DOI: 10.1021/acs.energyfuels.5b00007
Energy Fuels 2015, 29, 2738−2751

Biomass: Performance and Cost Analysis. *Energy Fuels* **2011**, *25*, 415−437.
(13) Kaniyal, A. A.; van Eyk, P. J.; Nathan, G. J. Dynamic Modeling of the Coproduction of Liquid Fuels and Electricity from a Hybrid Solar Gasifier with Various Fuel Blends. *Energy Fuels* **2013**, *27* (6), 3556−3569.
(14) Piatkowski, N.; Wieckert, C.; Weimer, A. W.; Steinfeld, A. Solar-driven gasification of carbonaceous feedstock-a review. *Energy Environ. Sci.* **2011**, *4* (1), 73−82.
(15) Sudiro, M.; Bertucco, A. Synthetic fuels by a limited CO_2 emission process which uses both fossil and solar energy. *Energy Fuels* **2007**, *21* (6), 3668−3675.
(16) Puig-Arnavat, M.; Tora, E. A.; Bruno, J. C.; Coronas, A. State of the art on reactor designs for solar gasification of carbonaceous feedstock. *Sol. Energy* **2013**, *97*, 67−84.
(17) Gregg, D. W.; Taylor, R. W.; Campbell, J. H.; Taylor, J. R.; Cotton, A. Solar Gasification of Coal, Activated Carbon, Coke and Coal and Biomass Mixtures. *Sol. Energy* **1980**, *25* (4), 353−364.
(18) Taylor, R. W.; Berjoan, R.; Coutures, J. P. Solar Gasification of Carbonaceous Materials. *Sol. Energy* **1983**, *30* (6), 513−525.
(19) Piatkowski, N.; Steinfeld, A. Solar-driven coal gasification in a thermally irradiated packed-bed reactor. *Energy Fuels* **2008**, *22* (3), 2043−2052.
(20) Piatkowski, N.; Wieckert, C.; Steinfeld, A. Experimental investigation of a packed-bed solar reactor for the steam-gasification of carbonaceous feedstocks. *Fuel Process. Technol.* **2009**, *90* (3), 360−366.
(21) Kodama, T.; Kondoh, Y.; Tamagawa, T.; Funatoh, A.; Shimizu, K. I.; Kitayama, Y. Fluidized bed coal gasification with CO_2 under direct irradiation with concentrated visible light. *Energy Fuels* **2002**, *16* (5), 1264−1270.
(22) Murray, J. P.; Fletcher, E. A. Reaction of Steam with Cellulose in a Fluidized-Bed Using Concentrated Sunlight. *Energy* **1994**, *19* (10), 1083−1098.
(23) Kodama, T.; Gokon, N.; Enomoto, S.; Itoh, S.; Hatamachi, T. Coal Coke Gasification in a Windowed Solar Chemical Reactor for Beam-Down Optics. *J. Sol. Energy Eng.* **2010**, *132* (4).
(24) Gokon, N.; Ono, R.; Hatamachi, T.; Li, L. Y.; Kim, H. J.; Kodama, T. CO_2 gasification of coal cokes using internally circulating fluidized bed reactor by concentrated Xe-light irradiation for solar gasification. *Int. J. Hydrogen Energy* **2012**, *37* (17), 12128−12137.
(25) Sheu, E. J.; Mitsos, A.; Eter, A. A.; Mokheimer, E. M. A.; Habib, M. A.; Al-Qutub, A. A Review of Hybrid Solar-Fossil Fuel Power Generation Systems and Performance Metrics. *J. Sol. Energy Eng.* **2012**, *134* (4).
(26) Z'Graggen, A.; Haueter, P.; Maag, G.; Romero, M.; Steinfeld, A. Hydrogen production by steam-gasification of carbonaceous materials using concentrated solar energy - IV. Reactor experimentation with vacuum residue. *Int. J. Hydrogen Energy* **2008**, *33* (2), 679−684.
(27) Z'Graggen, A.; Haueter, P.; Maag, G.; Vidal, A.; Romero, M.; Steinfeld, A. Hydrogen production by steam-gasification of petroleum coke using concentrated solar power - III. Reactor experimentation with slurry feeding. *Int. J. Hydrogen Energy* **2007**, *32* (8), 992−996.
(28) Z'Graggen, A.; Steinfeld, A. Hydrogen production by steam-gasification of carbonaceous materials using concentrated solar energy - V. Reactor modeling, optimization, and scale-up. *Int. J. Hydrogen Energy* **2008**, *33* (20), 5484−5492.
(29) Nickerson, T. A.; Hathaway, B. J.; Smith, T. M.; Davidson, J. H. Economic assessment of solar and conventional biomass gasification technologies: Financial and policy implications under feedstock and product gas price uncertainty. *Biomass Bioenergy* **2015**, *74* (0), 47−57.
(30) Hathaway, B. J.; Kittelson, D. B.; Davidson, J. H. Integration of Solar Gasification With Conventional Fuel Production: The Roles of Storage and Hybridization. *J. Sol. Energy Eng.* **2014**, *136* (1).
(31) Saw, W. L.; Pang, S. S. Co-gasification of blended lignite and wood pellets in a 100 kW dual fluidised bed steam gasifier: The influence of lignite ratio on producer gas composition and tar content. *Fuel* **2013**, *112*, 117−124.
(32) Kern, S. J.; Pfeifer, C.; Hofbauer, H. Cogasification of Polyethylene and Lignite in a Dual Fluidized Bed Gasifier. *Ind. Eng. Chem. Res.* **2013**, *52* (11), 4360−4371.
(33) Hofbauer, H.; Rauch, R.; Bosch, K.; Koch, R.; Aichernig, C. Biomass CHP Plant Güssing: A Success Story. In *Pyrolysis and Gasification of Biomass and Waste*; Bridgewater, A. V., Ed.; CPL Press: U.K., 2003; pp 527−36.
(34) Ma, Z.; Glatzmaier, G.; Mehos, M. Fluidized bed technology for concentrating solar power with thermal energy storage. *J. Sol. Energy Eng.* **2014**, *136* (3), 031014.
(35) Kern, S.; Pfeifer, C.; Hofbauer, H. Gasification of lignite in a dual fluidized bed gasifier - Influence of bed material particle size and the amount of steam. *Fuel Process. Technol.* **2013**, *111*, 1−13.
(36) Kern, S.; Pfeifer, C.; Hofbauer, H. Co-Gasification of Wood and Lignite in a Dual Fluidized Bed Gasifier. *Energy Fuels* **2013**, *27* (2), 919−931.
(37) Basu, P., Hydrodynamics. In *Combustion and Gasification in Fluidized Beds*; CRC Press: Boca Raton, FL, 2006; pp 35−42.
(38) Alonso, E.; Romero, M. Review of experimental investigation on directly irradiated particles solar reactors. *Renewable Sustainable Energy Rev.* **2015**, *41*.
(39) Ho, C. K.; Iverson, B. D. Review of high-temperature central receiver designs for concentrating solar power. *Renewable Sustainable Energy Rev.* **2014**, *29*, 835−846.
(40) Koppatz, S.; Pfeifer, C.; Hofbauer, H. Comparison of the performance behaviour of silica sand and olivine in a dual fluidised bed reactor system for steam gasification of biomass at pilot plant scale. *Chem. Eng. J.* **2011**, *175*, 468−483.
(41) Kuhn, J. N.; Zhao, Z. K.; Felix, L. G.; Slimane, R. B.; Choi, C. W.; Ozkan, U. S. Olivine catalysts for methane- and tar-steam reforming. *Appl. Catal., B* **2008**, *81* (1−2), 14−26.
(42) Christian, J.; Ho, C. Alternative designs of a high efficiency, north-facing, solid particle receiver. *Procedia* **2014**, *49*, 314−323.
(43) Meier, A.; Gremaud, N.; Steinfeld, A. Economic evaluation of the industrial solar production of lime. *Energy Convers. Manage.* **2005**, *46* (6), 905−926.
(44) Segal, A.; Epstein, M.; Yogev, A. Hybrid concentrated photovoltaic and thermal power conversion at different spectral bands. *Sol. Energy* **2004**, *76* (5), 591−601.
(45) Wei, X. D.; Lu, Z. W.; Wang, Z. F.; Yu, W. X.; Zhang, H. X.; Yao, Z. H. A new method for the design of the heliostat field layout for solar tower power plant. *Renewable Energy* **2010**, *35* (9), 1970−1975.
(46) Fernandez, P.; Miller, F.; McDowell, M.; Hunt, A. Design space exploration of a 5 MWth small particle solar receiver. *Procedia* **2014**, *49*, 344−353.
(47) Zhang, H. L.; Wang, Z. F.; Guo, M. H.; Liang, W. F. Cosine efficiency distribution of heliostats field of solar thermal power tower plants. In *Asia-Pacific Power and Energy Engineering Conference (Appeec)*, 2009.
(48) Kueh, K.; Nathan, G. J.; Saw, W. L. Sizing a Solar Thermal Plant for Continuous Power Output. *Sol. Energy* Submitted.
(49) Abdelouahed, L.; Authier, O.; Mauviel, G.; Corriou, J. P.; Verdier, G.; Dufour, A. Detailed Modeling of Biomass Gasification in Dual Fluidized Bed Reactors under Aspen Plus. *Energy Fuels* **2012**, *26* (6), 3840−3855.
(50) Goyal, A.; Rehmat, A. Modeling of a Fluidized-Bed Coal Carbonizer. *Ind. Eng. Chem. Res.* **1993**, *32* (7), 1396−1410.
(51) Spath, P.; Aden, A.; Eggeman, T.; Ringer, M.; Wallace, B.; Jechura, J. *Biomass to Hydrogen Production Detailed Design and Economics Utilizing the Battelle Columbus Laboratory Indirectly-Heated Gasifier*; NREL: Golden, CO, 2005.
(52) Chiesa, P.; Consonni, S.; Kreutz, T.; Williams, R. Co-production of hydrogen, electricity and CO_2 from coal with commercially ready technology. PartA: Performance and emissions. *Int. J. Hydrogen Energy* **2005**, *30* (7), 747−767.
(53) Laan, G. P. v. d. *Kinetics, Selectivity and Scale Up of the Fischer−Tropsch Synthesis*; University of Groningen: Groningen, The Netherlands, 1999.

DOI: 10.1021/acs.energyfuels.5b00007
Energy Fuels 2015, 29, 2738−2751

(54) NREL. National Solar Radiation Database 1991−2010 update. http://rredc.nrel.gov/solar/old_data/nsrdb/1991-2010/.
(55) Australian Government Bureau of Meteorology (BOM). One minute solar data. http://reg.bom.gov.au/climate/reg/oneminsolar/.
(56) Suuberg, E. M.; Peters, W. A.; Howard, J. B. Product Composition and Kinetics of Lignite Pyrolysis. *Ind. Eng. Chem. Process Des. Dev.* **1978**, *17* (1), 37−46.

DOI: 10.1021/acs.energyfuels.5b00007
Energy Fuels 2015, 29, 2738−2751

CHAPTER 4

SYSTEM OPTIMIZATION FOR FISCHER−TROPSCH LIQUID FUELS PRODUCTION VIA SOLAR HYBRIDIZED DUAL FLUIDIZED BED GASIFICATION OF SOLID FUELS

Peijun Guo[*,†,‡], Woei L. Saw[†,‡], Philip J. van Eyk[†,‡], Ellen B. Stechel[¤],

Peter J. Ashman[†,‡] and Graham J. Nathan[†,§]

[†]*Centre for Energy Technology,* [‡]*School of Chemical Engineering and* [§]*School of Mechanical Engineering, The University of Adelaide, SA 5005, Australia*
[¤]*Light Works, Arizona State University, Tempe, AZ, USA*

Energy & Fuels 31 (2017) 2033-2043

Statement of Authorship

Title of Paper	System optimization for Fischer-Tropsch liquid fuels production via solar hybridized dual fluidized bed gasification of solid fuels
Publication Status	☐ Published ☐ Accepted for Publication ☑ Submitted for Publication ☐ Unpublished and Unsubmitted work written in manuscript style
Publication Details	Guo, P., Saw, W. L., van Eyk, P. J., Stechel, E. B., Ashman, P. J., and Nathan, G. J. System optimization for Fischer-Tropsch liquid fuels production via solar hybridized dual fluidized bed gasification of solid fuels. Energy & Fuels, In revision for resubmitting.

Principal Author

Name of Principal Author (Candidate)	Peijun Guo
Contribution to the Paper	Performed the system modelling, interpreted results, wrote manuscript and acted as corresponding author.
Overall percentage (%)	65%
Certification:	This paper reports on original research I conducted during the period of my Higher Degree by Research candidature and is not subject to any obligations or contractual agreements with a third party that would constrain its inclusion in this thesis. I am the primary author of this paper.
Signature	Date: 6/10/2016

Co-Author Contributions

By signing the Statement of Authorship, each author certifies that:

i. the candidate's stated contribution to the publication is accurate (as detailed above);

ii. permission is granted for the candidate in include the publication in the thesis; and

iii. the sum of all co-author contributions is equal to 100% less the candidate's stated contribution.

Name of Co-Author	Woei L. Saw
Contribution to the Paper	Supervised development of work, helped in data interpretation and manuscript evaluation.
Signature	Date: 6/10/2016
Name of Co-Author	Philip J. van Eyk
Contribution to the Paper	Supervised development of work, helped in data interpretation and manuscript evaluation.
Signature	Date: 6/10/2016
Name of Co-Author	Ellen B. Stechel
Contribution to the Paper	Supervised development of work, helped in data interpretation and manuscript evaluation.
Signature	Date: 6/10/2016
Name of Co-Author	Peter J. Ashman
Contribution to the Paper	Supervised development of work, helped in data interpretation and manuscript evaluation.
Signature	Date: 7/10/16
Name of Co-Author	Graham J. Nathan
Contribution to the Paper	Supervised development of work, helped in data interpretation and manuscript evaluation.
Signature	Date: 6/10/2016

energy&fuels

Article

pubs.acs.org/EF

System Optimization for Fischer–Tropsch Liquid Fuels Production via Solar Hybridized Dual Fluidized Bed Gasification of Solid Fuels

Peijun Guo,*[,†,‡] Woei L. Saw,[†,‡] Philip J. van Eyk,[†,‡] Ellen B. Stechel,[∥] Peter J. Ashman,[†,‡] and Graham J. Nathan[‡,§]

[†]Centre for Energy Technology, [‡]School of Chemical Engineering, and [§]School of Mechanical Engineering, The University of Adelaide, Adelaide, South Australia 5005, Australia

[∥]Light Works, Arizona State University, Tempe, Arizona 85281, United States

Supporting Information

ABSTRACT: A new configuration of solar hybridized dual fluidized bed (DFB) gasification process is proposed with char separation for the production of Fischer–Tropsch (FT) liquid fuels from solid fuels of biomass and/or coal. The addition of carbon capture with sequestration and FT reactor tail-gas recycle configurations is also assessed. The studied FT liquid fuels production systems are simulated by using a pseudodynamic model incorporating a year long, hourly averaged solar insolation time-series. For the case with a solar multiple (i.e., the heliostat field area relative to that required to meet the demand of the DFB gasifier at the point of peak solar thermal output) of 2.64 and bed material storage capacity of 16 h, the calculated annual solar share of the solar hybridized coal-to-liquids system can be increased from 12.2 to 20.3% by the addition of the char separation for a char gasification conversion of 80%. To achieve the well-to-wheel greenhouse gas emissions for FT liquid fuels parity with diesel derived from mineral crude oil, a calculated biomass fraction of 58% is required for the nonsolar coal case, also with a char gasification conversion of 80%. This fraction can be reduced to 30% by carbon capture and sequestration and further reduced to 17% by the integration of solar energy, based on a solar multiple of 2.64 and bed material storage capacity of 16 h. This reduction is significant given that biomass is much more expensive than coal. However, because of the higher content of light hydrocarbons content in the syngas produced with the studied biomass gasification, the specific FT liquids output per unit feedstock of the system decreases with an increase in the biomass fraction. As the biomass fraction is increased from 0 to 100%, this specific output is decreased from 59.6 to 48.3% but can be increased to 71.5 and 70.9%, respectively, by incorporating tail-gas recycle.

1. INTRODUCTION

Fischer–Tropsch (FT) liquid fuels are expected to play an important role in meeting the long-term demand for reliable alternative sources of liquid transport fuels.[1] FT liquid fuels production via coal gasification has received much interest due to the plentiful reserves of coal and their low cost.[2−5] However, the implementation of coal-to-liquids (CTL) systems is constrained by their high greenhouse gas (GHG) emissions.[6−8] As a potential path to mitigate these emissions, two kinds of promising renewable energy, biomass and solar energy, have received growing attention as partial or total substitutes for the coal feed. The gasification of biomass and its cogasification with coal are well-demonstrated, especially in fluidized beds[9−11] and have also been assessed for FT liquid fuels production systems.[12−14] Solar gasification has also been proposed, utilizing concentrated solar thermal energy to drive the endothermic gasification reactions, thereby reducing both the GHG emissions and the feedstock consumption.[15] However, less attention has been paid to the comprehensive analysis of the FT liquid fuels production by solar hybridized gasification of biomass and/or coal, so there is significant potential to improve on the concepts proposed previously.[8,16,17] Hence, the overall objective of current investigation is to identify preferred configurations of solar hybridized coal and/or biomass to FT liquid fuels systems.

Of the recent solar hybridized coal and/or biomass to FT liquid fuels systems, the high gasification temperature (>1200 °C),[8,16] the need for storage of syngas,[8,16,18] and the need for high-temperature molten salt storage[19,20] has impeded their application. To lower these challenges, Guo et al.[17] proposed a solar hybridized CTL (SCTL) system with a solar hybridized dual fluidized bed (SDFB) gasifier and sensible heat storage of the hot solid bed material. This system uses solid bed material as a medium to transfer heat from the fast fluidized bed combustor and/or the solar receiver to the bubbling fluidized bed gasifier. Due to the separation of the gasification and combustion processes in SDFB gasifier and the utilization of sensible heat storage of the hot solid bed material, the steady and high-quality (i.e., with low N_2 content) syngas output can be achieved without the need for an expensive air separation unit. For a solar multiple of 3 and a bed material storage capacity of 16 h, they reported an increase of 32.6% in annual FT liquids output per unit feedstock and a reduction of 34.1% in mine-to-tank GHG emissions for this SCTL system relative to the equivalent nonsolar CTL system, as the char gasification conversion was assumed to be 100%. However, they also found that the mine-to-tank GHG emissions for FT liquid fuels produced with coal as the feedstock are still higher than those associated with producing liquid fuels from conventional mineral crude. In addition, the solar share of this SCTL system

Received: July 18, 2016
Revised: December 8, 2016
Published: December 12, 2016

DOI: 10.1021/acs.energyfuels.6b01755
Energy Fuels 2017, 31, 2033−2043

depends strongly on the char gasification conversion,[17] which was measured to be only 50−60% for lab-/pilot-scale dual fluidized bed (DFB) gasification of lignite.[10,21,22] This char conversion can potentially be improved by increasing the scale and by better gasifier design, but the extent to which this can be achieved is yet to be reported. Therefore, new approaches are needed with which to further improve the energetic and environmental performance of the SCTL system, especially under relatively low char gasification conversions. Three potential approaches to achieve this are proposed and assessed in this study: (1) char separation from the output solid mixture of the bubbling fluidized gasifier; (2) cogasification of biomass and lignite with and without carbon capture and sequestration (CCS) technology; and (3) FT reactor tail-gas recycle. Hence, the present study aims to assess the influences of these new approaches on the energetic and environmental performance of the coal and/or biomass-to-liquids systems via an SDFB gasifier.

The combustion of unconverted char in the fast fluidized bed combustor was found to limit the solar input to the SDFB gasifier.[17] The proposed integration of char separation has potential to enable a greater share of solar energy to heat the bed material by avoiding combustion when solar energy is available. It further allows the potential for the storage of char when the solar resource is available for use in the fluidized bed combustor when fuel is needed. The binary mixture of bed material and char can potentially be separated using a fluidized bed due to the significant difference in the density and size of the two types of particle. Such a fluidized bed system has been demonstrated in a continuous biochar separation experiment with over 90% separation efficiency.[23] However, the influence of the char separation on the performance of the solar hybridized coal and/or biomass-to-liquids systems has not been assessed yet.

Both the cogasification of biomass with coal and the use of CCS technology have been widely studied with a view to lowering the GHG emissions from the production of FT liquid fuels to below the reference case of conventional mineral crude. Parity of the life cycle GHG emissions for the liquid fuels produced from conventional mineral crude oil was shown to be possible for FT liquid fuels produced from coal and biomass-to-liquids (CTL_{bio}) system with CCS technology and 9% biomass fraction (higher heating value (HHV) basis).[12−14] Furthermore, these GHG emissions can potentially be reduced to zero if the biomass fraction is increased to 37.4%.[13] To reduce the mine-to-tank GHG emissions for the FT liquid fuels to below that for the diesel derived from mineral crude, a 53% biomass cogasification fraction, by weight, is required for the solar hybrid CTL_{bio} ($SCTL_{bio}$) system with a solar hybrid vortex flow gasifier[15] in which the solid particles are distributed in a cloud close to the wall and the solar radiation is introduced to the reaction zones directly through a window.[16] However, for the nonsolar equivalent, this biomass cogasificaiton fraction is 65%. This reduction in the required biomass fraction with the use of solar is significant both because of challenge of maintaining a steady and sustainable supply of biomass, especially for large-scale applications and because of the challenges of high biomass blend ratios in a gasifier design.[24,25] In addition, economic benefits can also be achieved by reducing the biomass fraction because biomass is typically 3−4 times more expensive than coal.[25−27] However, no equivalent study has been reported for the $SCTL_{bio}$ system with an SDFB gasifier, which should be more suitable for cogasification of biomass and coal than the vortex flow gasifier.[10,11] Moreover, the influence of CCS technology on the performance of this $SCTL_{bio}$ system is also yet to be reported.

To increase the FT liquid fuels output, it has been proposed that the tail gases from the FT reactor and FT liquids upgrading system be recycled back to the FT reactor via an auto−thermal reformer which converts the light gases to syngas.[2,3,12−14,27−29] Compared with the once-through CTL system, another 11.8% of the input energy to the CTL system with tail-gas recycle is transferred into FT liquid fuels.[12,13] However, no equivalent investigation has been reported for the coal and/or biomass-to-liquids systems with an SDFB gasifier. In addition, there are potential benefits from incorporating an indirectly heated tubular reformer into the gasifier to eliminate the expensive air separation unit that is usually required for an autothermal reformer.[2,16] Moreover, the endothermic reforming reactions occurred in the indirect heat reformer can also been driven by solar thermal heat as gasification reactions, thus increasing the solar share of the solar hybridized coal and/or biomass-to-liquids systems.

In summary, the present paper proposes new approaches to optimize the performance of the solar hybridized FT liquid fuels production system via an SDFB gasifier, notably the addition of char separation, the cogasification of biomass with coal, the incorporation of carbon capture with sequestration and the use of tail-gas recycle. It then aims to assess the influences of these approaches on the performance of the system.

2. METHODOLOGY

2.1. System Description. Figure 1 presents a simplified flowsheet of the coal and/or biomass-to-liquids system studied in the present paper. This extends further the system proposed previously by Guo et al.[17] by the addition of the configurations of CCS and tail-gas recycle. The feedstock of the system can be coal and/or biomass. The use of

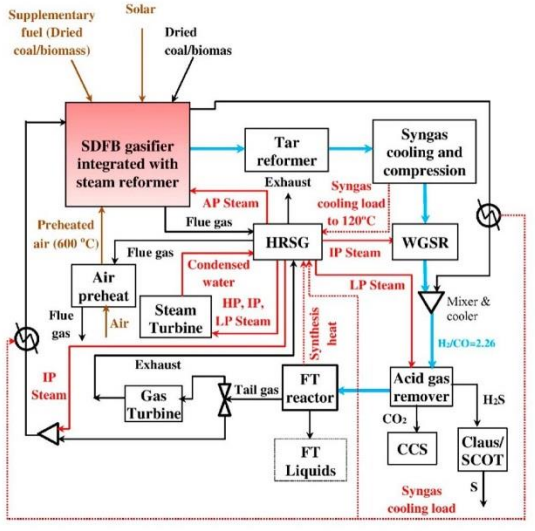

Figure 1. Simplified flowsheet of the proposed solar hybridized coal and/or biomass-to-liquids process with the proposed solar hybridized dual fluidized bed (SDFB) gasifier, carbon capture and sequestration (CCS), and tail-gas recycle.

DOI: 10.1021/acs.energyfuels.6b01755
Energy Fuels 2017, 31, 2033−2043

CCS is assumed to be applied only to the pure CO_2 stream from the acid gas remover, for subsequent compression and sequestration, while the stream of dilute CO_2 from both the fluidized bed combustor and the gas turbine are assumed to be vented. The configuration with tail-gas recycle assumes that the tail-gas from the FT reactor be mixed with steam and then preheated with the hot syngas from the steam reformer. The steam reforming reactions are assumed to occur within the steam reformer while the syngas from the steam reformer is proposed to be further cooled down by the heat recovery and steam generator (HRSG) before being recycled back to the FT reactor via an acid gas remover.

Figure 2 presents a system diagram of the SDFB gasifier studied in the present paper. This extends further the SDFB system proposed

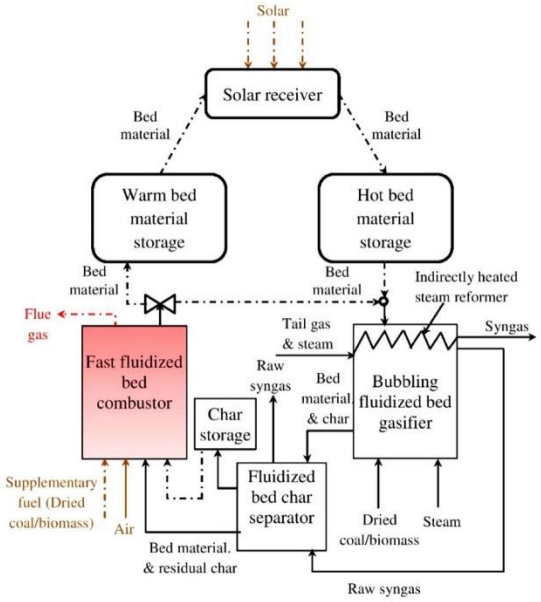

Figure 2. Flowsheet of the proposed SDFB gasifier with an integrated solar receiver, sensible heat storage of bed material, char separator, and tail-gas steam reformer. The dotted−dashed lines represent unsteady streams, while the solid lines represent steady streams.

previously by Guo et al.[17] by the addition of configurations of char separation and steam reformer. In present study, a fluidized bed char separator is proposed to separate the char using the raw syngas from the bubbling fluidized bed gasifier as fluidizing agent. This concept can also further increase the char gasification conversion and reduce the tar content in the raw syngas. The sensible heat of the separated char is proposed to be recovered via the inlet steam to the bubbling fluidized bed gasifier. An indirectly heated steam reformer (detailed in section 2.2.4) is proposed to be integrated with the bubbling fluidized bed gasifier while the steam reforming reactions in the reformer are proposed to be driven by the heat from the hot bed material fed to the bubbling fluidized bed gasifier.

To accommodate the intermittent and variable solar resource, the control of the SDFB gasifier is based on the operational strategy described by Guo et al.[17] This approach allows the gasifier, the steam reformer, and the fluidized bed char separator to all be operated at steady state. The solar variability is accommodated upstream from the gasifier, and the supplementary fuel is employed only when both the solar energy and the stored char are insufficient.

2.2. Process Model. In the present investigation, the simulation of the solar hybridized coal and/or biomass-to-liquids systems is based on the pseudodynamic model described previously.[8,17] This model was employed by assuming a steady-state operation for each 1 h time-step in a 1 year time series of historical direct normal insolation (DNI) data and by following the operational strategy proposed by the authors previously.[17] The time series of the solar resource used in the present investigation was for the summer-to-summer period June 1, 2004 to May 31, 2005 at Farmington, in northern New Mexico, USA, whose latitude is 37° N.[17,30] In addition, the models of the additional configurations proposed in the present paper are described in the following sections.

2.2.1. Char Separation. The DFB gasifier model is based on that developed by Guo et al.[17] with the following additional assumptions and specifications: (i) The purity of the separated char (i.e., the mass fraction of the char in the total separated solids) is assumed to be 100%. (ii) The outlet temperatures of the separated char, fluidizing agent, and bed material from the fluidized bed char separator are all assumed to be 850 °C. (iii) The hot separated char is assumed to be cooled to 150 °C by the steam input to the bubbling fluidized bed gasifier. In addition, the temperature of the char in the char storage unit is assumed to be 25 °C. (iv) The char overall gasification conversion ($X_{char,G}$) is defined to include both the conversion of the char in the bubbling fluidized bed gasifier and fluidized bed char separator. (v) The heat losses from the wall of the fluidized bed char separator are assumed to be 1% of the higher heating value of the total input fuel to the DFB gasifier when operated under non solar conditions. These heat losses are assumed to be independent from the introduction of solar energy. (vi) The stored char is assumed to be only an intermediated product rather than a final product. We therefore impose the condition that the stored char be consumed completely by the end of the time series investigated (1 year).

2.2.2. Cogasification of Coal and Biomass. The properties of the selected feedstock, Montana lignite[31,32] and spruce wood,[33,34] are shown in Table 1. The fuel blend of coal and biomass is assumed to be

Table 1. Proximate and Ultimate Analysis of Montana Lignite[31,32] and Spruce Wood[33,34]

	Montana lignite	spruce wood
	Proximate Analysis (wt %)	
fixed carbon	46.4	15.1
volatile matter	36.9	77.7
moisture	6.8	7
ash	9.9	0.3
	Ultimate Analysis (wt % dry)	
C	63.6	48
H	4.1	6.2
O	19.5	45.6
N	2	0.2
Cl	0	
S	1.3	
ash	10.6	0.3

dried to 2% (weight basis) moisture. The simulation of the wood pyrolysis process is based on the experimentally determined correlations reported in the literature.[33,34] The carbon closure of the biomass is assumed to be 85% in present investigation to account for the GHG emissions associated with the cultivation, harvest, transportation, and so on.[35,36] For each scenario investigated here, the conversions of biochar and coal char gasification are assumed to be the same. In addition, the char separation efficiencies (i.e., the fraction of the separated char relative to the total char in the input mixture) of the biochar and coal char are assumed to be the same for a system with char separation.

2.2.3. Carbon Capture and Sequestration (CCS). As described in section 2.1, only the pure CO_2 stream from acid gas remover is proposed to be compressed for sequestration. A four-staged intercooled compressor is proposed to compress this pure CO_2 stream to 120 bar with an assumed isentropic efficiency of 83%.

DOI: 10.1021/acs.energyfuels.6b01755
Energy Fuels 2017, 31, 2033−2043

This assumed pressure is suitable for the CO_2 transportation and sequestration into deep saline formations.[37]

2.2.4. Tail-Gas Recycle. To improve the FT liquids output from the solar hybridized coal and/or biomass-to-liquids system, part of the FT reactor tail-gas is proposed to be recycled back to FT reactor via a steam reformer integrated in the bubbling fluidized bed gasifier and then via an acid gas remover. The assumptions and specifications for this are as follows: (i) It is assumed that the tail-gas is split into two streams, with 90% sent to the steam reformer and the remainder sent to the gas turbine. (ii) The input molar ratio of steam to carbon (in the hydrocarbons) for the steam reformer is assumed to be 2.[12] (iii) The operating temperature of the reformer is assumed to be 850 °C,[2,12] while the temperature of the hot bed material fed to the bubbling fluidized bed gasifier was set to be 950 °C following Guo et al.[17] This hot bed material supplies the heat required by the steam reformer. (iv) The RGibbs reactor module of Aspen Plus V7.1 was used to model the steam reformer by minimizing the Gibbs free energy to determine the equilibrium composition of the outlet.[12] (v) The input tail-gas and steam to the steam reformer are proposed to be preheated to 500 °C by the hot output syngas from the steam reformer. This hot output syngas is proposed to be further cooled down to 120 °C by the HRSG. (vi) The water−gas shift reactor (WGSR) is proposed here to maintain a constant H_2/CO ratio (~2.26) in the syngas input to the FT reactor.

2.3. System Performance Analysis. The influences of the options proposed above are investigated by comparing the performance of the solar hybridized FTL fuels production systems with these various proposed additions with the performance of the previously proposed system[17] without these additions. To better understand the impact of the proposed new configurations, the performance of the systems is assessed by varying systematically the bed material sensible heat storage capacity (SC_{BM}, i.e., maximum operation hours without both solar radiation and supplementary feed, eq 1), the solar multiple (SM,[17] eq 2), the biomass fraction in the blend of biomass and coal based on higher heating value (HHV) ($F_{bio,HHV}$, eq 3), the char gasification conversion ($X_{char,G}$) and the char separation efficiency ($\eta_{char\text{-}sep}$, i.e., the fraction of the separated char relative to the total char in the input mixture).

$$SC_{BM} = \frac{m_{store,BM}}{\dot{m}_{G,BM}} \quad (1)$$

$$SM = \frac{A_{coll}}{A_{coll}^{DFB}} \quad (2)$$

$$F_{bio,HHV} = \frac{\dot{Q}_{bio,HHV}}{\dot{Q}_{feed,HHV}} \quad (3)$$

Here, $m_{store,BM}$ is the mass capacity of the hot bed material storage unit; $\dot{m}_{G,BM}$ is the mass flow rate of hot bed material to the gasifier; A_{coll} is the heliostat collector area; A_{coll}^{DFB} is the heliostat field area required to generate the net heat required by the DFB gasifier at the annual peak solar resource;[17] and $\dot{Q}_{bio,HHV}$ and $\dot{Q}_{feed,HHV}$ are the higher heating values of the input biomass and the input feedstock (i.e., of both coal and biomass), respectively.

To evaluate the annual performance of the solar hybridized coal and/or biomass to liquids system, the following metrics were used:

annual solar share,[17,38] SS_{ann}:

$$SS_{ann} = \frac{(Q_{net,sol})_{ann}}{(Q_{net,sol})_{ann} + (Q_{feed,HHV})_{ann}} \times 100\% \quad (4)$$

annual specific FT liquids output per unit of feedstock, $Q_{s,FTL,ann}$:

$$Q_{s,FTL,ann} = \frac{(Q_{FTL,HHV})_{ann}}{(Q_{feed,HHV})_{ann}} \times 100\% \quad (5)$$

annual specific net electricity output per unit of feedstock, $W_{s,net,ann}$:

$$W_{s,net,ann} = \frac{(W_{net})_{ann}}{(Q_{feed,HHV})_{ann}} \times 100\% \quad (6)$$

annual well-to-wheel (WTW) CO_2 emissions, $E_{CO_2,eq,ann}$:

$$E_{CO_2,eq,ann} = \frac{(m_{CO_2,eq})_{ann}}{(Q_{FTL,HHV})_{ann} + (W_{net})_{ann}} \quad (7)$$

Here, $(Q_{feed,HHV})_{ann}$ is the HHV of the annual input of feedstock to the DFB gasifier, $(Q_{FTL,HHV})_{ann}$ is the HHV of the annual FT liquids output, $(W_{net})_{ann}$ is the annual net electricity output from the system, and $(m_{CO_2,eq})_{ann}$ is the annual mass-based WTW equivalent CO_2 emissions associated with the FT liquid fuels production. The emission sources accounted for herein are those from mining the coal resource,[39] FT liquids production process, FT synthetic fuel to diesel refinery process,[7,39] FT liquid fuels combustion process, and transportation emissions for coal and FT liquid fuels.[7,39] However, those emissions associated with the plant construction are not included here since its contribution is small over the life of the plant. Furthermore, the carbon closure is assumed to be 85% for biomass.[35,36]

3. RESULTS AND DISCUSSION

3.1. Effect of Char Separation. Figure 3 presents the calculated annual supplementary feed to the combustor

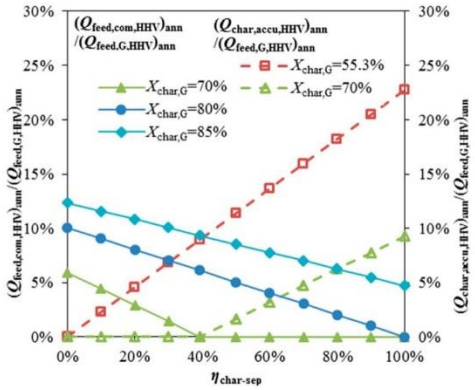

Figure 3. Calculated annual net supplementary feed required for combustor ($(Q_{feed,com,HHV})_{ann}$) or annual char accumulation ($(Q_{char,accu,HHV})_{ann}$), normalized by the annual feed to bubbling fluidized bed gasifier ($(Q_{feed,G})_{ann,HHV}$) as a function of char separation efficiency for various of char gasification conversions ($X_{char,G}$). Conditions: Solar multiple = 2.64, bed material storage capacity = 16 h.

($(Q_{feed,com,HHV})_{ann}$) and the annual char accumulation ($(Q_{char,accu,HHV})_{ann}$) normalized by the annual feed into the gasifier ($(Q_{feed,G,HHV})_{ann}$) as a function of char separation efficiency ($\eta_{char\text{-}sep}$, i.e., the fraction of the separated char relative to the total char in the input mixture) for various of char gasification conversions ($X_{char,G}$). These are calculated for a solar multiple (SM) of 2.64 and for a bed material storage capacity (SC_{BM}) of 16 h. In addition, in this section, only coal is considered as the feedstock. As shown in Figure 3, for the case of $X_{char,G}$ = 55.3%, the annual accumulation of char cannot be avoid unless the $\eta_{char\text{-}sep}$ is 0. This implies that this conversion corresponds to case where the amount of char generated by the

DOI: 10.1021/acs.energyfuels.6b01755
Energy Fuels 2017, 31, 2033−2043

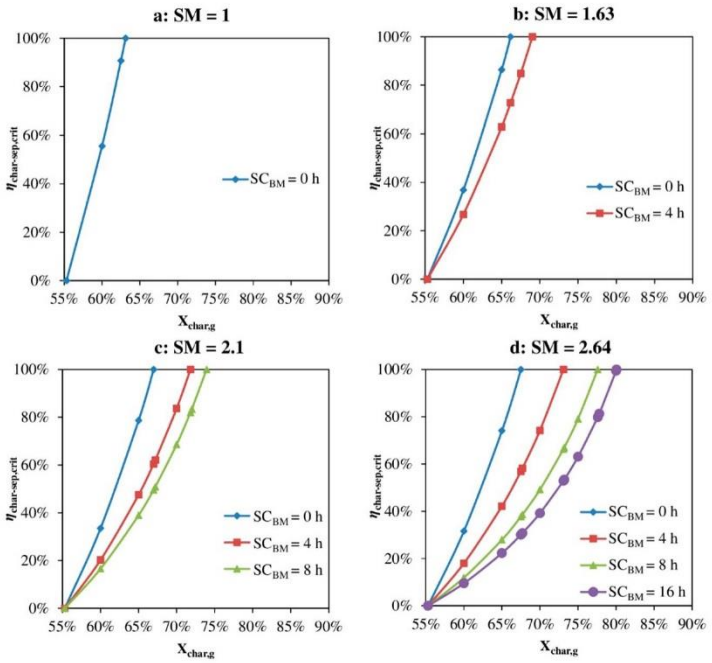

Figure 4. Calculated dependence on char gasification conversion ($X_{char,G}$) of the critical char separation efficiency ($\eta_{char-sep,crit}$) to avoid both annual char accumulation and annual supplementary feed, for various solar multiples (SM) and bed material storage capacities (SC_{BM}). Note: The $\eta_{char-sep,crit}$ of 100% corresponds to the critical $X_{char,G}$.

gasifier exactly matches the energy required to be supplied by the combustor. Any separation of char when solar energy is available will lead to annual char accumulation. For this reason, the minimum conversion investigated here is $X_{char,G}$ = 55.3%. In contrast, the case of $X_{char,G}$ = 80% corresponds to the condition in which no char is accumulated after 1 year of operation even with a $\eta_{char-sep}$ of 100%. However, for a lower $\eta_{char-sep}$, some supplementary feed will be required. Hence, this char gasification conversion is termed the critical char gasification conversion ($X_{char,G,crit}$). For conversions above this, such as $X_{char,G}$ = 85% shown in Figure 3, no char is accumulated over the year, but instead some supplementary feed is required. However, for any value of $X_{char,G}$ between 55.3% and the critical conversion (e.g., $X_{char,G}$ = 70%), there is also a critical value of $\eta_{char-sep}$ (here 39.3%) required to avoid both annual char accumulation and supplementary feed. For efficiencies greater than this critical char separation efficiency ($\eta_{char-sep,crit}$), char will be accumulated over the year, while the supplementary feed will be required for those efficiencies lower than this $\eta_{char-sep,crit}$.

Figure 4 presents the calculated dependence on char gasification conversion ($X_{char,G}$) of the critical char separation efficiency ($\eta_{char-sep,crit}$), the $\eta_{char-sep}$ required to avoid both annual char accumulation and supplementary feed for various solar multiples (SM = 1, 1.63, 2.1 and 2.64), and bed material storage capacities (SC_{BM} = 0, 4, 8, and 16 h). The upper limit of 90% for $X_{char,G}$ has been imposed because the high ash content and low heating value of the present char is anticipated to make operation of char separation impractical. As reported by Guo et al.,[17] for each SM, there is a threshold bed material storage capacity required to avoid solar dumping ($SC_{BM,no-dump}$), as shown in Table 2. For this reason, any SC_{BM} larger than

Table 2. Selected Solar Multiples (SM) and the Corresponding Threshold Capacities of Bed Material Storage Required to Avoid Solar Dumping ($SC_{BM,no-dump}$)

	SM = 1	SM = 1.63	SM = 2.1	SM = 2.64
$SC_{BM,no-dump}$ (h)	0	4	8	16

$SC_{BM,no-dump}$ should be avoided and was not investigated in present study. It can be seen that $\eta_{char-sep,crit}$ increases monotonically from 0 to 100% as the $X_{char,G}$ is increased from 55.3%. In addition, the $\eta_{char-sep,crit}$ of 100% corresponds to the critical $X_{char,G}$ ($X_{char,G,crit}$). It can also been seen that an increase in either the SM or the SC_{BM} increases the $X_{char,G,crit}$. For SC_{BM} = 0 h, the $X_{char,G,crit}$ increases from 63.1 to 67.5% with an increase in SM from 1 to 2.64. This $X_{char,G,crit}$ can is further increased to 80% with an increase in SC_{BM} from 0 to 16 h.

3.1.1. Effect of Char Separation on the Performance of the SCTL System. Figure 5 presents the calculated annually averaged solar share (SS_{ann}) of the SCTL system with and without char separation as a function of char gasification conversion ($X_{char,G}$) for various values of solar multiple (SM) and bed material storage capacity (SC_{BM}). Here, we have set $\eta_{char-sep}$ as equal to $\eta_{char-sep,crit}$ (shown in Figure 4) for $X_{char,G} \leq X_{char,G,crit}$ (shown in Figure 4) and to 100% for $X_{char,G} > X_{char,G,crit}$ both to avoid annual char accumulation and to minimize the requirement for supplementary feed. It can be seen that for the same values of SM and SC_{BM} the value of SS_{ann} with char separation is greater than that for the SCTL system without char separation. Moreover, this difference increases to a peak as $X_{char,G}$ is increased toward $X_{char,G,crit}$. For the case SM = 1 and SC_{BM} = 0, the value of SS_{ann} without char separation can be increased monotonically from 0 to 6% as $X_{char,G}$ is increased

DOI: 10.1021/acs.energyfuels.6b01755
Energy Fuels 2017, 31, 2033−2043

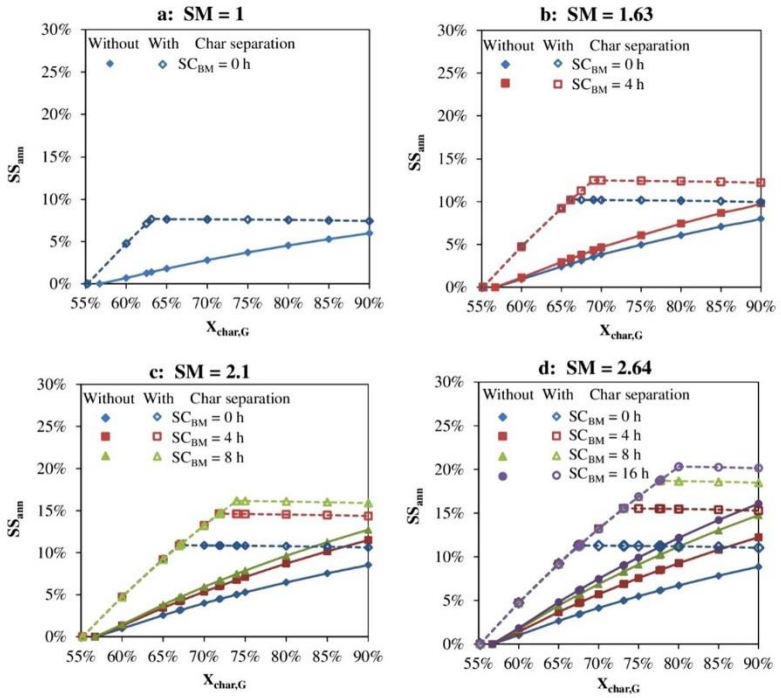

Figure 5. Calculated annually averaged solar share (SS_{ann}) for the SCTL system with and without char separation as a function of char gasification conversion ($X_{char,G}$) for various values of solar multiple (SM) and bed material storage capacities (SC_{BM}). The char separation efficiencies are set to critical values (shown in Figure 4) for $X_{char,G}$ less than its critical value (shown in Figure 4) and to 100% for $X_{char,G}$ greater than the critical value.

from 55.3 to 90% (Figure 5a). In contrast, the value of SS_{ann} with char separation increases further to 7.4% with an increase in $X_{char,G}$ from 55.3 to 63.1%. This increase is caused by the increase in $\eta_{char\text{-}sep}$ (from 0 to 100%). An increase in $\eta_{char\text{-}sep}$ results in less char combustion in the combustor and a higher solar input for the case with char separation, thus increasing SS_{ann}. However, SS_{ann} reaches an almost constant value for $X_{char,G} > X_{char,G,crit}$. For the maximum value of $\eta_{char\text{-}sep}$ (100%), an increase in $X_{char,G}$ reduces the amount of char generated by gasifier which leads to higher supplementary fuel requirement, thus limiting the SS_{ann}. While fluidized bed char separation technology has not yet been demonstrated commercially, developments are in progress to separate char within a bubbling fluidized bed separator.[23] Therefore, it is possible to separate char within the bubbling fluidized bed gasifier of the proposed SDFB system rather than build an additional char separator. This has potential to significantly reduce the additional cost of char separation.

It can also be seen that for the case $X_{char,G} < X_{char,G,crit}$ the value of SS_{ann} with char separation is almost independent from SM and SC_{BM} since the $\eta_{char\text{-}sep,crit}$ is assumed here. As discussed above, both the char accumulation over the year and the requirement of supplementary feed can be avoided for the case with $\eta_{char\text{-}sep,crit}$. Therefore, the heat required by the gasification process is only provided by the char combustion and solar thermal energy. For a certain $X_{char,G}$, both the heat required by the gasification and the amount of char from the bubbling fluidized bed gasifier are constant. Therefore, even for different values of SM and SC_{BM}, the annual solar inputs are similar which results in the similar SS_{ann}. However, for $X_{char,G} > X_{char,G,crit}$, an increase in SM and/or SC_{BM} results in a significant increase in SS_{ann}. For $X_{char,G}$ = 80%, SM = 2.64, and SC = 16 h, the value of the SS_{ann} is 20.3%. However, the SS_{ann} decreases to 11.2% as SC_{BM} is decreased to 0 h and to 7.6% for SM = 1 and SC_{BM} = 0 h.

3.2. Effects of Biomass Cogasification and Carbon Capture and Sequestration (CCS). Figures 6–9 present the

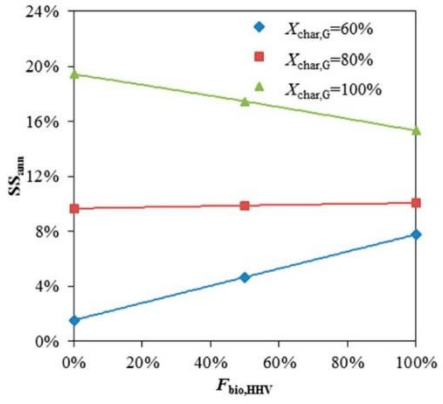

Figure 6. Calculated annually averaged solar share (SS_{ann}) of the solar hybridized coal and biomass-to-liquids ($SCTL_{bio}$) system as a function of biomass fraction based on HHV ($F_{bio,HHV}$) for various values of char gasification conversion ($X_{char,G}$).

DOI: 10.1021/acs.energyfuels.6b01755
Energy Fuels 2017, 31, 2033–2043

effects of biomass cogasification and CCS on the performance of the SCTL system without char separation. Note that the values of SM and SC_{BM} are set to 2.64 and 16 h, respectively. Due to the negligible effect of char gasification conversion ($X_{char,G}$) on the assessed performance of the CTL_{bio} system,[17,40] the performance of the CTL_{bio} system is not assessed for various $X_{char,G}$. Here, the $X_{char,G}$ is set as 80% for the CTL_{bio} system.

3.2.1. Solar Share. Figure 6 presents the calculated annually averaged solar share (SS_{ann}) of the $SCTL_{bio}$ system as a function of the biomass fraction based on HHV ($F_{bio,HHV}$) for various values of char gasification conversion ($X_{char,G}$). As expected, the value of SS_{ann} decreases with a decrease in $X_{char,G}$. However, the effect of $X_{char,G}$ on SS_{ann} decreases with an increase in $F_{bio,HHV}$ due to the lower fixed carbon content in the selected biomass compared with the selected lignite. For $X_{char,G}$ = 100%, the value of SS_{ann} decreases from 15.4 to 12.1%, almost linearly, as $F_{bio,HHV}$ is increased from 0 to 100%. However, for $X_{char,G}$ = 60%, the value of SS_{ann} increases from 1.5 to 7.8%, as $F_{bio,HHV}$ is increased from 0 to 100%.

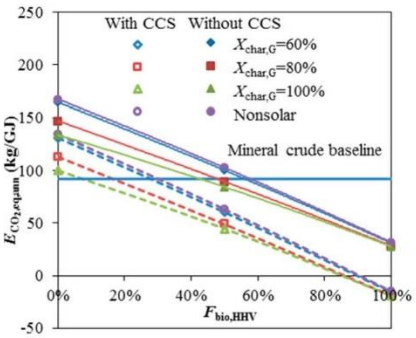

Figure 7. Calculated annual well-to-wheel (WTW) CO_2 emissions ($E_{CO_2,eq,ann}$) for liquid fuels produced by solar hybridized coal/biomass blends with and without carbon capture and sequestration (CCS) as a function of biomass fraction based on HHV ($F_{bio,HHV}$) for various values of char gasification conversion ($X_{char,G}$). The nonsolar CTL_{bio} systems with and without CCS and conventional mineral crude baseline are also shown for comparison.

3.2.2. CO_2 Emissions. Figure 7 presents the calculated well-to-wheel (WTW) CO_2 emissions ($E_{CO_2,eq,ann}$) of the liquid fuels produced by $SCTL_{bio}$ systems with and without CCS as a function of $F_{bio,HHV}$ for various values of $X_{char,G}$. Also shown is $E_{CO_2,eq,ann}$ for the liquid fuels produced by CTL_{bio} systems with and without CCS. To match the WTW CO_2 emissions for the diesel produced from conventional mineral crude oil,[7,39] a value of $F_{bio,HHV}$ = 58% is required for the CTL_{bio} system without CCS, but this is reduced to $F_{bio,HHV}$ = 30% by the integration of CCS. For the same WTW CO_2 emission target and $X_{char,G}$ = 80%, the $F_{bio,HHV}$ is reduced to 47.9% for the CTL_{bio} system without CCS and to 17% with CCS by the integration of solar energy. These reductions of $F_{bio,HHV}$ are significant given that biomass is typically more expensive and less available than lignite. It can also been seen that the effect of solar energy integration on $E_{CO_2,eq,ann}$ for liquid fuels produced from CTL_{bio} system decreases with an increase in $F_{bio,HHV}$. This is to be expected because the biomass is assumed to have a carbon closure of 85%. The additional cost of CCS is around \$15−80 per ton of CO_2 avoided.[41−43] The application of CCS depends strongly on local carbon policy and/or the cost of biomass.

3.2.3. Energetic Output. Figure 8 presents the calculated specific energetic output per unit feedstock of the $SCTL_{bio}$

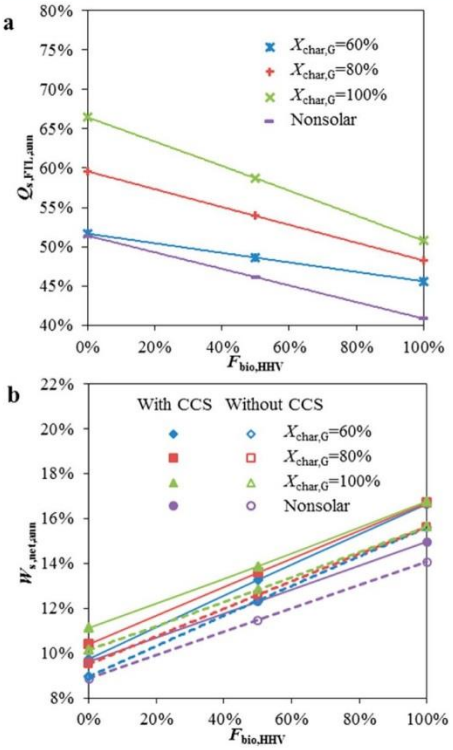

Figure 8. Calculated annual specific FT liquids output per unit feedstock ($Q_{s,FTL,ann}$) and annual specific electricity output per unit feedstock ($W_{s,net,ann}$) of the solar hybridized coal and biomass-to-liquids ($SCTL_{bio}$) systems for the cases with and without carbon capture and sequestration (CCS) as a function of biomass fraction based on HHV ($F_{bio,HHV}$) for various values of char gasification conversion ($X_{char,G}$). $Q_{s,FTL,ann}$ and $W_{s,net,ann}$ of nonsolar CTL_{bio} systems with and without CCS are also shown as a comparison; the influence of CCS on $Q_{s,FTL,ann}$ is negligible and is not shown here.

system with and without CCS as a function of $F_{bio,HHV}$ for various values of $X_{char,G}$. It can be seen that the annual specific electricity output per unit feedstock ($W_{s,net,ann}$) is decreased by using CCS due to the electricity consumed by the CO_2 compression. However, electricity is only a byproduct of the $SCTL_{bio}$ system and is enough to enable self-sufficiency even with CCS incorporated. For this reason, further $SCTL_{bio}$ systems are all assessed for the case with CCS unless otherwise stated, owing to its potential to significantly reduce net CO_2 emissions. It can also be seen that $W_{s,net,ann}$ and $Q_{s,FTL,ann}$ decrease with a decrease in $X_{char,G}$. However, the effect of $X_{char,G}$ on $Q_{s,FTL,ann}$ decreases with an increase in $F_{bio,HHV}$ because of the lower fixed carbon content in the selected biomass compared with the selected lignite. Furthermore, an increase in $F_{bio,HHV}$ results in an increase in $W_{s,net,ann}$ but a

DOI: 10.1021/acs.energyfuels.6b01755
Energy Fuels 2017, 31, 2033−2043

reduction in $Q_{s,FTL,ann}$. This is to be expected because of the increased content of light hydrocarbons in the syngas for the $SCTL_{bio}$ system with a higher $F_{bio,HHV}$.[10,11] In the once-through $SCTL_{bio}$ system assessed here, the increased light hydrocarbon content results in less carbon being stored in FT liquids together with an increased electricity generation from the combined cycle in which the tail-gas from the FT reactor is combusted. For the case with $X_{char,G}$ = 80%, $Q_{s,FTL,ann}$ decreases from 59.6 to 48.3%, while $W_{s,net,ann}$ increases from 10.4 to 16.7% as $F_{bio,HHV}$ is increased from 0 to 100%.

3.3. Effect of Tail-Gas Recycle and Char Separation on Performance. All of the remaining assessments of the influence of tail gas recycle and char separation are undertaken for $X_{char,G}$ = 80%, $\eta_{char\text{-}sep}$ = 80% and with CCS, unless otherwise stated.

3.3.1. Improvement on Annual Solar Share (SS_{ann}). Figure 9 presents the effect of tail-gas recycle and char separation on

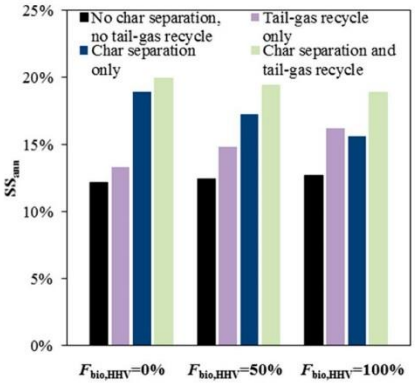

Figure 9. Effect of tail-gas recycle and char separation on annual solar share (SS_{ann}) for the solar hybridized coal and biomass-to-liquids ($SCTL_{bio}$) system with various values of biomass fraction based on HHV ($F_{bio,HHV}$). Conditions: char gasification conversion ($X_{char,G}$) is 80%, and char separation efficiency is 80%.

SS_{ann} for the $SCTL_{bio}$ system with various values of $F_{bio,HHV}$. It can be seen that the addition of char separation and tail-gas recycle both increase SS_{ann}. However, the influence of char separation on the SS_{ann} is decreased by increasing $F_{bio,HHV}$, while the influence of tail-gas recycle is increased by increasing $F_{bio,HHV}$. Char separation increases the solar input when solar is available and decreases feedstock consumption when it is not, thus increasing the solar share. However, the lower fixed carbon content of the selected biomass relative to that of the selected coal results in a weaker influence of char separation. For example, for the case of $F_{bio,HHV}$ = 0%, the integration of char separation increases SS_{ann} for the $SCTL_{bio}$ system without tail-gas recycle by 55.2%, from 12.2 to 18.9%. However, for $F_{bio,HHV}$ = 100%, this SS_{ann} is only increased by 27.3% from 12.7 to 16.2%.

For the $SCTL_{bio}$ system with tail-gas recycle, the endothermic reforming reactions in the steam reformer increase the heat demand of the gasifier, into which the steam reformer is integrated, thus increasing the solar input and solar share. For a higher $F_{bio,HHV}$, the increased content of light hydrocarbons in the syngas from gasifier results in an increased content of light hydrocarbons in the tail-gas from FT reactor, thus increasing the heat demand for steam reformer. This higher heat demand results in a higher SS_{ann} improvement caused by the addition of tail-gas recycle. As shown in Figure 9, for the case of $F_{bio,HHV}$ = 0%, the addition of tail-gas recycle can increase the SS_{ann} of the $SCTL_{bio}$ system without char separation by about 9%, i.e., from 12.2 to 13.3%. However, for $F_{bio,HHV}$ = 100%, this SS_{ann} is increased by about 27.3%, i.e., from 12.7 to 16.2%. Moreover, the influence of $F_{bio,HHV}$ on SS_{ann} is relatively small for the case with both char separation and tail-gas recycle under the studied conditions due to the counter effect of $F_{bio,HHV}$ on the influences of the addition of tail-gas recycle and char separation.

3.3.2. Improvement on Energetic Output. Figure 10 presents the effect of tail-gas recycle and char separation on

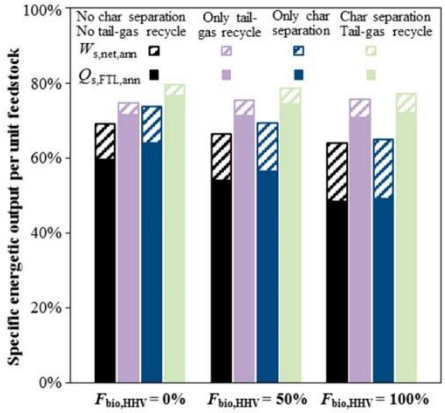

Figure 10. Effect of tail-gas recycle and char separation on the annual specific FT liquids output per unit feedstock ($Q_{s,FTL,ann}$) and on annual specific electricity output per unit feedstock ($W_{s,net,ann}$) for the solar hybridized coal and biomass-to-liquids ($SCTL_{bio}$) systems with various values of biomass fraction based on HHV ($F_{bio,HHV}$). Assumptions: carbon capture and sequestration (CCS) is included, char gasification conversion is 80%, and char separation efficiency is 80%.

the specific energetic output per unit feedstock of the $SCTL_{bio}$ system for various values of $F_{bio,HHV}$. It can be seen that the addition of char separation increases both the annual specific electricity output per unit feedstock ($W_{s,net,ann}$) and the annual specific FT liquids output per unit feedstock ($Q_{s,FTL,ann}$). This is due to the increased SS_{ann}, as shown in Figure 9. Moreover, similar to the effect of char separation on the SS_{ann}, the effect of char separation on the specific energetic output (both $Q_{s,FTL,ann}$ and $W_{s,net,ann}$) of the $SCTL_{bio}$ system also decreases with $F_{bio,HHV}$. The integration of char separation increases $Q_{s,FTL,ann}$ and $W_{s,net,ann}$ of the $SCTL_{bio}$ system without tail-gas recycle by 7.3 and 4.3%, respectively, for $F_{bio,HHV}$ = 0%, while by 4.6 and 3.3% for $F_{bio,HHV}$ = 100%.

The addition of tail-gas recycle increases both $Q_{s,FTL,ann}$ and the total energetic output ($Q_{s,FTL,ann}$ + $W_{s,net,ann}$) for the $SCTL_{bio}$ system, while decreasing $W_{s,net,ann}$. As discussed above, an increase in $F_{bio,HHV}$ increases the content of light hydrocarbons in the tail-gas from the FT reactor, thus increasing the amount of syngas (including the CO and H_2 from reforming reactions) recycled back to the FT reactor. Therefore, the influence of the addition of tail-gas recycle is increased by $F_{bio,HHV}$, as shown in Figure 10. The addition of tail-gas recycle can increase the $Q_{s,FTL,ann}$ of the $SCTL_{bio}$ system without char separation by 46.9% for $F_{bio,HHV}$ = 100%, but only by 20% for $F_{bio,HHV}$ = 0%. It can also been seen that both

DOI: 10.1021/acs.energyfuels.6b01755
Energy Fuels 2017, 31, 2033−2043

$Q_{s,FTL,ann}$ and the total energetic output from the $SCTL_{bio}$ systems with tail-gas recycle changes only slightly with $F_{bio,HHV}$, while that of the $SCTL_{bio}$ systems without tail-gas recycle decreases more significantly with $F_{bio,HHV}$. The economic impact of the requirement for a steam reformer in the tail-gas recycle process is expected to be relatively small since most of the syngas is converted into liquids in the upstream FT reactor. In addition, the current proposed indirectly heated tubular steam reformer is expected to be cost competitive compared with the autothermal reformer since the expensive air separation unit is not required. As suggested by Adams and Barton,[2] the capital cost of the indirectly heated tubular steam reformer is less than 5% of the FT reactor.

3.3.3. Effect on WTW CO_2 Emissions. Figure 11 presents the effect of tail-gas recycle and char separation on the annual WTW CO_2 emissions ($E_{CO_2,eq,ann}$) for the liquid fuels produced from the $SCTL_{bio}$ systems with and without CCS for various values of $F_{bio,HHV}$. It can be seen that the addition of tail-gas recycle decreases $E_{CO_2,eq,ann}$ for the liquid fuels produced from the $SCTL_{bio}$ system without CCS. This is to be expected because of the higher total energetic output per unit feedstock results from the addition of tail-gas recycle, as discussed above. The higher energetic output per unit feedstock of the $SCTL_{bio}$ system reduces the feedstock requirement per GJ of output, which lowers $E_{CO_2,eq,ann}$. This follows because the carbon in the feedstock is the main source of CO_2 emissions. However, this effect is reduced by $F_{bio,HHV}$ because the biomass is largely carbon neutral. However, for the $SCTL_{bio}$ system with CCS, the addition of tail-gas recycle decreases the $E_{CO_2,eq,ann}$ by 6.74 kg/GJ of output for $F_{bio,HHV}$ = 0 while increasing $E_{CO_2,eq,ann}$ by 12.6 kg/GJ of output for $F_{bio,HHV}$ = 100%. The methane reforming reaction produces syngas with a higher H_2/CO ratio (of about 3), which reduces the amount of CO_2 generated from the water−gas shift reaction, and the amount of CO_2 removed from the acid gas remover because the required H_2/CO ratio in the present study is set to 2.26 for the FT synthesis process. In the present paper, the energy requirement for CCS is only limited to that required to compress the pure CO_2 from the acid gas remover to sequestration pressure. Therefore, the addition of tail-gas recycle reduces the effect of CCS on $E_{CO_2,eq,ann}$. Furthermore, this reduction is more significant for a higher $F_{bio,HHV}$ due to the higher methane content in the syngas from the gasifier. It can also be seen that for $F_{bio,HHV}$ > 50% the addition of tail-gas recycle increases $E_{CO_2,eq,ann}$ for the liquid fuels produced from the present system with CCS.

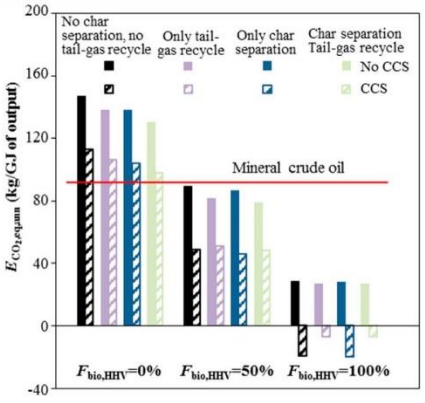

Figure 11. Effect of tail-gas recycle and char separation on annual well-to-wheel (WTW) CO_2 emissions ($E_{CO_2,eq,ann}$) for the liquid fuels produced from the solar hybridized coal and biomass-to-liquids ($SCTL_{bio}$) systems with and without carbon capture and sequestration (CCS) for various values of the biomass fraction based on HHV ($F_{bio,HHV}$). Assumptions: char gasification conversion ($X_{char,G}$) is 80%, and char separation efficiency is 80%.

The addition of char separation also decreases $E_{CO_2,eq,ann}$ for the liquid fuels for both the cases with and without CCS, although the effect of char separation is reduced by increasing $F_{bio,HHV}$. This effect of char separation is consistent with that on SS_{ann} shown above in Figure 9 (section 3.3.1). Moreover, for $F_{bio,HHV}$ = 0, the value of $E_{CO_2,eq,ann}$ for the liquid fuels produced from the $SCTL_{bio}$ system with all these configurations including char separation, tail-gas recycle, and CCS is only about 6.3 kg/GJ higher than that for the liquid fuels produced from conventional mineral crude oil.

4. CONCLUSION

In summary, it is found that the proposed approaches of incorporating char separation, cogasification of biomass with coal, carbon capture and sequestration (CCS), and tail-gas recycle can significantly improve the energetic and/or environmental performance of an FT liquid fuels production system using a solar hybridized dual fluidized bed (SDFB) gasifier.

The calculated WTW CO_2 emissions for the liquid fuels produced with conventional mineral oil process can be achieved for the present studied FT liquid fuels production system by integrating biomass cogasification and/or CCS technology. For the nonsolar coal and biomass-to-liquids (CTL_{bio}) system, a biomass fraction of 58% based on HHV is required to achieve the above WTW CO_2 emissions target, with a char gasification conversion ($X_{char,G}$) of 80%. This biomass fraction can be decreased to about 47.9% by solar hybridization of the case with a solar multiple (SM) = 2.64 and bed material storage capacity (SC_{BM}) = 16 h and to about 30% by incorporating CCS. Furthermore, by incorporating both solar energy and CCS, this biomass fraction can be further decreased to about 17%. However, as the biomass fraction is increased from 0 to 100%, the specific FT liquids output per unit feedstock ($Q_{s,FTL,ann}$) of the solar hybridized CTL_{bio} ($SCTL_{bio}$) system decreased gradually from 59.6 to 48.3%, while the specific electricity output per unit feedstock ($W_{s,net,ann}$) increased gradually from 10.4 to 16.7%. Furthermore, the addition of CCS results in a lower $W_{s,net,ann}$. However, the electricity is sufficient for self-sufficiency even for the system with CCS.

The addition of tail-gas recycle to the $SCTL_{bio}$ system is found to significantly increase the calculated $Q_{s,FTL,ann}$ and annual solar share (SS_{ann}) while decreasing $W_{s,net,ann}$, especially for the case with a high biomass fraction. For SM = 2.64, SC_{BM} = 16 h, $X_{char,G}$ = 80%, and a biomass fraction of 0, $Q_{s,FTL,ann}$ and SS_{ann} are increased by 20 and 9%, respectively, by the addition of tail-gas recycle. For a biomass fraction of 100%, $Q_{s,FTL,ann}$ and SS_{ann} can be increased by 49.6 and 27.3%, respectively.

The addition of char separation can significantly increase the calculated SS_{ann} of the $SCTL_{bio}$ system, especially under relatively low char gasification conversions. For SM = 2.64, SC_{BM} = 16 h, and $X_{char,G}$ = 80%, SS_{ann} of the studied SCTL system is increased from 12.2 to 20.3% by the integration of

DOI: 10.1021/acs.energyfuels.6b01755
Energy Fuels 2017, 31, 2033−2043

char separation. Nevertheless, the influence of char separation on the performance of the $SCTL_{bio}$ system decreases with an increase in both the biomass fraction and the char gasification conversion because of the decreased amount of char from the gasifier.

■ ASSOCIATED CONTENT

Supporting Information

The Supporting Information is available free of charge on the ACS Publications website at DOI: 10.1021/acs.energyfuels.6b01755.

Process simulation results and mass/energy/carbon flows of a proposed solid fuels to Fischer–Tropsch liquid fuels system via solar hybridized dual fluidized bed gasifier (PDF)

■ AUTHOR INFORMATION

Corresponding Author

*Phone: +61406887246. E-mail: peijun.guo@adelaide.edu.au.

ORCID

Peijun Guo: 0000-0001-6631-7818

Notes

The authors declare no competing financial interest.

■ ACKNOWLEDGMENTS

This work was supported by the Australian Solar Thermal Research Initiative (ASTRI), a project supported by the Australian Government, through the Australian Renewable Energy Agency (ARENA). The Australian Government, through ARENA, supports Australian research and development in solar photovoltaic and solar thermal technologies to help solar power become cost competitive with other energy sources. P.G. also thanks the generous support of the Chinese Scholarship Council (CSC) who provides the scholarship for his Ph.D. study. P.J.v.E. acknowledges the support of the Australian Solar Institute (ASI) for providing a postdoctoral fellowship. G.J.N. thanks the Australian Research Council (ARC) for the Discovery Outstanding Researcher Award used to support this work.

■ NOMENCLATURE

A = area (m^2)
AP = atmospheric pressure
CCS = carbon capture and storage
CTL = coal-to-liquids
DFB = dual fluidized bed
DNI = direct normal insolation
E = emission per unit output (kg/GJ)
FT = Fischer–Tropsch
GHG = greenhouse gas
HHV = higher heating value (J/kg)
HP = high pressure
HRSG = heat recovery and steam generation
IP = intermediate pressure
LP = low pressure
m = mass capacity (kg)
$\dot{m}$ = mass flow rate (kg/s)
Q = heating value of fuel, heat flow (J)
$\dot{Q}$ = heat flow rate (W)
SC = storage capacity (hours)
SCTL = solar hybridized coal-to-liquids
SDFB = solar hybridized dual fluidized bed
SM = the ratio of the heliostat field area relative to that required to meet the demands of the DFB gasifier and the steam reformer unit at the point of peak solar thermal output
SS = solar share
W = electricity output (J)
WGSR = water–gas-shift reactor
WTW = well-to-wheel
X = conversion of reactant

Greek Letters

η = efficiency

Subscripts

ann = annual
bio = biomass
BM = bed material
char-sep = char separation
coll = heliostat collector
com = combustor
crit = critical
G = gasification
FTL = Fischer–Tropsch liquids
no-dump = no dumping
s = specific (output per unit feedstock)

■ REFERENCES

(1) Takeshita, T.; Yamaji, K. Important roles of Fischer–Tropsch synfuels in the global energy future. *Energy Policy* **2008**, *36* (8), 2773–2784.

(2) Adams, T.; Barton, P. Combining coal gasification and natural gas reforming for efficient polygeneration. *Fuel Process. Technol.* **2011**, *92* (3), 639.

(3) Chen, Y.; Adams, T.; Barton, P. Optimal Design and Operation of Flexible Energy Polygeneration Systems. *Ind. Eng. Chem. Res.* **2011**, *50* (8), 4553.

(4) Meerman, J. C.; Ramírez, A.; Turkenburg, W. C.; Faaij, A. P. C. Performance of simulated flexible integrated gasification polygeneration facilities. Part A:A technical-energetic assessment. *Renewable Sustainable Energy Rev.* **2011**, *15* (6), 2563–2587.

(5) Sudiro, M.; Bertucco, A. Production of synthetic gasoline and diesel fuel by alternative processes using natural gas and coal: Process simulation and optimization. *Energy* **2009**, *34* (12), 2206.

(6) Lattanzio, R. K. *Canadian Oil Sands: Life-Cycle Assessments of Greenhouse Gas Emissions*; Congressional Research Service: Pittsburgh, PA, 2012; p 31.

(7) Gerdes, K. J.; Skone, T. J. *An Evaluation of the Extraction, Transport and Refining of Imported Crude Oils and the Impact on Life Cycle Greenhouse Gas Emissions*; NETL: Washington D.C., 2009; p 42.

(8) Kaniyal, A. A.; van Eyk, P. J.; Nathan, G. J.; Ashman, P. J.; Pincus, J. J. Polygeneration of Liquid Fuels and Electricity by the Atmospheric Pressure Hybrid Solar Gasification of Coal. *Energy Fuels* **2013**, *27* (6), 3538–3555.

(9) Hofbauer, H.; Rauch, R.; Bosch, K.; Koch, R.; Aichernig, C., Biomass CHP Plant Güssing: A Success Story. In *Pyrolysis and Gasification of Biomass and Waste*; Bridgewater, A. V., Ed.; CPL Press: Newbury, U.K., 2003; pp 527–36.

(10) Kern, S.; Pfeifer, C.; Hofbauer, H. Co-Gasification of Wood and Lignite in a Dual Fluidized Bed Gasifier. *Energy Fuels* **2013**, *27* (2), 919–931.

(11) Saw, W. L.; Pang, S. S. Co-gasification of blended lignite and wood pellets in a 100 kW dual fluidised bed steam gasifier: The influence of lignite ratio on producer gas composition and tar content. *Fuel* **2013**, *112*, 117–124.

(12) Kreutz, T. G.; Larson, E. D.; Liu, G.; Williams, R. H. Fischer–Tropsch Fuels from Coal and Biomass. In *Proceedings of 25th Annual International Pittsburgh Coal Conference, Pittsburgh, Pennsylvania, USA, 2008*; Morsi, B. I., Ed.; Curan: Pittsburgh, PA, 2008.

DOI: 10.1021/acs.energyfuels.6b01755
Energy Fuels 2017, 31, 2033–2043

(13) Larson, E. D.; Fiorese, G.; Liu, G. J.; Williams, R. H.; Kreutz, T. G.; Consonni, S. Co-production of decarbonized synfuels and electricity from coal plus biomass with CO_2 capture and storage: an Illinois case study. *Energy Environ. Sci.* **2010**, *3* (1), 28−42.
(14) Liu, G. J.; Larson, E. D.; Williams, R. H.; Kreutz, T. G.; Guo, X. B. Making Fischer−Tropsch Fuels and Electricity from Coal and Biomass: Performance and Cost Analysis. *Energy Fuels* **2011**, *25*, 415−437.
(15) Piatkowski, N.; Wieckert, C.; Weimer, A. W.; Steinfeld, A. Solar-driven gasification of carbonaceous feedstock-a review. *Energy Environ. Sci.* **2011**, *4* (1), 73−82.
(16) Kaniyal, A. A.; van Eyk, P. J.; Nathan, G. J. Dynamic Modeling of the Coproduction of Liquid Fuels and Electricity from a Hybrid Solar Gasifier with Various Fuel Blends. *Energy Fuels* **2013**, *27* (6), 3556−3569.
(17) Guo, P. J.; van Eyk, P. J.; Saw, W. L.; Ashman, P. J.; Nathan, G. J.; Stechel, E. B. Performance Assessment of Fischer−Tropsch Liquid Fuels Production by Solar Hybridized Dual Fluidized Bed Gasification of Lignite. *Energy Fuels* **2015**, *29* (4), 2738−2751.
(18) Kaniyal, A. A.; van Eyk, P. J.; Nathan, G. J. Storage capacity assessment of liquid fuels production by solar gasification in a packed bed reactor using a dynamic process model. *Appl. Energy* **2016**, *173*, 578−588.
(19) Nickerson, T. A.; Hathaway, B. J.; Smith, T. M.; Davidson, J. H. Economic assessment of solar and conventional biomass gasification technologies: Financial and policy implications under feedstock and product gas price uncertainty. *Biomass Bioenergy* **2015**, *74* (0), 47−57.
(20) Hathaway, B. J.; Kittelson, D. B.; Davidson, J. H. Integration of Solar Gasification With Conventional Fuel Production: The Roles of Storage and Hybridization. *J. Sol. Energy Eng.* **2014**, *136*, 011024.
(21) Kern, S. J.; Pfeifer, C.; Hofbauer, H. Cogasification of Polyethylene and Lignite in a Dual Fluidized Bed Gasifier. *Ind. Eng. Chem. Res.* **2013**, *52* (11), 4360−4371.
(22) Kern, S.; Pfeifer, C.; Hofbauer, H. Gasification of lignite in a dual fluidized bed gasifier - Influence of bed material particle size and the amount of steam. *Fuel Process. Technol.* **2013**, *111*, 1−13.
(23) Adegboye, M. O. Continuous segregation and removal of biochar from bubbling fluidized bed. Master of Engineering Science Thesis. University of Western Ontario, London, Ontario, Canada, 2014.
(24) Kirkels, A. F.; Verbong, G. P. J. Biomass gasification: Still promising? A 30-year global overview. *Renewable Sustainable Energy Rev.* **2011**, *15* (1), 471−481.
(25) Berndes, G.; Hoogwijk, M.; van den Broek, R. The contribution of biomass in the future global energy supply: a review of 17 studies. *Biomass Bioenergy* **2003**, *25* (1), 1−28.
(26) Sami, M.; Annamalai, K.; Wooldridge, M. Co-firing of coal and biomass fuel blends. *Prog. Energy Combust. Sci.* **2001**, *27* (2), 171−214.
(27) Tijmensen, M. J. A.; Faaij, A. P. C.; Hamelinck, C. N.; van Hardeveld, M. R. M. Exploration of the possibilities for production of Fischer−Tropsch liquids and power via biomass gasification. *Biomass Bioenergy* **2002**, *23* (2), 129−152.
(28) Dry, M. E. High quality diesel via the Fischer−Tropsch process - a review. *J. Chem. Technol. Biotechnol.* **2002**, *77* (1), 43−50.
(29) Rostrup-Nielsen, J. R. New aspects of syngas production and use. *Catal. Today* **2000**, *63* (2−4), 159−164.
(30) NREL. *National Solar Radiation Database*, 1991−2010 update. http://rredc.nrel.gov/solar/old_data/nsrdb/1991-2010/.
(31) Goyal, A.; Rehmat, A. Modeling of a Fluidized-Bed Coal Carbonizer. *Ind. Eng. Chem. Res.* **1993**, *32* (7), 1396−1410.
(32) Suuberg, E. M.; Peters, W. A.; Howard, J. B. Product Composition and Kinetics of Lignite Pyrolysis. *Ind. Eng. Chem. Process Des. Dev.* **1978**, *17* (1), 37−46.
(33) Abdelouahed, L.; Authier, O.; Mauviel, G.; Corriou, J. P.; Verdier, G.; Dufour, A. Detailed Modeling of Biomass Gasification in Dual Fluidized Bed Reactors under Aspen Plus. *Energy Fuels* **2012**, *26* (6), 3840−3855.
(34) Dufour, A.; Girods, P.; Masson, E.; Rogaume, Y.; Zoulalian, A. Synthesis gas production by biomass pyrolysis: Effect of reactor temperature on product distribution. *Int. J. Hydrogen Energy* **2009**, *34* (4), 1726−1734.
(35) Carpentieri, M.; Corti, A.; Lombardi, L. Life cycle assessment (LCA) of an integrated biomass gasification combined cycle IBGCC with CO2 removal. *Energy Convers. Manage.* **2005**, *46* (11−12), 1790−1808.
(36) Mann, M.; Spath, P. *Life cycle assessment of a biomass gasification combined-cycle power system*; NREL: Golden, CO, 1997.
(37) Herzog, H.; Golomb, D. Carbon Capture and Storage from Fossil Fuel Use. In *Encyclopedia of Energy*; Elsevier: Amsterdam, 2004; Vol. *1*.
(38) Sheu, E. J.; Mitsos, A.; Eter, A. A.; Mokheimer, E. M. A.; Habib, M. A.; Al-Qutub, A. A Review of Hybrid Solar-Fossil Fuel Power Generation Systems and Performance Metrics. *J. Sol. Energy Eng.* **2012**, *134* (4), 041006.
(39) Skone, J.; Gerdes, K. J. *Development of Baseline Data and Analysis of Life Cycle Greenhouse Gas Emissions of Petroleum-Based Fuels*; NETL: South Park Township, PA, 2008.
(40) Guo, P.; Saw, W. L.; Van Eyk, P. J.; Ashman, P. J.; Nathan, G. J.; Stechel, E. B. Fischer−Tropsch liquid fuel production by co-gasification of coal and biomass in a solar hybrid dual fluidized bed gasifier. *Energy Procedia* **2015**, *69*, 1770−1779.
(41) Saw, W.; Kaniyal, A.; van Eyk, P.; Nathan, G.; Ashman, P. Solar Hybridized Coal-to-liquids via Gasification in Australia: Techno-economic Assessment. *Energy Procedia* **2015**, *69*, 1819−1827.
(42) Herzog, H. J. The economics of CO_2 separation and capture. *Tech.-Elmsford-J. Franklin Inst. J. Sci. Legislative Reg. Judicial Sys.*, **2000**, *7*, 13−24.
(43) Azar, C.; Lindgren, K.; Larson, E.; Möllersten, K. Carbon capture and storage from fossil fuels and biomass - Costs and potential role in stabilizing the atmosphere. *Clim. Change* **2006**, *74* (1−3), 47−79.

DOI: 10.1021/acs.energyfuels.6b01755
Energy Fuels 2017, 31, 2033−2043

CHAPTER 5

GASIFICATION REACTIVITY AND PHYSICOCHEMICAL PROPERTIES OF THE CHARS FROM RAW AND TORREFIED WOOD, GRAPE MARC, AND MACROALGAE

Peijun Guo[*,†,‡], Woei L. Saw[†,‡], Philip J. van Eyk[†,‡], Ellen B. Stechel[¤], Rocky de Nys,[‖] Peter J. Ashman[†,‡] and Graham J. Nathan[†,§]

[†]*Centre for Energy Technology,* [‡]*School of Chemical Engineering and* [§]*School of Mechanical Engineering, The University of Adelaide, SA 5005, Australia*

[¤]*Light Works, Arizona State University, Tempe, AZ, USA*

[‖]*MACRO − The Centre for Macroalgal Resources and Biotechnology, College of Science and Engineering, James Cook University, Townsville Qld 4811, Australia*

Energy & Fuels 31(2017) 2246-2259

Statement of Authorship

Title of Paper	Gasification reactivity and physiochemical properties of the chars from raw and torrefied wood, grape marc and macroalgae
Publication Status	☐ Published ☐ Accepted for Publication ☑ Submitted for Publication ☐ Unpublished and Unsubmitted work written in manuscript style
Publication Details	Guo, P., Saw, W. L., van Eyk, P. J., Stechel, E. B., de Nys, R., Ashman, P. J., and Nathan, G. J. Gasification reactivity and physiochemical properties of the chars from raw and torrefied wood, grape marc and macroalgae. Energy & Fuels, Submitted

Principal Author

Name of Principal Author (Candidate)	Peijun Guo
Contribution to the Paper	Performed experiments, interpreted data, wrote manuscript and acted as corresponding author.
Overall percentage (%)	70%
Certification:	This paper reports on original research I conducted during the period of my Higher Degree by Research candidature and is not subject to any obligations or contractual agreements with a third party that would constrain its inclusion in this thesis. I am the primary author of this paper.
Signature	Date 6/10/2016

Co-Author Contributions

By signing the Statement of Authorship, each author certifies that:

i. the candidate's stated contribution to the publication is accurate (as detailed above);
ii. permission is granted for the candidate in include the publication in the thesis; and
iii. the sum of all co-author contributions is equal to 100% less the candidate's stated contribution.

Name of Co-Author	Woei L. Saw
Contribution to the Paper	Supervised development of work, helped in data interpretation and manuscript evaluation.
Signature	Date 6/10/2016
Name of Co-Author	Philip J. van Eyk
Contribution to the Paper	Supervised development of work, helped in data interpretation and manuscript evaluation.
Signature	Date 6/10/2016
Name of Co-Author	Ellen B. Stechel
Contribution to the Paper	Supervised development of work, helped in data interpretation and manuscript evaluation.
Signature	Date 6/10/2016
Name of Co-Author	Rocky de Nys
Contribution to the Paper	Helped in data interpretation and manuscript evaluation.
Signature	Date 7/10/16
Name of Co-Author	Peter J. Ashman
Contribution to the Paper	Supervised development of work, helped in data interpretation and manuscript evaluation.
Signature	Date 7/10/16
Name of Co-Author	Graham J. Nathan
Contribution to the Paper	Supervised development of work, helped in data interpretation and manuscript evaluation.
Signature	Date 6/10/2016

energy&fuels

Article

pubs.acs.org/EF

Gasification Reactivity and Physicochemical Properties of the Chars from Raw and Torrefied Wood, Grape Marc, and Macroalgae

Peijun Guo,[*,†,‡] Woei L. Saw,[†,‡] Philip J. van Eyk,[†,‡] Ellen B. Stechel,[§] Rocky de Nys,[∥] Peter J. Ashman,[†,‡] and Graham J. Nathan[†,⊥]

[†]Centre for Energy Technology, [‡]School of Chemical Engineering, and [⊥]School of Mechanical Engineering, The University of Adelaide, Adelaide, South Australia 5005, Australia

[§]LightWorks, Arizona State University, Tempe, Arizona 85281, United States

[∥]MACRO—The Centre for Macroalgal Resources and Biotechnology, College of Science and Engineering, James Cook University, Townsville Queensland 4811, Australia

ABSTRACT: The gasification reactivity of the chars from both raw and torrefied wood, grape marc, and macroalgae has been investigated in this paper. The variations in char gasification reactivity were explained using further investigation of the physicochemical characteristics of the char that can influence the gasification reactivity, i.e., specific surface area, uniformity of the carbonaceous structure, and concentration of alkali metals (Na and K). It was found that the influence of the torrefaction process on the char gasification reactivity strongly depends upon the solid fuel properties and pyrolysis conditions. For a pyrolysis temperature of 800 °C, the gasification reactivity of the chars from both the torrefied grape marc and the torrefied macroalgae was lower than that of the chars from their corresponding raw fuels. This is mainly due to a lower specific surface area and a lower content of alkali metals (Na and/or K) in the chars produced from both the torrefied grape marc and the torrefied macroalgae than for those chars produced from their corresponding raw fuels. However, the opposite influence of torrefaction was found for the macroalgae char when the pyrolysis temperature was increased to 1000 °C. This is attributed mostly to the higher Na content and the more amorphous carbonaceous structure for the torrefied macroalgae char than for the raw macroalgae char.

1. INTRODUCTION

The ongoing depletion of fossil fuel reserves, high greenhouse gas (GHG) emissions, and increasing global population provide motivation for the development of renewable energy and alternative fuels. As one of the most promising renewable energy sources, biomass is expected to play an important role in the future energy supply.[1] In addition to the widely studied woody biomass, the utilization of agricultural and industrial residues and algal biomass has also received much attention. Agricultural and industrial residues have significant economic advantage, while algal biomass has merits that include a high areal energy yield, an adaptability to a diverse range of aquatic environments, and an avoidance of any requirement for arable land.[2−5] In Australia, wineries produce several hundred thousand tonnes of grape marc every year, which needs to be properly processed to avoid environmental damage and to achieve economic benefits. One potential approach to use the grape marc is to convert it into valuable syngas by gasification.[6] In addition, freshwater macroalgae is considered as an important future energy resource because it is expected to play a growing role in the treatment of wastewater.[7,8] Therefore, grape marc and macroalgae were selected as the biomass fuels for the present investigation together with the more conventional biomass feedstock of wood.

Despite its strong potential, biomass can exhibit some properties, e.g., high oxygen content, high moisture content, low calorific value, hygroscopic nature, and low density, which can result in a low conversion efficiency and difficulties during collection, grinding, transportation, and storage. Torrefaction is a mild thermal pretreatment (200−300 °C) technology that has been widely studied and demonstrated to mitigate these challenges.[9−13] The torrefaction of a wide range of biomass has been studied, including woody biomass,[14−18] agriculture and industry residues,[16−19] microalgae,[20−22] and grassy biomass.[23,24] After torrefaction, solid fuels have a lower moisture content, higher heating value, hydrophobicity, better grindability, and more uniform properties than the corresponding raw material. In addition, torrefaction reduces the O/C and H/C ratios for the biomass, thus making it more like coal. All of these merits can make the torrefied biomass easier to use than the raw biomass in existing reactors without significant modification to the feeding system.[12]

Gasification technology is considered as one of the most promising technologies to convert low-value biomass to high-value syngas.[9,25] The syngas product can be used in gas turbines, engines, or fuel cells to generate electricity with higher efficiency than through a direct biomass combustion process. Alternatively, the syngas can be converted to high-value chemicals, such as Fischer−Tropsch liquid fuels and methanol. As a result of the merits of the torrefaction discussed above, the gasification of the torrefied biomass has attracted great interest

Special Issue: In Honor of Professor Brian Haynes on the Occasion of His 65th Birthday

Received: September 1, 2016
Revised: January 31, 2017
Published: February 1, 2017

DOI: 10.1021/acs.energyfuels.6b02215
Energy Fuels 2017, 31, 2246−2259

in recent years.[25−28] In the gasification process, both pyrolysis and biochar gasification occur simultaneously. However, the rate of pyrolysis is much faster than the gas−solid reactions, so that the char gasification reactions are regarded as the rate-determining process for the gasifier design and operation. Therefore, much attention has been focused on the influence of torrefaction on the biomass char gasification rate.[29−36] However, no consistent explanation for the influence of torrefaction on the overall gasification rate of biochar has been found. The variability was found to strongly depend upon the biomass species and biochar preparation conditions (e.g., temperature and heating rate). Torrefaction was found to reduce the carbon conversion of forest residues and spruce gasification in an entrained-flow reactor operated at 1000−1400 °C.[32,36] The gasification experiments under various CO_2 concentrations at 800−1000 °C showed that the char reactivity of torrefied olive stones was lower than that of raw olive stones, while the char prepared from torrefied straw had higher reactivity than that from raw straw.[30] Moreover, torrefaction had little effect on the char reactivity of pine shells.[30] Fisher et al.[31] found that torrefied willow char had lower combustion and gasification reactivity than the raw willow char and that a higher heating rate of pyrolysis could enhance this influence of torrefaction. However, no investigation of the influence of torrefaction on the char gasification rate of the grape marc and macroalgae has yet been reported. In addition, little work has been performed to explain these various changes in char reactivity caused by torrefaction via investigating char-reactivity-affecting factors. Thus, the present study aims to fill this gap.

Char reactivity can be influenced by the char characteristics, including the particle specific surface area (SSA), the concentration of catalytic elements (such as Na, K, Fe, and Ca), and the uniformity of the carbonaceous structure. Therefore, to better understand the observed variation of the gasification rate caused by torrefaction, new investigations are required. The Brunauer−Emmett−Teller (BET) surface area of the char produced in CDS 2000 Pyroprobe from both raw and torrefied willow (290 °C and 30 min) were analyzed and compared to each other.[37] With a pyrolysis temperature of 1000 °C and a high heating rate of around 1000 K/s, the torrefied willow char was found to have higher a BET surface area than that of the raw willow char. However, with the same raw and torrefied willow (at 290 °C and 30 min) pyrolyzed in a drop tube furnace at 1100 °C, the torrefied willow char was found to have a lower BET surface area than the raw willow char.[38] The BET surface area of the char pyrolyzed at 550 °C from torrefied rice husks was found to be lower than that of the raw rice husk char pyrolyzed under the same conditions.[39] Therefore, the influence of torrefaction on the BET surface area is strongly dependent upon the torrefaction and pyrolysis conditions as well as the biomass type. In addition, the surface area of micropores was found to be important for the char material, especially for the raw char.[40] The method of CO_2 adsorption at 273 K has been widely used to characterize the SSA of the char because the method of N_2 adsorption at 77 K for BET surface area analysis is not very suitable to be used to evaluate the microporosity (<0.7 nm) of char as a result of the restrictive activated diffusion effect.[41] As a result of the larger kinetic energy resulting from the higher adsorption temperature (in contrast to N_2 adsorption at 77 K for the BET surface area test), the CO_2 molecules can penetrate into narrow pores (<0.7 nm).[41] However, no investigation has been reported on the influence of the torrefaction on the SSA (especially via CO_2 adsorption at 273 K) of both the grape marc and macroalgae char.

Metal catalysts (especially Na, K, Ca, Fe, and Mg) have been found to have a significant effect on the gasification reactivity of biochar.[42] The reactivity of fir char under CO_2 gasification was found to be increased through the addition of metal catalysts, in the order of K > Na > Ca > Fe > Mg.[42] On the other hand, the CO_2 gasification reactivity of pistachios nut shell char was found to be increased through the addition of metal catalysts, in the order of Na > Ca > Fe > K > Mg.[43] Besides, other than the loaded metal catalysts, the metal elements in the raw biomass can also influence the gasification reactivity of the char. Therefore, the migration of the elemental metals, especially the alkali (K and Na), alkaline earth (Ca and Mg), and transition (Fe) metals, during the pyrolysis and gasification process can influence the instantaneous reactivity of the char significantly. Previous studies on the release of elemental metals during biomass pyrolysis and gasification process found that the extent to which an elemental metal is released to the gas phase or is retained in the solid residue depends upon both feedstock composition and operating conditions, such as reaction temperature, heating rate, and gas environment.[44,45] In addition, the monovalent species (Na and K) were found to be usually volatilized to a much larger extent than the divalent species (Ca, Mg, and Fe).[45] Because torrefaction significantly changes the properties of biomass, the above findings suggest that torrefaction may influence the release of the elemental metal during the pyrolysis and gasification process and, therefore too, the reactivity of the char. However, no assessment of these effects is available. Therefore, the present investigation aims to investigate the possible influence of torrefaction on reactivity through its influence on metal elements (Na and K) in both the char (pyrolysis product) and ash (gasification product) from raw and torrefied biomass.

Raman spectroscopy is one of the most powerful techniques to study the structural features of carbonaceous material because it is sensitive to both the crystalline and amorphous structures. It has been used to correlate the structural features of coal and biomass with char reacitivty.[46−51] However, little work has been performed to evaluate the influence of torrefaction on the char structure using the Raman technique.

The first aim of this study is to demonstrate the influence of torrefaction on the overall CO_2 gasification reactivity of char from winery residue grape marc, macroalgae, and conventional biomass wood. The second aim is to explore the reasons why the torrefaction changes the overall gasification reactivity of the biochar by investigating the SSA, carbon structure, and catalytic metal element concentration of the chars prepared from raw and torrefied fuels.

2. METHODOLOGY

2.1. Fuels. Three types of biomass, i.e., wood, grape marc, and macroalgae, were selected with widely differing chemical compositions. Not only does this allow for the influence of torrefaction on char reactivity for being assessed for significantly different species, it also allows for an assessment of whether torrefaction reduces this variability. The selected wood is a commercial Swedish wood (WD) from Skellefteå Kraft. The grape marc (GM) used in the present study is shiraz grape marc supplied by the Waite campus of The University of Adelaide. The selected macroalgae was *Oedogonium intermedium*,[8] which was cultured in 10 000 L parabolic tanks at James Cook University, Townsville, Queensland, Australia. The tanks were stocked at 0.5 g L^{-1} in dechlorinated water with the addition of microalgae food (MAF) (0.1 g L^{-1}) and harvested after 7 days by filtration

DOI: 10.1021/acs.energyfuels.6b02215
Energy Fuels 2017, 31, 2246−2259

through mesh bags (100 μm), which were subsequently spin drier (Fisher and Paykell Application, Ltd.). All of the fuels were air-dried until the moisture content was less than 10 wt % to reduce the energy penalty during the torrefaction process resulting from moisture evaporation. According to the location of biomass, species of biomass, etc., the approach of biomass drying in real application varies significantly, thus leading to a considerable difference in the energy penalty for the drying processes. However, this is beyond the scope of the present study. The particle size range for the biomass feedstock used in the torrefaction and pyrolysis experiments was 0.5−1.6 mm. Samples of the raw and torrefied biomass were further milled to pass through a 250 μm sieve for fuel analysis.

2.2. Reactor Setup. The torrefied biomass, char, and ash were prepared in the laboratory-scale, fixed-bed, and batch reactors shown in Figure 1. This compromises a 1.4 m long, 46 mm inner diameter,

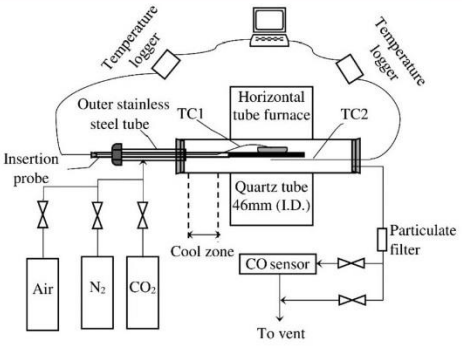

Figure 1. Schematic diagram of the fixed-bed reactor used for the torrefaction, pyrolysis, and gasification experiments.

quartz tube, which was horizontally positioned inside a 0.8 m, three-zone, electrically heated furnace. That is, the tube extends 0.3 m from both the front and back ends of the furnace. Both ends of the quartz tube were sealed with tapered silicone plugs. A stainless-steel tube welded to a high-temperature stainless-steel (253MA) rod was used as a sample insertion probe. A rack was manufactured using the 253MA high-temperature stainless-steel rod at one end of the probe (rod end) to locate the crucible, while a rubber plug was used to seal the tube of the probe at the other end. A K-type thermocouple (TC1) was located in the crucible to monitor the sample temperature, and another K-type thermocouple (TC2) was located in the middle of the quartz tube to monitor the gas temperature. Samples (0.5−4 g) were loaded into 25 mL alumina crucibles without compressing the fuel bed. A cool zone of an inert gas atmosphere was established at one end of the reactor both to hold the sample below 60 °C before its insertion into the furnace and to cool the sample after the experiment was finished. The insertion probe was supported by an outer stainless-steel tube. One end of the outer tube was installed through the tapered silicone plug, while the other end was fit with a nut and seal to tighten and seal the probe with the outer tube.

High-purity N_2 was used in the torrefaction and pyrolysis experiments, while both high-purity N_2 and CO_2 were used in the gasification experiments. Compressed air was used in the ash-producing experiments at 550 °C. The gases were fed to the quartz tube through the outer stainless-steel tube. Product gas was passed through a quartz wool filter to remove the tar and monitored for CO concentration before being vented to exhaust. A separate non-dispersive infrared gas analyzer was used to measure the CO concentration for the char gasification experiments and confirm the completion of the gasification process.

2.3. Torrefaction. The torrefaction experiments were carried out at 275 °C in the fixed-bed reactor for all of the selected biomass samples. The residues were weighed at the end of each test to determine the mass and energy yields of torrefaction according to eqs 1 and 2

$$\text{mass yield (\%)} = m_{T,daf}/m_{R,daf} \times 100\% \quad (1)$$

$$\text{energy yield (\%)} = (m_{T,d}\text{HHV}_{T,d})/(m_{R,d}\text{HHV}_{R,d}) \times 100\% \quad (2)$$

where $m_{T,daf}$ and $m_{R,daf}$ are the dry and ash-free weights of the torrefied and raw biomass, respectively, $m_{T,d}$ and $m_{R,d}$ are the dry weights of the torrefied and raw biomass, respectively, and $\text{HHV}_{T,d}$ and $\text{HHV}_{R,d}$ are the higher heating values of the dry torrefied and raw biomass, respectively. The HHV (MJ/kg) of each fuel is calculated according to eq 3, which was proposed by Channiwala and Parikh[52]

$$\text{HHV} = 0.3491\text{C} + 1.1783\text{H} + 0.1005\text{S} - 0.1034\text{O} - 0.0151\text{N} - 0.0211\text{ash} \quad (3)$$

where C, H, S, O, N, and ash represent carbon, hydrogen, sulfur, oxygen, nitrogen, and ash mass percentages in the dry fuels, respectively.

At the start of the each torrefaction experiment, the empty crucible was kept in an oven at 105 °C and then weighed before being loaded with the sample. After loading, the sample was dried in an oven at 105 °C for 3 h, weighed, and transferred to the cool zone with a N_2 purge [1.0 L/min at standard temperature and pressure (STP)]. When the gas temperature reached 275 °C, as determined with TC2, the sample was moved to the middle of the furnace. The sample was held in the furnace for 30 min after reaching the torrefaction temperature (275 °C based on TC1) and then pulled back to the cool zone. After the sample temperature reached 105 °C, the crucible was removed from the quartz tube and weighted immediately. The weight of the torrefied sample can be achieved by subtracting the weight of the empty 105 °C oven-dried crucible. All of the torrefied biomass samples, i.e., torrefied wood (T-WD), torrefied grape marc (T-GM), and torrefied macroalgae (T-MA), were stored in the desiccator together with the crucible for further char preparation.

2.4. Char and Ash Preparation. The char was prepared in the fixed-bed reactor described above at various pyrolysis temperatures (T_P) between 800 and 1100 °C for the following tests. Because the pyrolysis at these temperatures was vigorous, a relatively high flow rate of N_2 (4.0 L/min at STP) was used to achieve sufficient purge, thus avoiding any significant secondary reactions of tar. In addition to the higher temperatures, another difference in the operating procedure for char preparation from torrefaction was the residence. After being moved to the middle of the furnace, the sample was held in the furnace for 60 min to remove all of the volatiles. The char was then ground and sieved to achieve a particle size of <150 μm for further investigations. The char yield was calculated according to eq 4

$$\text{char yield (\%)} = m_{C,daf}/m_{R,daf} \times 100\% \quad (4)$$

where $m_{C,daf}$ and $m_{R,daf}$ are the dry and ash-free weights of the char and raw biomass, respectively.

The char samples were ashed in the furnace at 550 °C in air for 12 h to oxidize all of the organic matter. These ash samples were used for the subsequent digestion and inductively coupled plasma optical emission spectrometry (ICP−OES) analysis to determine the inorganic matter content in the char produced from the pyrolysis process. Alternatively, to investigate the retention of inorganic matter after a gasification process, char samples were gasified at temperatures from 800 to 1000 °C in pure CO_2 gas to produce the ash for an inorganic element analysis. The gasification temperature of 1100 °C was not investigated here because the ash started to melt and stick on the crucible at this temperature.

The inorganic matter content in wood char and ash was not investigated in the present study because the ash content in the wood is very low (~0.3%). In addition, the scale of our reactor is too small to produce enough wood ash sample for the digestion and ICP−OES analysis because of the low ash content in the wood.

2.5. Char Gasification Rate Measurements. The CO_2 gasification rate of char samples was determined for various gasification temperatures (T_G = 750−1000 °C) using thermogravimetric analysis

DOI: 10.1021/acs.energyfuels.6b02215
Energy Fuels 2017, 31, 2246−2259

Table 1. Characteristics of Raw and Torrefied Wood (R-WD and T-WD), Grape Marc (R-GM and T-GM), and Macroalgae (R-MA and T-MA)

	R-MA	T-MA	R-GM	T-GM	R-WD	T-WD
			Proximate Analysis (wt %)			
moisture	7.55 ± 0.35	3.38 ± 0.22	2.87 ± 0.31	2.59 ± 0.3	7.5 ± 0.42	2.8 ± 0.21
volatile matter	67.03 ± 1.05	48.88 ± 0.92	64.65 ± 1.23	51.46 ± 1.1	75.6 ± 1.42	72.58 ± 1.33
fixed carbon	17.64 ± 0.6	34.34 ± 0.45	26.88 ± 0.71	38.3 ± 0.51	16.6 ± 0.78	24.21 ± 0.89
ash	7.78 ± 0.1	13.4 ± 0.25	5.6 ± 0.21	7.65 ± 0.29	0.3 ± 0.22	0.41 ± 0.23
HHV[a] (MJ/kg)	19.59	22.93	21.51	25.47	21.05	22.67
			Ultimate Analysis (wt %)[a]			
C	44.97 ± 0.05	54.54 ± 0.15	50.7 ± 0.1	60.03 ± 0.09	50.49 ± 0.3	54.52 ± 0.14
H	6.61 ± 0.22	5.33 ± 0.14	6.43 ± 0.05	6.06 ± 0.01	6.64 ± 0.4	6.48 ± 0.06
O[b]	35.59	19.64	35.06	23.62	42.52	38.57
N	4.22 ± 0.01	5.77 ± 0.01	2.19 ± 0.12	2.64 ± 0.03	0.05 ± 0.03	0.06 ± 0.01
S	0.14 ± 0.01	0.12 ± 0.01	0.13 ± 0.01	0.11 ± 0.01	<0.01	<0.01
C/O	1.26	2.78	1.45	2.54	1.19	1.41
C/H	6.80	10.24	7.88	9.91	7.60	8.41
			Inorganic Matter Analysis (wt %)[a]			
Cl	0.35 ± 0.01	0.56 ± 0.01	0.02	0.02	<0.01	<0.01
P	0.69 ± 0.02	1.2 ± 0.01	0.29 ± 0.01	0.39 ± 0.01	<0.01	<0.01
Na	0.71 ± 0.04	1.2 ± 0.02	0.02	0.03	<0.01	<0.01
K	1.59 ± 0.05	2.7 ± 0.06	1.99 ± 0.06	2.65 ± 0.07	0.04	0.05
Ca	0.52 ± 0.05	1.11 ± 0.07	0.64 ± 0.02	0.84 ± 0.02	0.07	0.09
Mg	0.45 ± 0.02	0.74 ± 0.02	0.11	0.15	0.01	0.01
Fe	0.12 ± 0.01	0.24 ± 0.02	0.02	0.02	<0.01	<0.01
Al	0.01	0.01	0.02	0.02	<0.01	<0.01

[a]Dry basis. [b]Calculated by difference.

(Mettler Toledo TGA-DSC2). A thin layer (approximate monolayer) of sample was loaded into an alumina crucible with a wall height of 1 mm to avoid any significant gas diffusion in the crucible. Each sample was heated to 105 °C in N_2 (30 mL/min balance gas N_2 + 120 mL/min at STP purge gas N_2) at the rate of 40 °C/min and held at 105 °C for 1 h to remove any residual moisture. The sample was then heated to the target gasification temperature at the rate of 40 °C/min and held at this temperature for 5 min. The purge gas was then switched from N_2 to CO_2 with the same gas flow rate to start the gasification process. The instantaneous gasification rate, r, can be obtained according to eq 5

$$r = \frac{dX}{dt}\frac{1}{1-X} \qquad X = \frac{m_i - m(t)}{m_i - m_f} \tag{5}$$

where X is the char conversion of the gasification process and m_i, $m(t)$, and m_f are the masses of the char at the start of the gasification, at time t, and at the end of the gasification, respectively.

In addition, to compare the reactivity of the chars, the conventional reactivity index (R_{50}) was calculated according to eq 6

$$R_{50} = \frac{50\%}{\tau_{50}} \tag{6}$$

where τ_{50} is the time for 50% char conversion during gasification.

2.6. Analysis of Char, Ash, and Raw and Torrefied Biomass. The analysis of C, H, and N was carried out in triplicate using an elemental analyzer (PerkinElmer 2400 Series II) for all of the raw and torrefied samples. The chlorine concentration was measured using ion chromatography (Dionex, ICS-2500 system), following extraction in water. This measurement was only conducted for the raw and torrefied samples. Sulfur and all other inorganic elements in all of the samples (i.e., raw and torrefied biomass and the ash prepared in section 2.4) were measured by ICP−OES (5100, Agilent Technologies), using a radial plasma viewing mode, following digestion in H_2O_2 (30%, v/v)/HNO_3 (68%, v/v)/HF (48%, v/v). Digested samples were dissolved and diluted with 5% (v/v) HNO_3. All plasticware was cleaned before use by soaking in a 6 M solution of HCl for a period of at least 12 h. ICP−OES and ion chromatography measurements of the solution were performed externally by Analytical Services Unit in Commonwealth Scientific and Industrial Research Organisation (CSIRO) Land and Water. All of the samples were digested and analyzed at least twice.

The char SSA was measured using adsorption of CO_2 at 273 K with a constant volume adsorption apparatus (BELSORP-MAX, BEL, Japan), while data analysis was performed using the density functional theory (DFT) method. Around 100 mg of char sample was loaded to the cell and degassed at 300 °C prior to the measurement for 4 h.

Raman spectroscopy was performed with a Labram HR Evolution spectrometer (Horiba Jobin-Ivon, France) equipped with a Synapse charge-coupled device detection system (Horiba Jobin-Ivon, France). A visible laser (532 nm, 2.33 eV) and an objective lens (50×) were used in the present study. A low laser power of 15 mW was used, which was found to be sufficient to avoid structural damage. For each Raman measurement, spectra were collected using an exposure time of 3 s with a step size of 6 μm in both x and y directions over 60 × 60 μm areas. The sum of the spectra collected from each mapping was used for each char sample.

3. RESULTS AND DISCUSSION

3.1. Sample Characterization and Torrefaction Yields. The proximate and elemental analyses of the raw and torrefied biomass samples are presented in Table 1. As expected, the ratios of C/O and C/H of the torrefied biomass samples were found to be higher than those of the parent fuels. The torrefied samples also have a higher dry-based HHV than the corresponding raw samples, which is primarily attributed to both the significant increase in the C content (dry based, shown in Table 1) and the decrease in the O content (dry based, shown in Table 1) during the torrefaction process. In addition, as a result of the release of volatile matter during the torrefaction process, the torrefied biomass has a lower volatile content but higher fixed carbon and ash contents than the parent biomass.

DOI: 10.1021/acs.energyfuels.6b02215
Energy Fuels 2017, 31, 2246−2259

Figure 2 presents the dry and ash-free yields of mass, energy, C, H, and O for the torrefied samples of macroalgae, grape

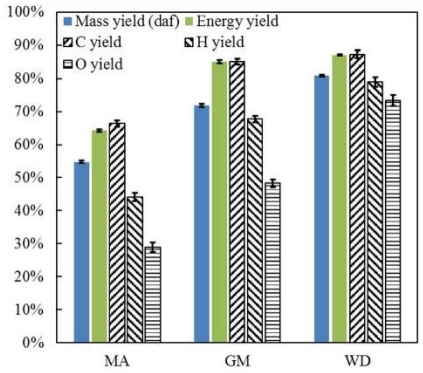

Figure 2. Yields of mass (dry and ash-free basis), energy, C, H, and O for the torrefied samples of macroalgae (MA), grape marc (GM), and wood (WD).

marc, and wood. The yields of C, H, and O were defined on the basis of the elemental retention in the solid phase after torrefaction. It can be seen that the highest mass yield achieved from the present cases was 81% for the wood, followed by 72.9% for the grape marc and 58.5% for the macroalgae. For macroalgae, the significant mass loss during the torrefaction process could be attributed to the high content of proteins and carbohydrates (the high activity organic constituents[53]), which are together typically greater than 50 wt %, on a dry basis.[54,55] The high mass yield achieved for the torrefaction of wood is deduced to be due to the relatively low content of hemicellulose (the high activity organic constituent), which is usually less than 30% for wood.[56] Interestingly, a similar energy yield of 87% was obtained for the torrefactions of both the grape marc and wood, even though the mass yield from the torrefaction of grape marc was much lower than that for wood. This is because there was a greater loss of oxygen during the torrefaction of grape marc than that for wood, as shown in Figure 2. Moreover, the energy yield for the torrefaction of macroalgae was lower than that for the other two feedstocks, which is attributed mostly to the significant loss of C and H during the torrefaction of macroalgae.

3.2. Char Yield from Pyrolysis. Figure 3 presents the dry and ash-free char mass yields based on dry parent biomass for both the raw and torrefied wood, grape marc, and macroalgae as a function of the pyrolysis temperature over the range of 800−1100 °C. It can be seen that a greater char yield (on the basis of the parent biomass) was obtained for all of the studied torrefied biomass samples than from their corresponding raw samples. This can be attributed to the cross-linking of cellulose that occurs during the biomass torrefaction process.[57,58] That is, torrefaction causes cellulose to depolymerize to form active cellulose, which then undergoes cross-linking. Cross-linked cellulose can form char through further polycondensation. During the subsequent pyrolysis process, the cross-linking and charring of cellulose during torrefaction predominantly promote the formation of char.[57,58] However, the reason for the increase of the char yield for the torrefied macroalgae is yet to be fully understood, and further study is required.

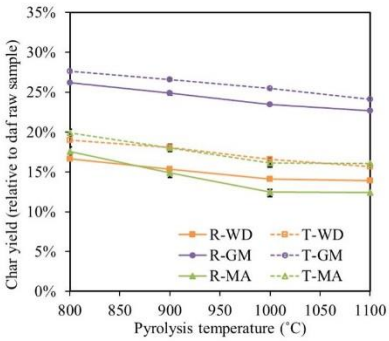

Figure 3. Char mass yield (dry and ash-free basis) relative to the raw biomass as a function of the pyrolysis temperature for both the raw and torrefied wood (R-WD and T-WD), grape marc (R-GM and T-GM), and macroalgae (R-MA and T-MA).

The char yield for all three materials, wood, grape marc, and macroalgae, was found to decrease with an increase in the pyrolysis temperature (800−1000 °C), for both the raw and torrefied forms. However, the decrease was found to be continued with a further increase in the pyrolysis temperature to 1100 °C for wood and grape marc, while for macroalgae, no further reduction in the char yield can be observed. The decrease in the char yield with an increase in the pyrolysis temperature is attributable mostly to the rearrangement of the carbon structure and the release of further volatiles.[59] In addition, high-temperature ash reactions (e.g., to form K_2CO_3) can also contribute to this decrease. These lead to the release of volatile ash (e.g., K_2CO_3) and affect the retention of organic matter.[60]

3.3. Catalytic Elements (Na and K). *3.3.1. Retentions of Na and K after Pyrolysis and Gasification.* Figure 4 presents the extent to which Na and/or K are retained (relative to the content of elements in the parent biomass) in the char after pyrolysis and in the ash after further char gasification as a function of the temperature for both the raw and torrefied (a) grape marc and (b) macroalgae. Here, the char used for each gasification experiment was produced at the same temperature as the gasification. A retention in the char of less than 100% implies that releases of Na and/or K have occurred during the pyrolysis process.[44,45] Besides, releases of further Na and/or K during the char gasification process may have occurred if a retention in the ash after char gasification is lower than that in the char after pyrolysis.[44,45] It can be seen from Figure 4a that no significant release of K occurs from either the raw or torrefied grape marc during the pyrolysis process over the temperature range from 800 to 900 °C. However, the retention of K decreases significantly for both the raw and torrefied grape marc chars with the pyrolysis temperature over the range of 1000−1100 °C. On the other hand, a significant release of K was found to occur during the gasification of both the raw and torrefied grape marc char at the temperature range from 800 to 1000 °C. However, no significant influence of torrefaction on the release of K from the grape marc char was found for either the gasification or pyrolysis process.

It can also be seen from Figure 4 that no significant release of K or Na was found for macroalgae during the pyrolysis process at 800 °C. However, the retention of both K and Na was found to decrease significantly with an increase in the pyrolysis temperature over the range from 800 to 1000 °C. In addition,

DOI: 10.1021/acs.energyfuels.6b02215
Energy Fuels 2017, 31, 2246−2259

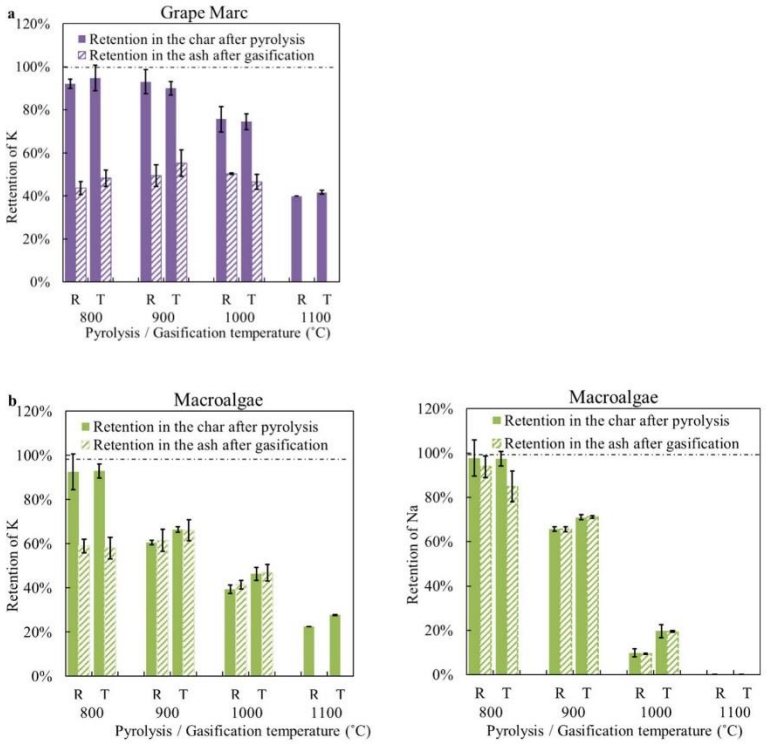

Figure 4. Retention of Na and/or K in the char after pyrolysis and in the ash after char gasification as a function of the temperature for the raw (R) and torrefied (T) (a) grape marc and (b) macroalgae. Conditions: The char used for each gasification experiment was produced at the same temperature as the gasification.

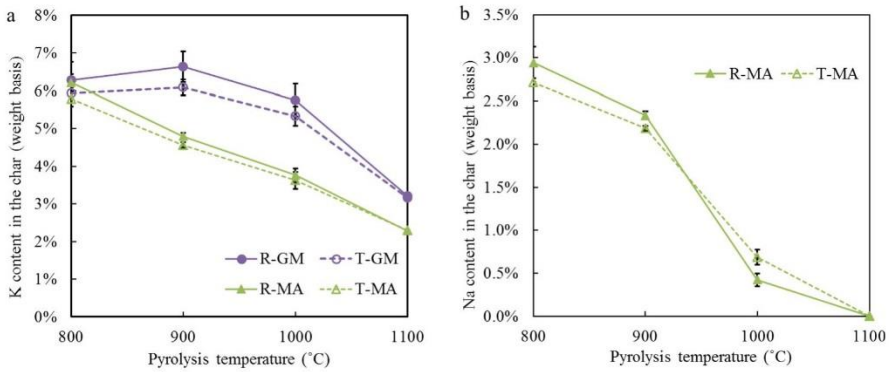

Figure 5. Dependence upon the pyrolysis temperature for the chars from both raw and torrefied grape marc (R-GM and T-GM) and/or macroalgae (R-MA and T-MA) of the contents of (a) K and (b) Na.

the release of K and Na during the char gasification process was found to be significant only at a temperature of 800 °C. However, no significant influence of torrefaction on the release of K was found for macroalgae during the char gasification process.

In addition, with an increase in the pyrolysis temperature, the torrefied macroalgae tends to release less Na and K than the raw macroalgae. At a pyrolysis temperature of 1000 °C, approximately 41.3% of K was found to be retained in the raw macroalgae char, while 11.6% of Na was found to be retained in the raw macroalgae char. However, for the torrefied macroalgae char, these two values were found to be increased to 49.3 and 22.2%, respectively. The reason for this difference is yet to be fully understood.

The release of K and Na can occur via many routes, including sublimation of chlorides (e.g., KCl and NaCl), decomposition of carbonates (e.g., K_2CO_3 and Na_2CO_3), vaporization of sulfates (e.g., K_2SO_4 and Na_2SO_4), vaporization of phosphates

DOI: 10.1021/acs.energyfuels.6b02215
Energy Fuels 2017, 31, 2246−2259

(e.g., KPO_3 and $NaPO_3$), etc.[44] Hence, it is plausible that torrefaction may influence the release of Na and K under high-temperature thermal processes via changing the chlorine content in the feedstock and/or transforming the alkali metals. However, this is not yet fully understood. In addition, no significant release of either Ca or Mg was found during either the pyrolysis or gasification processes for all of the char samples tested in the present study.

3.3.2. Content of Na and K in the Char. Figure 5 presents the dependence upon the pyrolysis temperature for the chars from both raw and torrefied grape marc and/or macroalgae of the content of (a) K and (b) Na. For pyrolysis temperatures over the range from 800 to 1000 °C, the torrefied grape marc char has a lower content of K than the raw grape marc char. This is attributed mostly to the higher char yield for the torrefied grape marc than for the raw grape marc, as shown in Figure 3. However, for the higher pyrolysis temperature of 1100 °C, the difference in the K content is negligible. In addition, for pyrolysis temperatures over the range from 800 to 1000 °C, no significant variation in the content of K was found for either the raw or torrefied grape marc chars. However, for the higher temperature of 1100 °C, the K content decreases significantly for both the raw and torrefied grape marc chars. It is deduced that this could result from the significant release of K, as discussed in section 3.3.1.

The contents of K and Na in the torrefied macroalgae char were both lower than in the raw macroalgae char for the pyrolysis temperature of 800 °C. As for the case of grape marc, this is attributed mostly to the higher char yield for the torrefied macroalgae than for the raw macroalgae. However, the content of K for the raw and torrefied macroalgae is approximately the same for the higher temperatures over the range from 1000 to 1100 °C. On the other hand, the content of Na in the torrefied macroalgae char was higher than that in the raw macroalgae char for the pyrolysis temperature of 1000 °C. This is attributed mostly to the lower release of K and Na during the pyrolysis process for the torrefied macroalgae than for the raw macroalgae, especially at higher temperatures, as shown in Figure 4. For the raw and torrefied macroalgae chars, the contents of both K and Na were found to decrease significantly with an increase in the pyrolysis temperature over the range from 800 to 1100 °C. This is attributed to the significant increase in the release of K and Na, as discussed in section 3.3.1. No Na was detected for the pyrolysis temperature of 1100 °C.

3.4. Char SSA. Figure 6 presents the SSA (determined by CO_2 adsorption at 273 K) of the char from the raw and torrefied wood, grape marc, and macroalgae as a function of the pyrolysis temperature. It can be seen that torrefaction has a small effect on the SSA of the wood char, which is attributed mostly to the insignificant mass loss during the wood torrefaction process. On the other hand, the SSA of both the torrefied grape marc char and torrefied macroalgae char was found to be lower than that of the char produced from their corresponding raw fuels. The lower SSA of the char could be due to the lower volatile content in the torrefied fuels compared to the raw fuels.[61]

In addition, the SSA for both the raw and torrefied wood chars was found to vary little with the pyrolysis temperature over the range from 800 to 1000 °C. This SSA is approximately 690 m^2/g, which is close to that (633 m^2/g) achieved in the literature for spruce wood char.[62] However, there was a significant decrease in these char SSAs for the higher pyrolysis

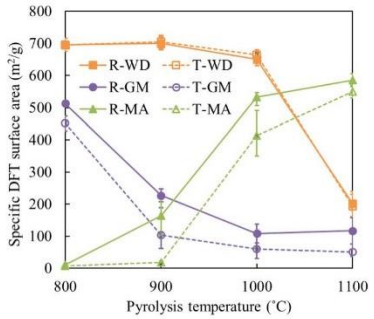

Figure 6. SSA (determined by CO_2 adsorption at 273 K) as a function of the pyrolysis temperature for both the raw and torrefied wood chars (R-WD and T-WD), grape marc chars (R-GM and T-GM), and macroalgae chars (R-MA and T-MA).

temperature of 1100 °C. Potential explanations for this are the reordering of the char structure, micropore coalescence, pore collapse, and ash (alkali compound) sintering.[63−65] For both the raw and torrefied grape marc chars, the SSA was found to decrease as the pyrolysis temperature was increased from 800 to 900 °C. A similar trend was also found for the grape seed (main components of grape marc) char in the literature.[66] In addition, the SSA for both the raw and torrefied macroalgae chars produced at 800 °C was found to be very low (<25 m^2/g) compared to that of the grape marc chars produced at the same temperature (>500 m^2/g). This could be due to the high content of Na in the macroalgae chars, which could lead to significant sintering at 800 °C.

However, at higher temperatures, the SSA of both the raw and torrefied macroalgae chars was found to increase with an increase in the pyrolysis temperature (from 800 to 1100 °C). A similar trend was also found in the literature for char produced from algae.[67] In contrast, no significant change of SSA was found for both the raw and torrefied grape marc chars over the temperature range from 900 to 1100 °C. A plausible explanation for this difference is that the release of alkali metals from the macroalgae char was found to increase significantly with the pyrolysis temperature, as shown in Figure 4, which would open the pores and counter the effect of ash sintering. For the grape marc chars, the significant release of K from both the raw and torrefied forms, especially from 900 to 1100 °C, will tend to increase the SSAs. Nevertheless, even though the concentration of K in the grape marc char can be deduced, it is still sufficient, even at the pyrolysis temperature of 1100 °C (see Figure 5), for ash sintering to inhibit such an increase in the SSA.

3.5. Raman Spectra Measurements. Figure 7 presents examples of Raman spectra normalized by the maximum intensity of the G band at approximately 1590 cm^{-1} for both the raw and torrefied grape marc chars prepared at the pyrolysis temperatures of 800 and 1000 °C. It can be seen that biomass chars exhibit two strong peaks at the D and G bands. The normalized intensity of the D band, which is associated with the Raman shift of 1300−1400 cm^{-1}, increases with the number of disordered structures in graphite or other highly ordered carbonaceous materials. In contrast, the intensity of the G band, which is associated with the Raman shift of 1550−1600 cm^{-1}, is attributed to the stretching vibration modes of graphite C=C bonds. Hence, the intensity of the G band (I_G) is sharpened as the degree of graphitization increases.[50] The V band lies at the

DOI: 10.1021/acs.energyfuels.6b02215
Energy Fuels 2017, 31, 2246−2259

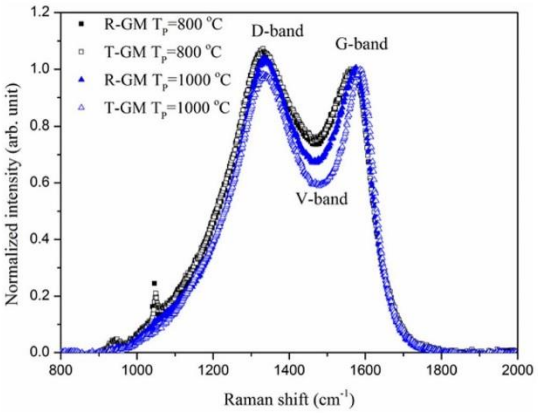

Figure 7. Examples of Raman spectra normalized by the maximum intensity of the G band, which peaks at approximately 1590 cm^{-1}, for both the raw and torrefied grape marc chars (R-GM and T-GM) prepared at the pyrolysis temperatures (T_p) of 800 and 1000 °C.

valley between the D and G bands, with a shift of approximately 1500 cm^{-1}. Its intensity increases with the number of amorphous carbon structures.[68] Therefore, the uniformity of the carbonaceous structure can be determined from the intensity ratio between the V and G bands (I_V/I_G).[50]

Figure 8 presents the intensity ratio I_V/I_G for all of the raw and torrefied biomass chars as a function of the pyrolysis

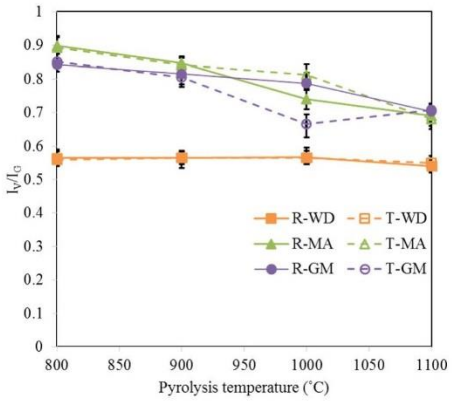

Figure 8. Intensity ratio I_V/I_G as a function of the pyrolysis temperature for the chars prepared from both the raw and torrefied wood (R-WD and T-WD), grape marc (R-GM and T-GM), and macroalgae (R-MA and T-MA).

temperature. It can be seen that, for the wood char, both the pyrolysis temperature and torrefaction process were found to have a negligible effect on I_V/I_G. Meanwhile, I_V/I_G was found to decrease with an increase in the pyrolysis temperature for both the grape marc and macroalgae chars. This decrease implies an increase in the uniformity of the carbonaceous structure, which is consistent with previous findings reported in the literature.[49] Moreover, the most significant effect of torrefaction on I_V/I_G was found for both the grape marc and macroalgae chars at 1000 °C. Torrefaction was found to increase I_V/I_G for the macroalgae char but to decrease that for the grape marc char.

3.6. Reactivity of CO_2 Gasification of Char. *3.6.1. Reactivity Index.* Figure 9a presents the reactivity index (R_{50}) of

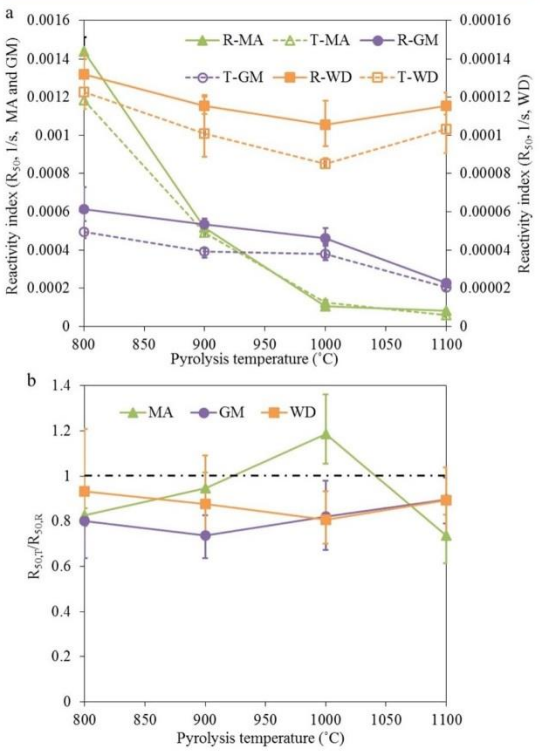

Figure 9. Dependence upon the pyrolysis temperature for the wood (WD), grape marc (GM), and macroalgae (MA): (a) CO_2 gasification reactivity index (R_{50}) of the char from raw (R) and torrefied (T) biomass and (b) R_{50} of the torrefied biomass char ($R_{50,T}$) normalized to that of the corresponding raw biomass char ($R_{50,R}$). Condition: the gasification temperature was set at 800 °C for all of the char samples.

the CO_2 gasification (T_G = 800 °C) of char as a function of the pyrolysis temperature for the raw and torrefied wood, grape marc, and macroalgae. It can be seen that the gasification reactivity decreases with an increase in the pyrolysis temperature for all of the studied chars, except for the wood, for which char reactivity increases between 1000 and 1100 °C. The initial decrease in reactivity for wood char could be attributed to the decrease in the concentration of catalytic inorganic matter (e.g., K), because no obvious change was found in the SSA or the uniformity of the carbonaceous structure[69] [note that the release of K was not measured in the present study for the case of wood as a result of its low ash content, while a significant release of K was found for the case of grape marc and macroalgae, especially at high pyrolysis temperatures (>900 °C)]. On the other hand, over the pyrolysis temperature range of 1000−1100 °C, some other factors that were not investigated in the present study, e.g., the transformation of catalytic inorganic elements, may contribute to the slight increase in the gasification reactivity of wood char.

The decrease in the char gasification reactivity with the pyrolysis temperature for both the raw and torrefied macroalgae was found to be significant over the temperature range of 800−

DOI: 10.1021/acs.energyfuels.6b02215
Energy Fuels 2017, 31, 2246−2259

1000 °C. This is consistent with the significant decrease in the content of alkali metals (as shown in Figure 5) and the increase in carbonaceous structure uniformity, as discussed in section 3.5,[50,69] suggesting that these effects outweigh the competing trend of an increase in SSA, which would lead to an increase in char reactivity. However, no significant decrease in the gasification reactivity of either the raw or torrefied macroalgae chars was found as the pyrolysis temperature was further increased from 1000 to 1100 °C, even though the decrease in the concentration of Na and K was still considerable. A likely explanation for this is that the most active Na and K compounds (e.g., alkali carbonates) are released below 1000 °C,[70] so that the remaining compounds are in a less active form (e.g., Na and K retention inside the char matrix instead of at the surface[69]).

The reactivity of both the raw and torrefied grape marc chars was found to decrease slightly over the pyrolysis temperature range from 800 to 1000 °C. However, the decrease for both the raw torrefied grape marc chars was found to be much more significant as the pyrolysis temperature was further increased to 1100 °C. This significant decrease can be explained by the significant decrease in the content of K over the temperature range of 1000−1100 °C (discussed in section 3.3.2).

Figure 9b presents the dependence upon the pyrolysis temperature of the CO_2 gasification reactivity index of the torrefied biomass char ($R_{s0,T}$) normalized by that of the corresponding raw biomass char ($R_{s0,R}$) for the wood, grape marc, and macroalgae. It can be seen that the torrefaction has little effect on the reactivity of wood char, which is consistent with the measurement of SSA (as discussed in section 3.4) and carbonaceous structure (as discussed in section 3.5). However, for macroalgae, torrefaction was found to decrease the char reactivity for a pyrolysis temperature of 800 °C and to increase it for 1000 °C. The reduction for 800 °C can be attributed primarily to the decrease in the reduction in the content of alkali metals, as discussed in section 3.3.2. In addition, the reduction in the concentration of Ca and Mg may also contribute to the lower reactivity of the torrefied biomass chars than for the corresponding raw biomass chars. This is consistent with the negligible release of either Ca or Mg during the pyrolysis process (section 3.3.1) and the char yield (on the basis of parent biomass) for the torrefied biomass being always higher than that for the corresponding raw biomass (Figure 3). For 1000 °C, the higher reactivity for the torrefied macroalgae char compared to the raw macroalgae char may be due to the greater concentration of Na (section 3.3.2) and the lower uniformity of the carbonaceous structure (section 3.5). In addition, at 1100 °C, the torrefied macroalgae char was found to have a lower reactivity than the raw macroalgae char. This is consistent with the lower SSA for the torrefied macroalgae char than for the raw macroalgae char. Interestingly, the content of Na was found to decrease to zero for both the raw and torrefied macroalgae chars at 1100 °C, so that it has no influence on the reactivity.

The torrefied grape marc char was found to exhibit a lower gasification reactivity than the raw grape marc char within the pyrolysis temperature range from 800 to 1000 °C. This is consistent with the lower content of K (section 3.3.2), the lower SSA (section 3.4), and the higher uniformity of the carbonaceous structure (at 1000 °C only; section 3.5). However, the influence of torrefaction was found to reduce with an increase in the pyrolysis temperature from 1000 to 1100 °C. This is attributed mostly to the negligible difference in the K content between the raw and torrefied grape marc char at 1100 °C, as shown in Figure 5.

Figure 10 presents the CO_2 gasification reactivity index (R_{s0}; T_G = 800 °C) as a function of the content of alkali metal (K + Na) for both the raw and torrefied (a) grape marc and (b) macroalgae chars. Because the content of the inorganic matter for the wood studied here is negligible compared to that in the studied grape marc and macroalgae, no data for wood chars is plotted in Figure 10. It can be seen that, for these conditions, a linear correlation is found between the logarithm of the reactivity index and the content of alkali metal for both the grape mar and macroalgae chars, although the slope is different for the grape marc and macroalgae chars. With an increase in the pyrolysis temperature, the significant decrease in gasification reactivity can therefore be attributed mostly to the decrease in the content of alkali metals. In addition, torrefaction reduces both the reactivity and the content of alkali metal for the chars prepared from both grape marc and macroalgae under all of the studied pyrolysis conditions, except for the char prepared from macroalgae at 1000 °C. For the case T_p = 1000

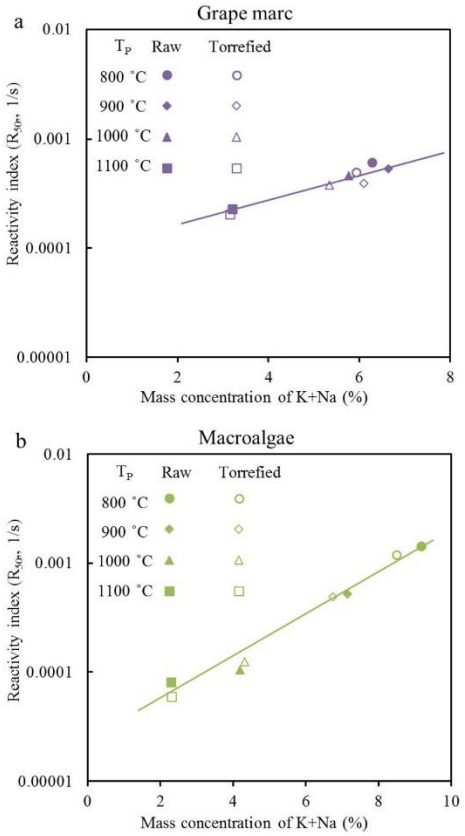

Figure 10. Reactivity index for CO_2 gasification (R_{s0}) as a function of the content of alkali metal (K + Na) for both the raw and torrefied (a) grape mar chars (R-GM and T-GM) and (b) macroalgae chars (R-MA and T-MA). Conditions: The pyrolysis temperature (T_p) was set in the range from 800 to 1100 °C, while the gasification temperature was set to be 800 °C.

DOI: 10.1021/acs.energyfuels.6b02215
Energy Fuels 2017, 31, 2246−2259

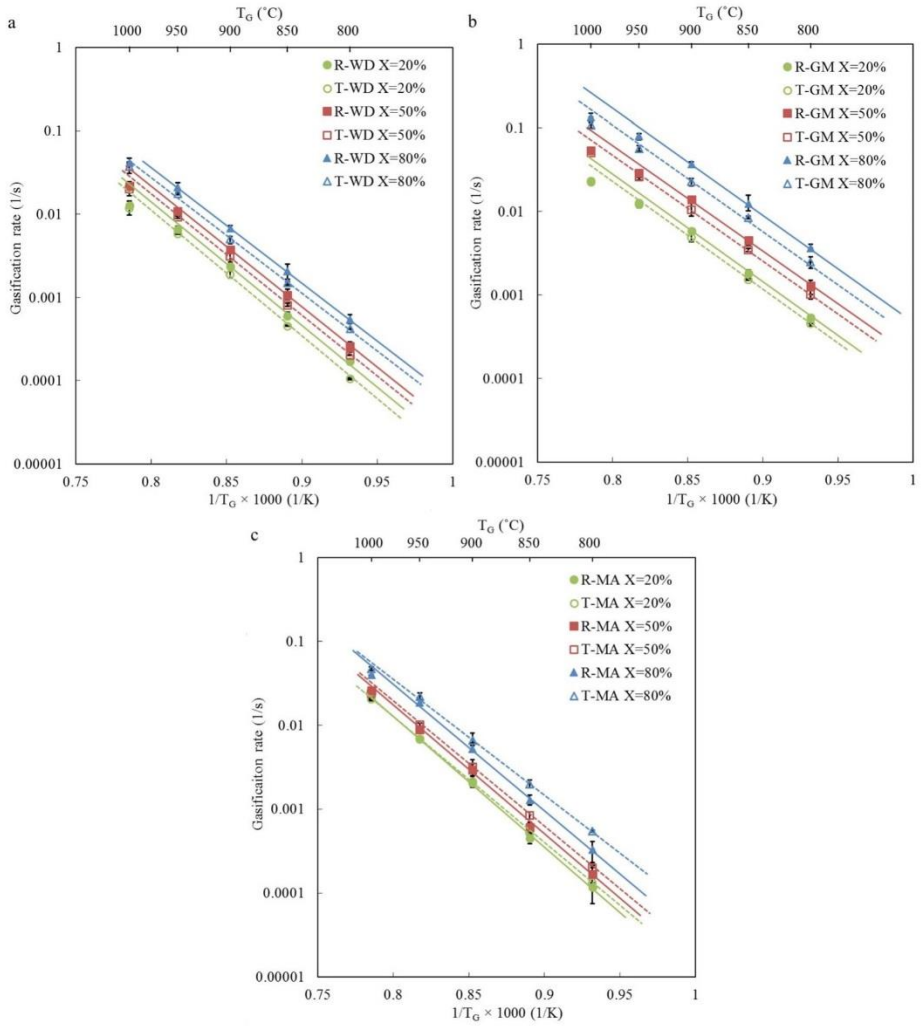

Figure 11. Arrhenius plots at various char gasification conversions (X) for the chars prepared at 1000 °C from both the raw (R) and torrefied (T) (a) wood (WD), (b) grape marc (GM), and (c) macroalgae (MA).

Table 2. Activation Energy (E_a) and Pre-exponential Factor (A) for Each of the Various Char Conversions (X) and for Each of the Studied Raw and Torrefied Chars Prepared at 1000 °C

		raw			torrefied		
		X = 20%	X = 50%	X = 80%	X = 20%	X = 50%	X = 80%
wood	E_a (kJ/mol)	303.5	298.1	290.9	304.8	297	291.2
	A (s^{-1})	7×10^{10}	7×10^{10}	7×10^{10}	7×10^{10}	5×10^{10}	5×10^{10}
grape marc	E_a (kJ/mol)	241.4	240.5	250.9	239.6	235.3	249.1
	A (s^{-1})	3×10^{8}	7×10^{8}	5×10^{9}	2×10^{8}	3×10^{8}	3×10^{9}
macroalgae	E_a (kJ/mol)	300.1	297.5	291.6	284.2	279.5	265.6
	A (s^{-1})	5×10^{10}	3×10^{10}	5×10^{10}	8×10^{9}	7×10^{9}	5×10^{9}

°C, torrefaction increases both the reactivity and the content of alkali metal for the macroalgae char. However, in comparison to the influence of the pyrolysis temperature on both the reactivity and the content of alkali metal in the studied chars, the influence of torrefaction is relatively small.

3.6.2. Arrhenius Plots. Figure 11 presents Arrhenius plots for all of the studied raw and torrefied chars prepared at 1000 °C, each for various char conversions (X = 20, 50, and 80%). For gasification temperatures below 900 °C, the linear correlation in each of these Arrhenius plots implies that these gasification

DOI: 10.1021/acs.energyfuels.6b02215
Energy Fuels 2017, 31, 2246−2259

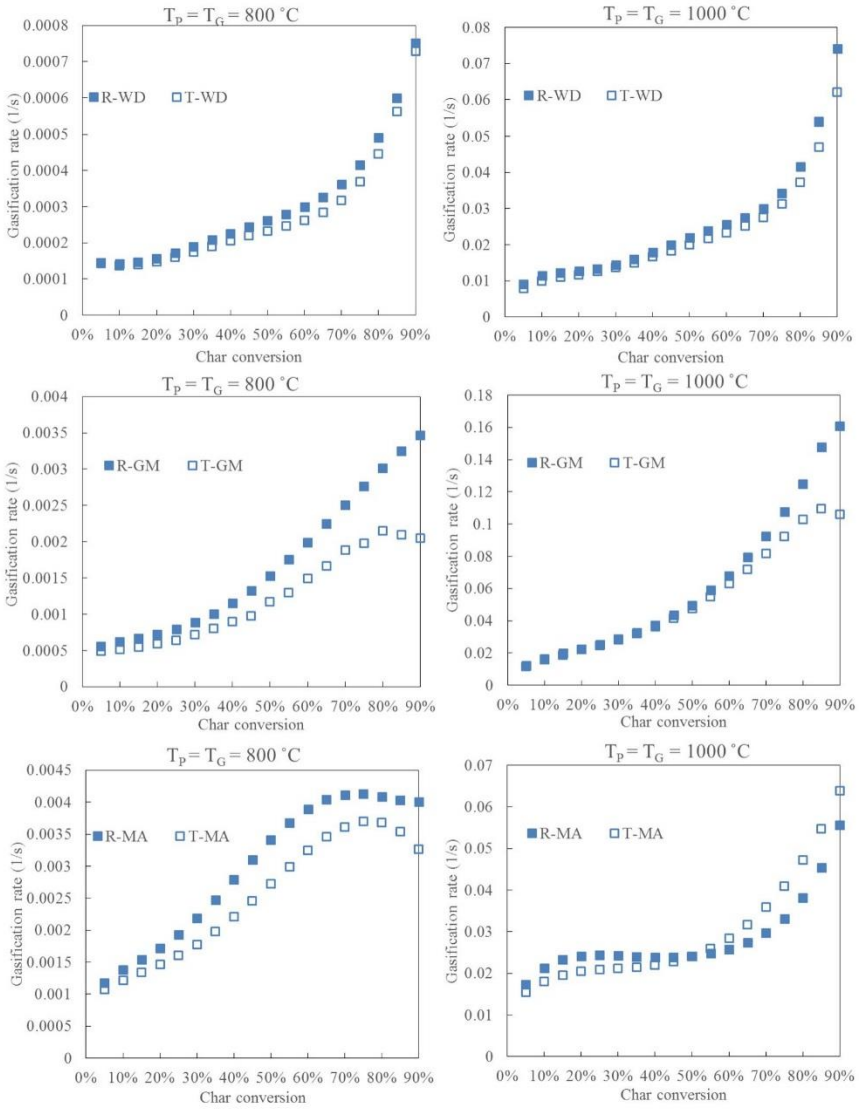

Figure 12. Gasification rate as a function of char conversion for both the raw and torrefied wood chars (R-WD and T-WD), grape marc chars (R-GM and T-GM), and macroalgae chars (R-MA and T-MA). Conditions: The pyrolysis temperature (T_P) and the gasification temperature (T_G) for each scenario were set to be the same (i.e., $T_P = T_G = 800$ °C, and $T_P = T_G = 1000$ °C).

reactions are all kinetically controlled throughout the measurement range.[40] Hence, the activation energy can be determined from the slope of the fitted line, while the pre-exponential factor can be determined from the intercept. The results of these measurements are shown in Table 2. This shows that the influence of the torrefaction and char conversion on the activation energy is small for the wood and grape marc chars. However, for the macroalgae char, torrefaction can be seen to reduce the activation energy, especially for the cases with higher char conversion. For the case $X = 80\%$, the activation energy for the raw macroalgae char is about 291.6 kJ/mol, while it is only about 265.6 kJ/mol for the torrefied macroalgae char. The difference in activation energy can be attributed to the measured differences in the content of Na and the uniformity of the carbonaceous structure, as presented in Figures 5 and 8, respectively.

However, for gasification temperatures of greater than 900 °C, the gasification reactions transition to the pore diffusion-controlled regime, in which the gasification rates depart from the linear correlation.

3.6.3. Trends in Gasification Rates. Figure 12 presents the gasification rate as a function of char conversion for each of the raw and torrefied chars prepared at the pyrolysis temperatures of 800 and 1000 °C. Here, each of the raw and torrefied biomass samples were first pyrolyzed and then gasified at the same temperature. The gasification rate can be seen to increase

DOI: 10.1021/acs.energyfuels.6b02215
Energy Fuels 2017, 31, 2246−2259

monotonously with the conversion for both the raw and torrefied wood char at 800 and 1000 °C. Furthermore, the rate of increase becomes greater with the char conversion. Potential explanations for this are the increase in the concentration of catalytic elements and/or the increase in porosity.[71,72]

Different from the above findings, for the raw grape marc chars prepared at both 800 and 1000 °C, even though the gasification rates both increase monotonously with the conversion, the rate of this increase tends to be constant over the conversion range from 50 to 90%. Furthermore, for the torrefied grape marc chars prepared at both 800 and 1000 °C, the gasification rates tend to decrease or be constant over the conversion range from 80 to 90%. A similar trend was found for both the raw and torrefied macroalgae chars at 800 °C, over the conversion range from 70 to 90%. This could be due to (i) the destruction of the physical structure of the char, (ii) the release of alkali metals (Figure 4), (iii) an increased concentration of condensed/graphitized carbonaceous matter, or (iv) an increased concentration of inert elements (e.g., Si and Al) on the char surface, which would impede the gasification reactions.[69,73]

On the other hand, for both the raw and torrefied macroalgae chars prepared at 1000 °C, the char reactivity is nearly constant for char conversions of less than 50%. However, it increases significantly as the char conversion is increased from 50 to 90%. It could be due to the synthetic influence of the factors discussed above regarding the concentration of catalysts, the carbonaceous structure, and the SSA of char. Therefore, to better understand the gasification rate variation with char conversions, more investigation on the variation of these factors needs to be carried out for various conversions.

4. CONCLUSION

In summary, it was found that torrefaction can influence char reactivity through its influence on the concentration of catalytic species, such as Na and K, through its influence on SSA and its influence on the carbonaceous structure.

For a pyrolysis temperature of 800 °C, the gasification reactivity of both the torrefied grape marc and the torrefied macroalgae chars were found to be lower than that of the chars prepared from their corresponding raw fuels. The decrease is attributed to a lower SSA and a lower concentration of the alkali metals (Na and/or K) in the char.

For a pyrolysis temperature of 1000 °C, the gasification reactivity for the torrefied macroalgae char was found to be higher than that of the raw macroalgae char. This is attributed to both the higher content of Na and the less uniform carbonaceous structure of the torrefied macroalgae char. On the other hand, the gasification reactivity for the torrefied grape marc char was found to be lower than that of the raw grape marc char. This was explained by both the lower content of K and the greater uniformity of the carbonaceous structure of the torrefied grape marc char.

For the present pyrolysis conditions (800−1100 °C, relatively low heating rate in tube furnace, and atmospheric pressure), the influence of torrefaction on char gasification reactivity and physicochemical properties was not remarkable. However, considering the increase in the char yield as a result of torrefaction, the carbon conversion of the torrefied fuel in a gasifier could be significantly different from that of the raw fuel. In particular, the influence of torrefaction on the char gasification reactivity and physicochemical properties could be greater at different values of the heating rate and pyrolysis pressure.

AUTHOR INFORMATION

Corresponding Author

*Telephone: +61406887246. E-mail: peijun.guo@adelaide.edu.au.

ORCID

Peijun Guo: 0000-0001-6631-7818

Notes

The authors declare no competing financial interest.

ACKNOWLEDGMENTS

The work was supported by the Australian Solar Thermal Research Initiative (ASTRI), a project supported by the Australian Government, through the Australian Renewable Energy Agency (ARENA). The Australian Government, through ARENA, supports Australian research and development in solar photovoltaic and solar thermal technologies to help solar power become cost-competitive with other energy sources. Peijun Guo thanks the generous support of the Chinese Scholarship Council (CSC), who provided the scholarship for his Ph.D. study. Philip J. van Eyk acknowledges the support of the Australian Solar Institute (ASI) for providing a postdoctoral fellowship. Graham J. Nathan thanks the Australian Research Council (ARC) for the Discovery Outstanding Researcher Award used to support this work.

REFERENCES

(1) International Energy Agency (IEA). *World Energy Outlook 2014*; IEA: Paris, France, 2014.

(2) Lawton, R. J.; Mata, L.; de Nys, R.; Paul, N. A. Selecting Reliable and Robust Freshwater Macroalgae for Biomass Applications. *PLoS One* **2013**, *8* (10), e77344.

(3) Stephens, E.; de Nys, R.; Ross, I. L.; Hankamer, B. Algae Fuels as an Alternative to Petroleum. *J. Pet. Environ. Biotechnol.* **2013**, *4* (4), 148.

(4) Kumar, K.; Ghosh, S.; Angelidaki, I.; Holdt, S. L.; Karakashev, D. B.; Morales, M. A.; Das, D. Recent developments on biofuels production from microalgae and macroalgae. *Renewable Sustainable Energy Rev.* **2016**, *65*, 235−249.

(5) Neveux, N.; Magnusson, M.; Mata, L.; Whelan, A.; de Nys, R.; Paul, N. A. The treatment of municipal wastewater by the macroalga Oedogonium sp. and its potential for the production of biocrude. *Algal Res.* **2016**, *13*, 284−292.

(6) van Eyk, P.; Muhlack, R.; Ashman, P. Gasification of grape marc in a circulating fluidized bed. *Proceedings of the Australian Combustion Symposium*; Brisbane, Queensland, Australia, Dec 2−4, 2009.

(7) Roberts, D. A.; Paul, N. A.; Bird, M. I.; de Nys, R. Bioremediation for coal-fired power stations using macroalgae. *J. Environ. Manage.* **2015**, *153*, 25−32.

(8) Lawton, R. J.; de Nys, R.; Skinner, S.; Paul, N. A. Isolation and Identification of Oedogonium Species and Strains for Biomass Applications. *PLoS One* **2014**, *9* (3), e90223.

(9) van der Stelt, M. J. C.; Gerhauser, H.; Kiel, J. H. A.; Ptasinski, K. J. Biomass upgrading by torrefaction for the production of biofuels: A review. *Biomass Bioenergy* **2011**, *35* (9), 3748−3762.

(10) Nanou, P.; Carbo, M. C.; Kiel, J. H. A. Detailed mapping of the mass and energy balance of a continuous biomass torrefaction plant. *Biomass Bioenergy* **2016**, *89*, 67−77.

(11) Thrän, D.; Witt, J.; Schaubach, K.; Kiel, J.; Carbo, M.; Maier, J.; Ndibe, C.; Koppejan, J.; Alakangas, E.; Majer, S.; Schipfer, F. Moving torrefaction towards market introduction − Technical improvements and economic-environmental assessment along the overall torrefaction

DOI: 10.1021/acs.energyfuels.6b02215
Energy Fuels 2017, 31, 2246−2259

supply chain through the SECTOR project. *Biomass Bioenergy* **2016**, *89*, 184−200.
(12) Chen, W. H.; Peng, J. H.; Bi, X. T. T. A state-of-the-art review of biomass torrefaction, densification and applications. *Renewable Sustainable Energy Rev.* **2015**, *44*, 847−866.
(13) Chew, J. J.; Doshi, V. Recent advances in biomass pretreatment − Torrefaction fundamentals and technology. *Renewable Sustainable Energy Rev.* **2011**, *15* (8), 4212−4222.
(14) Almeida, G.; Brito, J. O.; Perre, P. Alterations in energy properties of eucalyptus wood and bark subjected to torrefaction: The potential of mass loss as a synthetic indicator. *Bioresour. Technol.* **2010**, *101* (24), 9778−9784.
(15) Chen, W. H.; Cheng, W. Y.; Lu, K. M.; Huang, Y. P. An evaluation on improvement of pulverized biomass property for solid fuel through torrefaction. *Appl. Energy* **2011**, *88* (11), 3636−3644.
(16) Chang, S.; Zhao, Z. L.; Zheng, A. Q.; He, F.; Huang, Z.; Li, H. B. Characterization of Products from Torrefaction of Sprucewood and Bagasse in an Auger Reactor. *Energy Fuels* **2012**, *26* (11), 7009−7017.
(17) Sabil, K. M.; Aziz, M. A.; Lal, B.; Uemura, Y. Effects of torrefaction on the physiochemical properties of oil palm empty fruit bunches, mesocarp fiber and kernel shell. *Biomass Bioenergy* **2013**, *56*, 351−360.
(18) Medic, D.; Darr, M.; Shah, A.; Potter, B.; Zimmerman, J. Effects of torrefaction process parameters on biomass feedstock upgrading. *Fuel* **2012**, *91* (1), 147−154.
(19) Sadaka, S.; Negi, S. Improvements of Biomass Physical and Thermochemical Characteristics via Torrefaction Process. *Environ. Prog. Sustainable Energy* **2009**, *28* (3), 427−434.
(20) Wu, K.-T.; Tsai, C.-J.; Chen, C.-S.; Chen, H.-W. The characteristics of torrefied microalgae. *Appl. Energy* **2012**, *100*, 52−57.
(21) Chen, W.-H.; Huang, M.-Y.; Chang, J.-S.; Chen, C.-Y.; Lee, W.-J. An energy analysis of torrefaction for upgrading microalga residue as a solid fuel. *Bioresour. Technol.* **2015**, *185*, 285−293.
(22) Chen, W.-H.; Huang, M.-Y.; Chang, J.-S.; Chen, C.-Y. Torrefaction operation and optimization of microalga residue for energy densification and utilization. *Appl. Energy* **2015**, *154*, 622−630.
(23) Bridgeman, T. G.; Jones, J. M.; Shield, I.; Williams, P. T. Torrefaction of reed canary grass, wheat straw and willow to enhance solid fuel qualities and combustion properties. *Fuel* **2008**, *87* (6), 844−856.
(24) Xue, G.; Kwapinska, M.; Kwapinski, W.; Czajka, K. M.; Kennedy, J.; Leahy, J. J. Impact of torrefaction on properties of Miscanthus × giganteus relevant to gasification. *Fuel* **2014**, *121*, 189−197.
(25) Prins, M. J.; Ptasinski, K. J.; Janssen, F. J. J. G. More efficient biomass gasification via torrefaction. *Energy* **2006**, *31* (15), 3458−3470.
(26) Dudyński, M.; van Dyk, J. C.; Kwiatkowski, K.; Sosnowska, M. Biomass gasification: Influence of torrefaction on syngas production and tar formation. *Fuel Process. Technol.* **2015**, *131*, 203−212.
(27) Kwapinska, M.; Xue, G.; Horvat, A.; Rabou, L. P. L. M.; Dooley, S.; Kwapinski, W.; Leahy, J. J. Fluidized Bed Gasification of Torrefied and Raw Grassy Biomass (Miscanthus × gigantenus). The Effect of Operating Conditions on Process Performance. *Energy Fuels* **2015**, *29* (11), 7290−7300.
(28) Deng, J.; Wang, G.-j.; Kuang, J.-h.; Zhang, Y.-l.; Luo, Y.-h. Pretreatment of agricultural residues for co-gasification via torrefaction. *J. Anal. Appl. Pyrolysis* **2009**, *86* (2), 331−337.
(29) Weiland, F.; Nordwaeger, M.; Olofsson, I.; Wiinikka, H.; Nordin, A. Entrained flow gasification of torrefied wood residues. *Fuel Process. Technol.* **2014**, *125*, 51−58.
(30) Karlstrom, O.; Costa, M.; Brink, A.; Hupa, M. CO_2 gasification rates of char particles from torrefied pine shell, olive stones and straw. *Fuel* **2015**, *158*, 753−763.
(31) Fisher, E. M.; Dupont, C.; Darvell, L. I.; Commandre, J. M.; Saddawi, A.; Jones, J. M.; Grateau, M.; Nocquet, T.; Salvador, S. Combustion and gasification characteristics of chars from raw and torrefied biomass. *Bioresour. Technol.* **2012**, *119*, 157−165.
(32) Li, T.; Geier, M.; Wang, L.; Ku, X. K.; Güell, B. M.; Lovas, T.; Shaddix, C. R. Effect of Torrefaction on Physical Properties and Conversion Behavior of High Heating Rate Char of Forest Residue. *Energy Fuels* **2015**, *29* (1), 177−184.
(33) Kulkarni, A.; Baker, R.; Abdoulmomine, N.; Adhikari, S.; Bhavnani, S. Experimental study of torrefied pine as a gasification fuel using a bubbling fluidized bed gasifier. *Renewable Energy* **2016**, *93*, 460−468.
(34) Cerone, N.; Zimbardi, F.; Villone, A.; Strjiugas, N.; Kiyikci, E. G. Gasification of Wood and Torrefied Wood with Air, Oxygen, and Steam in a Fixed-Bed Pilot Plant. *Energy Fuels* **2016**, *30* (5), 4034−4043.
(35) Couhert, C.; Salvador, S.; Commandre, J. M. Impact of torrefaction on syngas production from wood. *Fuel* **2009**, *88* (11), 2286−2290.
(36) Ku, X. K.; Lin, J. Z.; Yuan, F. Y. Influence of Torrefaction on Biomass Gasification Performance in a High-Temperature Entrained-Flow Reactor. *Energy Fuels* **2016**, *30* (5), 4053−4064.
(37) Jones, J. M.; Bridgeman, T. G.; Darvell, L. I.; Gudka, B.; Saddawi, A.; Williams, A. Combustion properties of torrefied willow compared with bituminous coals. *Fuel Process. Technol.* **2012**, *101*, 1−9.
(38) McNamee, P.; Darvell, L. I.; Jones, J. M.; Williams, A. The combustion characteristics of high-heating-rate chars from untreated and torrefied biomass fuels. *Biomass Bioenergy* **2015**, *82*, 63−72.
(39) Zhang, S. P.; Hu, B.; Zhang, L.; Xiong, Y. Q. Effects of torrefaction on yield and quality of pyrolysis char and its application on preparation of activated carbon. *J. Anal. Appl. Pyrolysis* **2016**, *119*, 217−223.
(40) Kajitani, S.; Hara, S.; Matsuda, H. Gasification rate analysis of coal char with a pressurized drop tube furnace. *Fuel* **2002**, *81* (5), 539−546.
(41) Lozano-Castelló, D.; Cazorla-Amorós, D.; Linares-Solano, A. Usefulness of CO_2 adsorption at 273 K for the characterization of porous carbons. *Carbon* **2004**, *42* (7), 1233−1242.
(42) Huang, Y.; Yin, X.; Wu, C.; Wang, C.; Xie, J.; Zhou, Z.; Ma, L.; Li, H. Effects of metal catalysts on CO_2 gasification reactivity of biomass char. *Biotechnol. Adv.* **2009**, *27* (5), 568−572.
(43) Lahijani, P.; Zainal, Z. A.; Mohamed, A. R.; Mohammadi, M. CO_2 gasification reactivity of biomass char: Catalytic influence of alkali, alkaline earth and transition metal salts. *Bioresour. Technol.* **2013**, *144*, 288−295.
(44) Lane, D. J.; van Eyk, P. J.; Ashman, P. J.; Kwong, C. W.; de Nys, R.; Roberts, D. A.; Cole, A. J.; Lewis, D. M. Release of Cl, S, P, K, and Na during Thermal Conversion of Algal Biomass. *Energy Fuels* **2015**, *29* (4), 2542−2554.
(45) Li, C. Z.; Sathe, C.; Kershaw, J. R.; Pang, Y. Fates and roles of alkali and alkaline earth metals during the pyrolysis of a Victorian brown coal. *Fuel* **2000**, *79* (3−4), 427−438.
(46) Tay, H.-L.; Li, C.-Z. Changes in char reactivity and structure during the gasification of a Victorian brown coal: Comparison between gasification in O_2 and CO_2. *Fuel Process. Technol.* **2010**, *91* (8), 800−804.
(47) Morga, R. Micro-Raman spectroscopy of carbonized semi-fusinite and fusinite. *Int. J. Coal Geol.* **2011**, *87* (3−4), 253−267.
(48) Wang, M. J.; Roberts, D. G.; Kochanek, M. A.; Harris, D. J.; Chang, L. P.; Li, C. Z. Raman Spectroscopic Investigations into Links between Intrinsic Reactivity and Char Chemical Structure. *Energy Fuels* **2014**, *28* (1), 285−290.
(49) Sheng, C. Char structure characterised by Raman spectroscopy and its correlations with combustion reactivity. *Fuel* **2007**, *86* (15), 2316−2324.
(50) Okumura, Y.; Hanaoka, T.; Sakanishi, K. Effect of pyrolysis conditions on gasification reactivity of woody biomass-derived char. *Proc. Combust. Inst.* **2009**, *32*, 2013−2020.
(51) Asadullah, M.; Zhang, S.; Min, Z.; Yimsiri, P.; Li, C.-Z. Effects of biomass char structure on its gasification reactivity. *Bioresour. Technol.* **2010**, *101* (20), 7935−7943.

DOI: 10.1021/acs.energyfuels.6b02215
Energy Fuels 2017, 31, 2246−2259

(52) Channiwala, S. A.; Parikh, P. P. A unified correlation for estimating HHV of solid, liquid and gaseous fuels. *Fuel* **2002**, *81* (8), 1051−1063.
(53) Chen, W.-H.; Huang, M.-Y.; Chang, J.-S.; Chen, C.-Y. Thermal decomposition dynamics and severity of microalgae residues in torrefaction. *Bioresour. Technol.* **2014**, *169*, 258−264.
(54) Cole, A. J.; de Nys, R.; Paul, N. A. Biorecovery of nutrient waste as protein in freshwater macroalgae. *Algal Res.* **2015**, *7*, 58−65.
(55) Rodrigues, D.; Freitas, A. C.; Pereira, L.; Rocha-Santos, T. A. P.; Vasconcelos, M. W.; Roriz, M.; Rodríguez-Alcalá, L. M.; Gomes, A. M. P.; Duarte, A. C. Chemical composition of red, brown and green macroalgae from Buarcos bay in Central West Coast of Portugal. *Food Chem.* **2015**, *183*, 197−207.
(56) Peng, J.; Bi, X.; Lim, J.; Sokhansanj, S. Development of torrefaction kinetics for British Columbia softwood. *Int. J. Chem. React. Eng.* **2012**, *10* (1), 1−37.
(57) Elyounssi, K.; Collard, F.-X.; Mateke, J.-a. N.; Blin, J. Improvement of charcoal yield by two-step pyrolysis on eucalyptus wood: A thermogravimetric study. *Fuel* **2012**, *96*, 161−167.
(58) Zheng, A.; Zhao, Z.; Chang, S.; Huang, Z.; Wang, X.; He, F.; Li, H. Effect of torrefaction on structure and fast pyrolysis behavior of corncobs. *Bioresour. Technol.* **2013**, *128*, 370−377.
(59) Daud, W. M. A. W.; Ali, W. S. W.; Sulaiman, M. Z. Effect of carbonization temperature on the yield and porosity of char produced from palm shell. *J. Chem. Technol. Biotechnol.* **2001**, *76* (12), 1281−1285.
(60) Trubetskaya, A.; Jensen, P. A.; Jensen, A. D.; Garcia Llamas, A. D.; Umeki, K.; Glarborg, P. Effect of fast pyrolysis conditions on biomass solid residues at high temperatures. *Fuel Process. Technol.* **2016**, *143*, 118−129.
(61) Della Rocca, P. A.; Cerrella, E. G.; Bonelli, P. R.; Cukierman, A. L. Pyrolysis of hardwoods residues: On kinetics and chars characterization. *Biomass Bioenergy* **1999**, *16* (1), 79−88.
(62) Burhenne, L.; Aicher, T. Benzene removal over a fixed bed of wood char: The effect of pyrolysis temperature and activation with CO_2 on the char reactivity. *Fuel Process. Technol.* **2014**, *127*, 140−148.
(63) Huang, Y.; Jin, B.; Zhong, Z.; Zhong, W.; Xiao, R. Characteristic and mercury adsorption of activated carbon produced by CO_2 of chicken waste. *J. Environ. Sci.* **2008**, *20* (3), 291−296.
(64) Guerrero, M.; Ruiz, M. P.; Millera, Á.; Alzueta, M. U.; Bilbao, R. Characterization of Biomass Chars Formed under Different Devolatilization Conditions: Differences between Rice Husk and Eucalyptus. *Energy Fuels* **2008**, *22* (2), 1275−1284.
(65) Paethanom, A.; Yoshikawa, K. Influence of Pyrolysis Temperature on Rice Husk Char Characteristics and Its Tar Adsorption Capability. *Energies* **2012**, *5* (12), 4941.
(66) Jimenez-Cordero, D.; Heras, F.; Alonso-Morales, N.; Gilarranz, M. A.; Rodriguez, J. J. Porous structure and morphology of granular chars from flash and conventional pyrolysis of grape seeds. *Biomass Bioenergy* **2013**, *54*, 123−132.
(67) Chang, Y. M.; Tsai, W. T.; Li, M. H. Characterization of activated carbon prepared from chlorella-based algal residue. *Bioresour. Technol.* **2015**, *184*, 344−348.
(68) Li, X.; Hayashi, J.-i.; Li, C.-Z. FT-Raman spectroscopic study of the evolution of char structure during the pyrolysis of a Victorian brown coal. *Fuel* **2006**, *85* (12−13), 1700−1707.
(69) Quyn, D. M.; Wu, H.; Hayashi, J.-i.; Li, C.-Z. Volatilisation and catalytic effects of alkali and alkaline earth metallic species during the pyrolysis and gasification of Victorian brown coal. Part IV. Catalytic effects of NaCl and ion-exchangeable Na in coal on char reactivity. *Fuel* **2003**, *82* (5), 587−593.
(70) Chakrabarti, R.; Schmidt, L. D. Role of Potassium and Phosphorus in Catalytic Partial Oxidation in Short Contact Time Reactors. *Energy Fuels* **2015**, *29* (12), 8102−8109.
(71) Umeki, K.; Moilanen, A.; Gómez-Barea, A.; Konttinen, J. A model of biomass char gasification describing the change in catalytic activity of ash. *Chem. Eng. J.* **2012**, *207−208*, 616−624.
(72) Adschiri, T.; Furusawa, T. Relation between CO_2-reactivity of coal char and BET surface area. *Fuel* **1986**, *65* (7), 927−931.
(73) Fermoso, J.; Arias, B.; Pevida, C.; Plaza, M. G.; Rubiera, F.; Pis, J. J. Kinetic models comparison for steam gasification of different nature fuel chars. *J. Therm. Anal. Calorim.* **2008**, *91* (3), 779−786.

DOI: 10.1021/acs.energyfuels.6b02215
Energy Fuels 2017, 31, 2246−2259

CHAPTER 6

CONCLUSIONS AND RECOMMENDATIONS

6.1 Conclusions

A novel configuration of a solar hybridized coal to FTL fuels system via an SDFB gasifier has been proposed and analysed using a pseudo-dynamic model. This new concept has the potential to offer steady syngas output and sensible heat storage via solid particles. However, the calculated performance of the proposed solar hybridized FTL fuels production system is very sensitive to the char conversion in the gasification process. The addition of char separation has the potential to significantly increase the performance of the studied solar hybridized FTL fuels production system with relatively low char gasification conversion while the use of FT reactor tail-gas recycle has the potential to significantly increase the productivity of the main product FTL fuels. As expected, co-gasification of biomass with coal can significantly decrease the greenhouse gas emissions from the studied FTL fuels production systems compared with the equivalent systems via gasification of coal alone. However, the application of biomass is limited due to some properties, e.g., high oxygen content, high moisture content, low calorific value, hygroscopic nature and low density, which can result in low conversion efficiency and difficulties in collection, grinding, transportation and storage. Torrefaction can improve these properties, thus updating biomass to more attractive feedstock for gasification. However, torrefaction can also influence the char gasification reactivity, thereby affecting the design and operation of the gasification process. Therefore, the influence of torrefaction on the char characteristics was investigated to better understand the variation of the char gasification reactivity caused by torrefaction. It was found that the influence of torrefaction on the bio-char characteristics strongly depended on the biomass species and pyrolysis conditions.

6.1.1 Performance Assessment of Fischer−Tropsch Liquid Fuels Production by Solar Hybridized Dual Fluidized Bed Gasification of Lignite

The annual energetic and environmental performance of the solar hybridized coal to liquids (SCTL) system with an SDFB gasifier is achieved by using a pseudo-dynamic model that assumes steady state operation at each time step for a one-year, hourly integrated solar insolation. In addition, the sensitivity of annual performance of the present studied system to the solar multiple, bed material storage capacity, char gasification conversion, and the quality of solar resource was obtained. The solar multiple the ratio of the heliostat field area relative to that required to meet the demand of the DFB gasifier at the point of peak solar thermal output.

To maintain continuous and steady operation of the proposed SDFB gasifier without feeding any supplementary fuel into the combustion reactor, a huge calculated storage capacity (over 900 hours) is required, thus lowering the feasibility of the proposed system. Under this condition, the maximum values of the annual solar share (SS_{ann}) and the utilization factor of the heliostat collector ($\overline{U_{coll,ann}}$) are calculated to be 30.4% and 41.6%. Here, SS_{ann} is defined based on the energy input to present the percentage of solar energy in the total energy input, thus indicating the ratio of carbonless solar energy input to the carbonaceous fuel input. The maximum values of the percentage change in annual specific FTL output ($\Delta Q_{s,FTL,ann}$), the percentage change in annual specific net electricity output ($\Delta W_{s,net,ann}$) and annual reduction of CO_2 emissions ($\Delta E_{CO_2,ann}$) relative to their non-solar CTL counterparts are calculated to be 30.4%, 41.6%, 50.9%, 25.7%, and 46.9%, respectively, for a char gasification conversion of 100%.

In addition, significant improvements in the performance of the studied solar hybridized system compared with the equivalent non-solar system are also possible when coupled with a more realistic storage capacity, even though some dumping occurs. For a solar multiple of 3 and a storage capacity of 16 hours, the values of SS_{ann}, $\overline{U_{coll,ann}}$, $\Delta Q_{s,FTL,ann}$, $\Delta W_{s,net,ann}$, and $\Delta E_{CO_2,ann}$ are calculated to be 21.8%, 40.8%, 32.6%, 13.9%, and 34.1%, respectively.

On the other hand, both the energetic and environmental performance of the proposed SCTL system increases with the quality of the solar resource. The values of the calculated SS_{ann} of the proposed SCTL system are 21.8% by using the solar data in Farmington, NM, USA (2004/2005) and 14.6% by using the solar data in Dickinson, ND, USA (2004/2005). Moreover, the calculated performance of the studied SCTL system is also very sensitive to char gasification conversion. The SS_{ann} is reduced to zero as the char gasification conversion is reduced to 57%. In addition, for the presented studied case with lignite fuel as the feedstock, the calculated net mine-to-tank (MTT) CO_2 emissions exceed the value of the baseline case of diesel derived from mineral crude oil.

Therefore, new approaches are needed with which to further improve the energetic and environmental performance of the SCTL system, especially under relatively low char gasification conversions.

6.1.2 System optimization for Fischer−Tropsch liquid fuels production via solar hybridized dual fluidized bed gasification of solid fuels

New approaches, notably the incorporation of char separation, co-gasification of biomass and coal, the integration of carbon capture and sequestration (CCS) and the use of FT reactor tail-gas recycle, are proposed and found to be able to significantly improve the energetic and environmental performance of an FTL fuels production system using an SDFB gasifier.

To achieve the well-to-wheel (WTW) CO_2 emissions parity with the value of mineral fuel, a calculated biomass fraction of 47.9% based on HHV is required for the solar hybridized coal and biomass-to-liquids ($SCTL_{bio}$) system with a char gasification conversion of 80%, a solar multiple of 2.64 and a storage capacity of 16 h. The value of this calculated biomass fraction can be decreased to about 47.9% by solar hybridization in the case of a solar multiple of 2.64 and a storage capacity of 16 h. In addition, the value of this calculated biomass fraction can be decreased to about 17% by incorporating CCS.

On the other hand, an increase in the biomass fraction can result in a decrease in the calculated specific FT liquids output per unit feedstock ($Q_{s,FTL,ann}$) of the proposed $SCTL_{bio}$ system, alongside an increase in the calculated specific electricity output per unit feedstock ($W_{s,net,ann}$). As the biomass fraction is increased from 0 to 100%, the value of the calculated $Q_{s,FTL,ann}$ is decreased from 59.6% to 48.3% while the calculated $W_{s,net,ann}$ is increased from 10.4 to 16.7%. Furthermore, the addition of CCS results in a lower $W_{s,net,ann}$. However, the electricity is sufficient for self-sufficiency, even for the system with CCS.

The use of FT reactor tail-gas recycle to the $SCTL_{bio}$ system has the potential to significantly increase $Q_{s,FTL,ann}$ and SS_{ann} while decreasing $W_{s,net,ann}$, especially for cases with a high biomass fraction. For a solar multiple of 2.64, a storage capacity of 16 h, a char gasification conversion of 80% and a biomass fraction of 0, the calculated values of $Q_{s,FTL,ann}$ and SS_{ann} are increased by 20% and 9%, respectively, by the use of tail-gas recycle. For the case with only biomass as the feedstock, the calculated values of $Q_{s,FTL,ann}$ and SS_{ann} can be increased by 49.6% and 27.3%, respectively.

The addition of char separation also has the potential to significantly increase the performance of the proposed $SCTL_{bio}$ system. For a solar multiple of 2.64, a storage capacity of 16 h and a char gasification conversion of 80%, the calculated SS_{ann} of the studied SCTL system is increased from 12.2% to 20.3% by integrating char separation. Nevertheless, this influence decreases with an increase in both the biomass fraction and the char gasification conversion, due to the reduced amount of char from the gasifier (the fixed carbon content in the studied biomass (spruce wood) is lower than that in the studied lignite).

Even the co-gasification of biomass with coal can reduce CO_2 emissions from the proposed SCTL system significantly, large-scale application of the biomass is constrained by some biomass properties discussed in Section 1.1.3.2. In addition, torrefaction has been proven to be able to relieve this constraint. However, torrefaction can also influence the char gasification reactivity, thus affecting the design and operation of the gasification process.

6.1.3 Gasification reactivity and physicochemical properties of the chars from raw and torrefied wood, grape marc and macroalgae

In this study, it was found that torrefaction can influence the characteristics (i.e., specific surface area (SSA), concentration of catalytic species and the carbonaceous structure) of the char, thus influencing the char reactivity. In addition, the influences of the torrefaction process on char reactivity and char characteristics strongly depend on the biomass species and pyrolysis conditions.

For a pyrolysis temperature of 800 ºC, the SSA and the concentration of the alkali metals (Na and/or K) of both the torrefied grape marc and the torrefied macroalgae chars were both found to be lower than those of the chars prepared from their corresponding raw fuels. These decreases can result in a lower gasification reactivity of the char which is consistent with the findings of the present study.

For a pyrolysis temperature of 1000 ºC, the gasification reactivity for the torrefied grape marc char was also found to be lower than that of the raw grape marc char. On the other hand, the gasification reactivity for the torrefied macroalgae char was found to be higher than that of the char prepared from raw macroalgae. This increase is attributed to both the higher content of Na and the less uniform carbonaceous structure of the torrefied macroalgae char.

The influence of torrefaction on both char gasification reactivity and physicochemical properties is not remarkable for the selected species of biomass and conditions of pyrolysis (800−1100 ˚C, a relatively low heating rate in the tube furnace and atmospheric pressure). However, considering the increase in the char yield resulting from torrefaction, the carbon conversion of the torrefied fuel in a gasifier could be significantly different from that of the corresponding raw fuel. In addition, this

influence of torrefaction could be greater at different heating rates and pyrolysis pressures.

6.2 Recommendations for future work

Further studies are necessary to demonstrate the proposed configuration of solar hybridized coal/biomass to FTL fuels system via an SDFB gasifier and to improve understanding of the influence of torrefaction on the biomass char properties. The detailed recommendations are:

1. One of the main challenges of the proposed SDFB gasifier is the method with which the concentrated solar energy is to be integrated to heat the bed material that is used to drive the gasification process. Therefore, a technically feasible and economically affordable configuration of the solar particle receiver, together with a possible particle transportation (e.g., from the ground to the tower) system can be proposed, assessed (by using a dynamic model to understand the impact of start-up and shut-down) and demonstrated.
2. Another challenge of the proposed SDFB gasifier is the high temperature particle storage. Since the particles undergo the high heat flux in the solar receiver, some tiny particles could be overheated. Moreover, due to the severe conditions in the SDFB gasifier (e.g., ash coating, high temperature oxidization and reduction atmosphere), agglomeration could occur in the particle storage units. Therefore, further investigation can be performed to avoid the agglomeration in the particle storage units by better storage system design, better particle selection and so on.

3. Economic analysis of the currently proposed solar hybridized FTL fuels production systems can be performed in the future to further evaluate their viability.
4. Demonstration of char separation from the mixture of char and sand in the future. Demonstration of char storage is recommended since the high reactivity of it.
5. In the present study, it was found that the influence of torrefaction on the biomass char properties strongly depends on the pyrolysis temperature. However, the dependences on the other pyrolysis conditions, i.e., heating rate, pyrolysis pressure and pyrolysis time can also be studied in the future.
6. To understand the gasification performance (e.g., carbon conversion, tar generation, syngas composition, etc) of torrefied biomass in a DFB gasifier, relevant experiments of the DFB gasification of torrefied biomass need to be performed in the future.

REFERENCES

The following references are cited in Chapters 1, 2 and 6. References for Chapter 3-5 are included within each of those chapters.

Abdelouahed, L., Authier, O., Mauviel, G., Corriou, J. P., Verdier, G., and Dufour, A. (2012). Detailed Modeling of Biomass Gasification in Dual Fluidized Bed Reactors under Aspen Plus. *Energy & Fuels, 26*(6), 3840-3855.

Adams, T., and Barton, P. (2011). Combining coal gasification and natural gas reforming for efficient polygeneration. *Fuel Processing Technology*, *92*(3).

Adinberg, R., Epstein, M., and Karni, J. (2004). Solar Gasification of Biomass: A Molten Salt Pyrolysis Study. *Journal of Solar Energy Engineering, 126*(3), 850-857.

Aigner, I., Pfeifer, C., and Hofbauer, H. (2011). Co-gasification of coal and wood in a dual fluidized bed gasifier. *Fuel, 90*(7), 2404-2412.

Ail, S. S., and Dasappa, S. (2016). Biomass to liquid transportation fuel via Fischer Tropsch synthesis – Technology review and current scenario. *Renewable and Sustainable Energy Reviews, 58*, 267-286.

Asadullah, M., Zhang, S., Min, Z., Yimsiri, P., and Li, C.-Z. (2010). Effects of biomass char structure on its gasification reactivity. *Bioresour Technol, 101*(20), 7935-7943.

Baliban, R. C., Elia, J. A., and Floudas, C. A. (2013). Novel Natural Gas to Liquids Processes: Process Synthesis and Global Optimization Strategies. *Aiche Journal, 59*(2), 505-531.

Bayarsaikhan, B., Hayashi, J.-i., Shimada, T., Sathe, C., Li, C.-Z., Tsutsumi, A., and Chiba, T. (2005). Kinetics of steam gasification of nascent char from rapid pyrolysis of a Victorian brown coal. *Fuel, 84*(12–13), 1612-1621.

Bell, D. A., Towler, B. F., and Fan, M. (2011). *Coal gasification and its application*: Elsevier.

Bertocchi, R., Karni, J., and Kribus, A. (2004). Experimental evaluation of a non-isothermal high temperature solar particle receiver. *Energy, 29*(5–6), 687-700.

Brown, R. C., Liu, Q., and Norton, G. (2000). Catalytic effects observed during the co-gasification of coal and switchgrass. *Biomass and Bioenergy, 18*(6), 499-506.

C.K. Ho, J.M. Christian, J. Yellowhair, K. Armijo, and S. Jeter. (2016). *Performance Evaluation of a high-temperature falling particle receiver*. *ASME Power & Energy Conference*, Charlotte, NC.

C.K. Ho, J.M. Christian, J. Yellowhair, N. Siegel, S. Jeter, M. Golob, S.I. Abdel-Khalik, C. Nguyen, and Al-Ansary, H. (2015). *On sun testing of an advanced falling particle receiver system*. *SolarPACES 2015*, Cape Town, South Africa.

Cerone, N., Zimbardi, F., Villone, A., Strjiugas, N., and Kiyikci, E. G. (2016). Gasification of Wood and Torrefied Wood with Air, Oxygen, and Steam in a Fixed-Bed Pilot Plant. *Energy & Fuels, 30*(5), 4034-4043.

Chen, W. H., Peng, J. H., and Bi, X. T. T. (2015). A state-of-the-art review of biomass torrefaction, densification and applications. *Renewable & Sustainable Energy Reviews, 44*, 847-866.

Chew, J. J., and Doshi, V. (2011). Recent advances in biomass pretreatment – Torrefaction fundamentals and technology. *Renewable and Sustainable Energy Reviews, 15*(8), 4212-4222.

Couhert, C., Salvador, S., and Commandre, J. M. (2009). Impact of torrefaction on syngas production from wood. *Fuel, 88*(11), 2286-2290.

Ding, L., Zhou, Z., Guo, Q., Huo, W., and Yu, G. (2015). Catalytic effects of Na_2CO_3 additive on coal pyrolysis and gasification. *Fuel, 142*, 134-144.

Dry, M. E. (2002). The Fischer-Tropsch process: 1950-2000. *Catalysis Today, 71*(3-4), 227-241.

Dry, M. E. (2004). Chapter 3 - Chemical concepts used for engineering purposes. In S. André & D. Mark (Eds.), *Studies in Surface Science and Catalysis*, vol. Volume 152 (pp. 196-257): Elsevier.

Dudyński, M., van Dyk, J. C., Kwiatkowski, K., and Sosnowska, M. (2015). Biomass gasification: Influence of torrefaction on syngas production and tar formation. *Fuel Processing Technology, 131*, 203-212.

Duman, G., Uddin, M. A., and Yanik, J. (2014). The effect of char properties on gasification reactivity. *Fuel Processing Technology, 118*, 75-81.

Elyounssi, K., Collard, F.-X., Mateke, J.-a. N., and Blin, J. (2012). Improvement of charcoal yield by two-step pyrolysis on eucalyptus wood: A thermogravimetric study. *Fuel, 96*, 161-167.

Feldman, H. F., Paisley, M. A., Appelbaum, H. R., and Taylor, D. R. (1988). *Conversion of Forest Residues to a Methane-Rich Gas in a high-Throughput gasifier*: Battelle Columbus Division

Fisher, E. M., Dupont, C., Darvell, L. I., Commandre, J. M., Saddawi, A., Jones, J. M., Grateau, M., Nocquet, T., and Salvador, S. (2012). Combustion and gasification characteristics of chars from raw and torrefied biomass. *Bioresour Technol, 119*, 157-165.

Flamant, G., Hernandez, D., Bonet, C., and Traverse, J.-P. (1980). Experimental aspects of the thermochemical conversion of solar energy; Decarbonation of $CaCO_3$. *Solar Energy, 24*(4), 385-395.

Fout, T., Zoelle, A., Keairns, D., Turner, M., Woods, M., Kuehn, N., Shah, V., Chou, V., and Hamilton, B. A. (2015). *Cost and Performance Baseline for Fossil Energy Plants Volume 1a: Bituminous Coal (PC) and Natural Gas to Electricity Revision 3*: NETL.

Gibson, P. (2007). *Coal to Liquids at Sasol*: Sasl Technology R&D.

Gil, A., Medrano, M., Martorell, I., Lázaro, A., Dolado, P., Zalba, B., and Cabeza, L. F. (2010). State of the art on high temperature thermal energy storage for power generation. Part 1—Concepts, materials and modellization. *Renewable and Sustainable Energy Reviews, 14*(1), 31-55.

Gokon, N., Izawa, T., Abe, T., and Kodama, T. (2014). Steam gasification of coal cokes in an internally circulating fluidized bed of thermal storage material for solar thermochemical processes. *International Journal of Hydrogen Energy, 39*(21), 11082-11093.

Gokon, N., Izawa, T., and Kodama, T. (2015). Steam gasification of coal cokes by internally circulating fluidized-bed reactor by concentrated Xe-light radiation for solar syngas production. *Energy, 79*, 264-272.

Gokon, N., Ono, R., Hatamachi, T., Li, L. Y., Kim, H. J., and Kodama, T. (2012). CO_2 gasification of coal cokes using internally circulating fluidized bed reactor by concentrated Xe-light irradiation for solar gasification. *International Journal of Hydrogen Energy, 37*(17), 12128-12137.

Gregg, D. W., Taylor, R. W., Campbell, J. H., Taylor, J. R., and Cotton, A. (1980). Solar Gasification of Coal, Activated Carbon, Coke and Coal and Biomass Mixtures. *Solar Energy, 25*(4), 353-364.

Guo, P. J., van Eyk, P. J., Saw, W. L., Ashman, P. J., Nathan, G. J., and Stechel, E. B. (2015). Performance Assessment of Fischer-Tropsch Liquid Fuels Production by Solar Hybridized Dual Fluidized Bed Gasification of Lignite. *Energy & Fuels*, *29*(4), 2738-2751.

Hamelinck, C., Faaij, A., den Uil, H., and Boerrigter, H. (2004). Production of FT transportation fuels from biomass, technical options, process analysis and optimisation, and development potential. *Energy, 29*(11).

Hathaway, B. J., Davidson, J. H., and Kittelson, D. B. (2011). Solar Gasification of Biomass: Kinetics of Pyrolysis and Steam Gasification in Molten Salt. *Journal of Solar Energy Engineering, 133*(2), 021011-021011.

Hathaway, B. J., Kittelson, D. B., and Davidson, J. H. (2014). Integration of Solar Gasification With Conventional Fuel Production: The Roles of Storage and Hybridization. *Journal of Solar Energy Engineering-Transactions of the Asme, 136*(1).

Henry Chen, Y. H., Reilly, J. M., and Paltsev, S. (2011). The prospects for coal-to-liquid conversion: A general equilibrium analysis. *Energy Policy, 39*(9), 4713-4725.

Higman, C., and van der Burgt, J. M. (2003). *Gasification*: Elsevier.

Ho, C., Christian, J., Gill, D., Moya, A., Jeter, S., Abdel-Khalik, S., Sadowski, D., Siegel, N., Al-Ansary, H., Amsbeck, L., Gobereit, B., and Buck, R. (2014). Technology Advancements for Next Generation Falling Particle Receivers. *Energy Procedia, 49*, 398-407.

Ho, C. K. (In Press). A review of high-temperature particle receivers for concentrating solar power. *Applied Thermal Engineering*.

Ho, C. K., and Iverson, B. D. (2014). Review of high-temperature central receiver designs for concentrating solar power. *Renewable and Sustainable Energy Reviews, 29*, 835-846.

Hofbauer, H., Rauch, R., Bosch, K., Koch, R., and Aichernig, C. (2003). Biomass CHP Plant Güssing: A Success Story. In A. V. Bridgewater (Ed.), *Pyrolysis and Gasification of Biomass and Waste*, (pp. 527-536). U.K.: CPL Press.

Hofbauer, H., Rauch, R., Löffler, G., Kaiser, S., Fercher, E., and Tremmel, H. (2002). *Six years experience with the FICFB-gasification process. 12th European Conference and Technology Exhibition on Biomass for Energy. Industry and Climate Protection*, Amsterdam.

Hruby, J. M. (1986). *Technical feasibility study of a solid particle solar central receiver for high temperature applications*: ; Sandia National Labs., Livermore, CA (USA).

Hu, J., Yu, F., and Lu, Y. (2012). Application of Fischer–Tropsch Synthesis in Biomass to Liquid Conversion. *Catalysts, 2*(2), 303.

Huang, Y., Yin, X., Wu, C., Wang, C., Xie, J., Zhou, Z., Ma, L., and Li, H. (2009). Effects of metal catalysts on CO_2 gasification reactivity of biomass char. *Biotechnol Adv, 27*(5), 568-572.

IEA. (2016). *China's Engagement in Global Energy Governance* International Energy Agency.

Jones, J. M., Bridgeman, T. G., Darvell, L. I., Gudka, B., Saddawi, A., and Williams, A. (2012). Combustion properties of torrefied willow compared with bituminous coals. *Fuel Processing Technology, 101*, 1-9.

Kajita, M., Kimura, T., Norinaga, K., Li, C.-Z., and Hayashi, J.-i. (2010). Catalytic and Noncatalytic Mechanisms in Steam Gasification of Char from the Pyrolysis of Biomass. *Energy & Fuels, 24*(1), 108-116.

Kajitani, S., Hara, S., and Matsuda, H. (2002). Gasification rate analysis of coal char with a pressurized drop tube furnace. *Fuel, 81*.

Kaniyal, A. A., van Eyk, P. J., and Nathan, G. J. (2013a). Dynamic Modeling of the Coproduction of Liquid Fuels and Electricity from a Hybrid Solar Gasifier with Various Fuel Blends. *Energy & Fuels, 27*(6), 3556-3569.

Kaniyal, A. A., van Eyk, P. J., and Nathan, G. J. (2016). Storage capacity assessment of liquid fuels production by solar gasification in a packed bed reactor using a dynamic process model. *Applied Energy, 173*, 578-588.

Kaniyal, A. A., van Eyk, P. J., Nathan, G. J., Ashman, P. J., and Pincus, J. J. (2013b). Polygeneration of Liquid Fuels and Electricity by the Atmospheric Pressure Hybrid Solar Gasification of Coal. *Energy & Fuels, 27*(6), 3538-3555.

Karlstrom, O., Costa, M., Brink, A., and Hupa, M. (2015). CO_2 gasification rates of char particles from torrefied pine shell, olive stones and straw. *Fuel, 158*, 753-763.

Keown, D. M., Favas, G., Hayashi, J.-i., and Li, C.-Z. (2005). Volatilisation of alkali and alkaline earth metallic species during the pyrolysis of biomass: differences between sugar cane bagasse and cane trash. *Bioresour Technol, 96*(14), 1570-1577.

Kern, S., Pfeifer, C., and Hofbauer, H. (2013a). Co-Gasification of Wood and Lignite in a Dual Fluidized Bed Gasifier. *Energy & Fuels, 27*(2), 919-931.

Kern, S., Pfeifer, C., and Hofbauer, H. (2013b). Gasification of lignite in a dual fluidized bed gasifier - Influence of bed material particle size and the amount of steam. *Fuel Processing Technology, 111*, 1-13.

Kern, S. J., Pfeifer, C., and Hofbauer, H. (2013c). Cogasification of Polyethylene and Lignite in a Dual Fluidized Bed Gasifier. *Industrial & Engineering Chemistry Research, 52*(11), 4360-4371.

Kim, Y.-D., Yang, C.-W., Kim, B.-J., Moon, J.-H., Jeong, J.-Y., Jeong, S.-H., Lee, S.-H., Kim, J.-H., Seo, M.-W., Lee, S.-B., Kim, J.-K., and Lee, U.-D. (2016). Fischer–tropsch diesel production and evaluation as alternative automotive fuel in pilot-scale integrated biomass-to-liquid process. *Applied Energy, 180*, 301-312.

Kodama, T., Enomoto, S.-i., Hatamachi, T., and Gokon, N. (2008). Application of an Internally Circulating Fluidized Bed for Windowed Solar Chemical Reactor with Direct Irradiation of Reacting Particles. *Journal of Solar Energy Engineering, 130*(1), 014504-014504.

Kodama, T., Gokon, N., Enomoto, S., Itoh, S., and Hatamachi, T. (2010). Coal Coke Gasification in a Windowed Solar Chemical Reactor for Beam-Down Optics. *Journal of Solar Energy Engineering-Transactions of the Asme, 132*(4).

Kodama, T., Kondoh, Y., Tamagawa, T., Funatoh, A., Shimizu, K. I., and Kitayama, Y. (2002). Fluidized bed coal gasification with CO_2 under direct irradiation with concentrated visible light. *Energy & Fuels, 16*(5), 1264-1270.

Kolb, G. J., Diver, R. B., and Siegel, N. (2006). Central-Station Solar Hydrogen Power Plant. *Journal of Solar Energy Engineering, 129*(2), 179-183.

Kopyscinski, J., Rahman, M., Gupta, R., Mims, C. A., and Hill, J. M. (2014). K_2CO_3 catalyzed CO_2 gasification of ash-free coal. Interactions of the catalyst with carbon in N_2 and CO_2 atmosphere. *Fuel, 117, Part B*, 1181-1189.

Kruesi, M., Jovanovic, Z. R., dos Santos, E. C., Yoon, H. C., and Steinfeld, A. (2013). Solar-driven steam-based gasification of sugarcane bagasse in a combined drop-tube and fixed-bed reactor – Thermodynamic, kinetic, and experimental analyses. *Biomass and Bioenergy, 52*, 173-183.

Kruesi, M., Jovanovic, Z. R., and Steinfeld, A. (2014). A two-zone solar-driven gasifier concept: Reactor design and experimental evaluation with bagasse particles. *Fuel, 117, Part A*, 680-687.

Ku, X. K., Lin, J. Z., and Yuan, F. Y. (2016). Influence of Torrefaction on Biomass Gasification Performance in a High-Temperature Entrained-Flow Reactor. *Energy & Fuels, 30*(5), 4053-4064.

Kulkarni, A., Baker, R., Abdoulmomine, N., Adhikari, S., and Bhavnani, S. (2016). Experimental study of torrefied pine as a gasification fuel using a bubbling fluidized bed gasifier. *Renewable Energy, 93*, 460-468.

Kumar, K., Ghosh, S., Angelidaki, I., Holdt, S. L., Karakashev, D. B., Morales, M. A., and Das, D. (2016). Recent developments on biofuels production from microalgae and macroalgae. *Renewable and Sustainable Energy Reviews, 65*, 235-249.

Kwapinska, M., Xue, G., Horvat, A., Rabou, L. P. L. M., Dooley, S., Kwapinski, W., and Leahy, J. J. (2015). Fluidized Bed Gasification of Torrefied and Raw Grassy Biomass (Miscanthus × gigantenus). The Effect of Operating Conditions on Process Performance. *Energy & Fuels, 29*(11), 7290-7300.

Lahijani, P., Zainal, Z. A., Mohamed, A. R., and Mohammadi, M. (2013). CO_2 gasification reactivity of biomass char: Catalytic influence of alkali, alkaline earth and transition metal salts. *Bioresour Technol, 144*, 288-295.

Lane, D. J., van Eyk, P. J., Ashman, P. J., Kwong, C. W., de Nys, R., Roberts, D. A., Cole, A. J., and Lewis, D. M. (2015). Release of Cl, S, P, K, and Na during Thermal Conversion of Algal Biomass. *Energy & Fuels, 29*(4), 2542-2554.

Larson, E. D. (2006). A review of life-cycle analysis studies on liquid biofuel systems for the transport sector. *Energy for Sustainable Development, 10*(2), 109-126.

Larson, E. D., Fiorese, G., Liu, G. J., Williams, R. H., Kreutz, T. G., and Consonni, S. (2010). Co-production of decarbonized synfuels and electricity from coal plus biomass with CO_2 capture and storage: an Illinois case study. *Energy & Environmental Science*, *3*(1), 28-42.

Lawton, R. J., de Nys, R., and Paul, N. A. (2013). Selecting Reliable and Robust Freshwater Macroalgae for Biomass Applications. *Plos One*, *8*(5), e77344.

Li, C. Z., Sathe, C., Kershaw, J. R., and Pang, Y. (2000). Fates and roles of alkali and alkaline earth metals during the pyrolysis of a Victorian brown coal. *Fuel, 79*(3-4), 427-438.

Li, J., Bonvicini, G., Tognotti, L., Yang, W., and Blasiak, W. (2014a). High-temperature rapid devolatilization of biomasses with varying degrees of torrefaction. *Fuel, 122*, 261-269.

Li, T., Geier, M., Wang, L., Ku, X. K., Gull, B. M., Lovas, T., and Shaddix, C. R. (2015). Effect of Torrefaction on Physical Properties and Conversion Behavior of High Heating Rate Char of Forest Residue. *Energy & Fuels*, *29*(1), 177-184.

Li, X., Hayashi, J.-i., and Li, C.-Z. (2006). FT-Raman spectroscopic study of the evolution of char structure during the pyrolysis of a Victorian brown coal. *Fuel, 85*(12–13), 1700-1707.

Li, X., and Li, C.-Z. (2006). Volatilisation and catalytic effects of alkali and alkaline earth metallic species during the pyrolysis and gasification of Victorian brown coal. Part VIII. Catalysis and changes in char structure during gasification in steam. *Fuel, 85*(10–11), 1518-1525.

Li, Y., Yang, H., Hu, J., Wang, X., and Chen, H. (2014b). Effect of catalysts on the reactivity and structure evolution of char in petroleum coke steam gasification. *Fuel, 117, Part B*, 1174-1180.

Lichty, P., Perkins, C., Woodruff, B., Bingham, C., and Weimer, A. (2010). Rapid High Temperature Solar Thermal Biomass Gasification in a Prototype Cavity Reactor. *Journal of Solar Energy Engineering, 132*(1), 011012-011012.

Lozano-Castelló, D., Cazorla-Amorós, D., and Linares-Solano, A. (2004). Usefulness of CO_2 adsorption at 273 K for the characterization of porous carbons. *Carbon, 42*(7), 1233-1242.

Lu, L., Kong, C., Sahajwalla, V., and Harris, D. (2002). Char structural ordering during pyrolysis and combustion and its influence on char reactivity. *Fuel, 81*(9), 1215-1225.

Ma, Z., Glatzmaier, G., and Mehos, M. (2014). Fluidized bed technology for concentrating solar power with thermal energy storage. *Journal of Solar Energy Engineering-Transactions of the Asme, 136*(3), 9.

Mani, S., Tabil, L. G., and Sokhansanj, S. (2004). Grinding performance and physical properties of wheat and barley straws, corn stover and switchgrass. *Biomass and Bioenergy, 27*(4), 339-352.

McKee, D. W. (1983). Mechanisms of the alkali metal catalysed gasification of carbon. *Fuel, 62*(2), 170-175.

McNamee, P., Darvell, L. I., Jones, J. M., and Williams, A. (2015). The combustion characteristics of high-heating-rate chars from untreated and torrefied biomass fuels. *Biomass and Bioenergy, 82*, 63-72.

Melchior, T., Perkins, C., Lichty, P., Weimer, A. W., and Steinfeld, A. (2009). Solar-driven biochar gasification in a particle-flow reactor. *Chemical Engineering and Processing, 48*(8), 1279-1287.

Mi, J., Wang, N., Wang, M., Huo, P., and Liu, D. (2015). Investigation on the catalytic effects of AAEM during steam gasification and the resultant char reactivity in oxygen using Shengli lignite at different forms. *International Journal of Coal Science & Technology, 2*(3), 223-231.

Murray, J. P., and Fletcher, E. A. (1994). Reaction of Steam with Cellulose in a Fluidized-Bed Using Concentrated Sunlight. *Energy, 19*(10), 1083-1098.

Natarajan, K., Leduc, S., Pelkonen, P., Tomppo, E., and Dotzauer, E. (2014). Optimal locations for second generation Fischer Tropsch biodiesel production in Finland. *Renewable Energy, 62*, 319-330.

Nathan, G. J., Dally, B. B., Alwahabi, Z. T., van Eyk, P. J., Jafarian, M., and Ashman, P. J. (2017). Research challenges in combustion and gasification arising from emerging technologies employing directly irradiated concentrating solar thermal radiation. *Proceedings of the Combustion Institute, 36*(2), 2055-2074.

Neveux, N., Magnusson, M., Mata, L., Whelan, A., de Nys, R., and Paul, N. A. (2016). The treatment of municipal wastewater by the macroalga Oedogonium sp. and its potential for the production of biocrude. *Algal Research, 13*, 284-292.

Nickerson, T. A., Hathaway, B. J., Smith, T. M., and Davidson, J. H. (2015). Economic assessment of solar and conventional biomass gasification technologies: Financial and policy implications under feedstock and product gas price uncertainty. *Biomass and Bioenergy, 74*(0), 47-57.

Noureldin, M. M. B., Bao, B. P., Elbashir, N. O., and El-Halwagi, M. M. (2014). Benchmarking, insights, and potential for improvement of Fischer-Tropsch-based biomass-to-liquid technology. *Clean Technologies and Environmental Policy, 16*(1), 37-44.

Okumura, Y., Hanaoka, T., and Sakanishi, K. (2009). Effect of pyrolysis conditions on gasification reactivity of woody biomass-derived char. *Proceedings of the Combustion Institute, 32*, 2013-2020.

Overett, M. J., Hill, R. O., and Moss, J. R. (2000). Organometallic chemistry and surface science: mechanistic models for the Fischer–Tropsch synthesis. *Coordination Chemistry Reviews, 206–207*, 581-605.

Perander, M., DeMartini, N., Brink, A., Kramb, J., Karlström, O., Hemming, J., Moilanen, A., Konttinen, J., and Hupa, M. (2015). Catalytic effect of Ca and K on CO_2 gasification of spruce wood char. *Fuel, 150*, 464-472.

Piatkowski, N., and Steinfeld, A. (2008). Solar-driven coal gasification in a thermally irradiated packed-bed reactor. *Energy & Fuels, 22*(3), 2043-2052.

Piatkowski, N., Wieckert, C., and Steinfeld, A. (2009). Experimental investigation of a packed-bed solar reactor for the steam-gasification of carbonaceous feedstocks. *Fuel Processing Technology, 90*(3), 360-366.

Piatkowski, N., Wieckert, C., Weimer, A. W., and Steinfeld, A. (2011). Solar-driven gasification of carbonaceous feedstock-a review. *Energy & Environmental Science, 4*(1), 73-82.

Popa, T., Fan, M., Argyle, M. D., Slimane, R. B., Bell, D. A., and Towler, B. F. (2013). Catalytic gasification of a Powder River Basin coal. *Fuel, 103*, 161-170.

Prins, M. J., Ptasinski, K. J., and Janssen, F. J. J. G. (2006). More efficient biomass gasification via torrefaction. *Energy, 31*(15), 3458-3470.

Puig-Arnavat, M., Tora, E. A., Bruno, J. C., and Coronas, A. (2013). State of the art on reactor designs for solar gasification of carbonaceous feedstock. *Solar Energy, 97*, 67-84.

Quyn, D. M., Wu, H., Hayashi, J.-i., and Li, C.-Z. (2003). Volatilisation and catalytic effects of alkali and alkaline earth metallic species during the pyrolysis and gasification of Victorian brown coal. Part IV. Catalytic effects of NaCl and ion-exchangeable Na in coal on char reactivity. *Fuel, 82*(5), 587-593.

Röger, M., Amsbeck, L., Gobereit, B., and Buck, R. (2011). Face-Down Solid Particle Receiver Using Recirculation. *Journal of Solar Energy Engineering, 133*(3), 031009-031009.

Salkuyeh, Y. K., and Adams Ii, T. A. (2013). Combining coal gasification, natural gas reforming, and external carbonless heat for efficient production of gasoline and diesel with CO_2 capture and sequestration. *Energy Conversion and Management, 74*, 492-504.

Samaras, P., Diamadopoulos, E., and Sakellaropoulos, G. P. (1996). The effect of mineral matter and pyrolysis conditions on the gasification of Greek lignite by carbon dioxide. *Fuel, 75*(9), 1108-1114.

Sauciuc, A., Abosteif, Z., Weber, G., Potetz, A., Rauch, R., Hofbauer, H., Schaub, G., and Dumitrescu, L. (2012). Influence of operating conditions on the performance of biomass-based Fischer–Tropsch synthesis. *Biomass Conversion and Biorefinery, 2*(3), 253-263.

Saw, W., Kaniyal, A., van Eyk, P., Nathan, G., and Ashman, P. (2015). Solar Hybridized Coal-to-liquids via Gasification in Australia: Techno-economic Assessment. *Energy Procedia, 69*, 1819-1827.

Saw, W. L., and Pang, S. S. (2013). Co-gasification of blended lignite and wood pellets in a 100 kW dual fluidised bed steam gasifier: The influence of lignite ratio on producer gas composition and tar content. *Fuel, 112*, 117-124.

Schmid, J. C., Wolfesberger, U., Koppatz, S., Pfeifer, C., and Hofbauer, H. (2012). Variation of feedstock in a dual fluidized bed steam gasifier—influence on product gas, tar content, and composition. *Environmental Progress & Sustainable Energy, 31*(2), 205-215.

Schulz, H. (1999). Short history and present trends of Fischer–Tropsch synthesis. *Applied Catalysis A: General, 186*(1–2), 3-12.

Senneca, O., Salatino, P., and Masi, S. (1998). Microstructural changes and loss of gasification reactivity of chars upon heat treatment. *Fuel, 77*(13), 1483-1493.

Sheng, C. (2007). Char structure characterised by Raman spectroscopy and its correlations with combustion reactivity. *Fuel, 86*(15), 2316-2324.

Sheu, E. J., Mitsos, A., Eter, A. A., Mokheimer, E. M. A., Habib, M. A., and Al-Qutub, A. (2012). A Review of Hybrid Solar-Fossil Fuel Power Generation Systems and Performance Metrics. *Journal of Solar Energy Engineering-Transactions of the Asme, 134*(4).

Siegel, N. P., Ho, C. K., Khalsa, S. S., and Kolb, G. J. (2010). Development and Evaluation of a Prototype Solid Particle Receiver: On-Sun Testing and Model Validation. *Journal of Solar Energy Engineering, 132*(2), 021008-021008.

Stephens, E., de Nys, R., Ross, I. L., and Hankamer, B. (2013). Algae Fuels as an Alternative to Petroleum. *J. Pet. Environ. Biotechnol., 4*(4), 148.

Struis, R. P. W. J., Von Scala, C., Stucki, S., and Prins, R. (2002). Gasification reactivity of charcoal with CO_2. Part II: Metal catalysis as a function of conversion. *Chemical Engineering Science, 57*(17), 3593-3602.

Sudiro, M., and Bertucco, A. (2007). Synthetic fuels by a limited CO_2 emission process which uses both fossil and solar energy. *Energy & Fuels, 21*(6), 3668-3675.

Sudiro, M., and Bertucco, A. (2009). Production of synthetic gasoline and diesel fuel by alternative processes using natural gas and coal: Process simulation and optimization. *Energy, 34*(12).

Sudiro, M., Bertucco, A., Ruggeri, F., and Fontana, M. (2008). Improving Process Performances in Coal Gasification for Power and Synfuel Production. *Energy & Fuels, 22*(6), 3894-3901.

Suzuki, T., Nakajima, H., Ikenaga, N.-o., Oda, H., and Miyake, T. (2011). Effect of mineral matters in biomass on the gasification rate of their chars. *Biomass Conversion and Biorefinery, 1*(1), 17-28.

Suzuki, T., Ohme, H., and Watanabe, Y. (1992). Alkali metal catalyzed carbon dioxide gasification of carbon. *Energy & Fuels, 6*(4), 343-351.

Swanson, R. M., Platon, A., Satrio, J. A., and Brown, R. C. (2010). Techno-economic analysis of biomass-to-liquids production based on gasification. *Fuel, 89, Supplement 1*, S11-S19.

Takeshita, T., and Yamaji, K. (2008). Important roles of Fischer-Tropsch synfuels in the global energy future. *Energy Policy, 36*(8), 2773-2784.

Tan, T., and Chen, Y. (2010). Review of study on solid particle solar receivers. *Renewable and Sustainable Energy Reviews, 14*(1), 265-276.

Tavasoli, A., Sadaghiani, K., Nakhaei Pour, A., and Ahangari, M. (2007). Cobalt Loading Effects on the Structure and Activity for Fischer-Tropsch and Water-Gas Shift Reactions of Co/Al_2O_3 Catalysts. *Iranian Journal of Chemistry and Chemical Engineering*.

Tay, H.-L., and Li, C.-Z. (2010). Changes in char reactivity and structure during the gasification of a Victorian brown coal: Comparison between gasification in O_2 and CO_2. *Fuel Processing Technology, 91*(8), 800-804.

Taylor, R. W., Berjoan, R., and Coutures, J. P. (1983). Solar Gasification of Carbonaceous Materials. *Solar Energy, 30*(6), 513-525.

Thrän, D., Witt, J., Schaubach, K., Kiel, J., Carbo, M., Maier, J., Ndibe, C., Koppejan, J., Alakangas, E., Majer, S., and Schipfer, F. (2016). Moving torrefaction towards market introduction – Technical improvements and economic-environmental assessment along the overall torrefaction supply chain through the SECTOR project. *Biomass and Bioenergy, 89*, 184-200.

Tijmensen, M. J. A., Faaij, A. P. C., Hamelinck, C. N., and van Hardeveld, M. R. M. (2002). Exploration of the possibilities for production of Fischer Tropsch liquids and power via biomass gasification. *Biomass and Bioenergy, 23*(2), 129-152.

Toda, Y., Hatami, M., Toyoda, S., Yoshida, Y., and Honda, H. (1971). Micropore structure of coal. *Fuel, 50*(2), 187-200.

Trimm, D. L., and Adesina, A. A. (1996). Chemical Engineering and CatalysisHydrocarbon synthesis via Fischer-Tropsch reaction: travails and triumphs. *Applied Catalysis A: General, 138*(2), 345-367.

Tuinstra, F., and Koenig, J. L. (1970). Raman Spectrum of Graphite. *The Journal of Chemical Physics, 53*(3), 1126-1130.

Vallejos-Burgos, F., Díaz-Pérez, N., Silva-Villalobos, Á., Jiménez, R., García, X., and Radovic, L. R. (2016). On the structural and reactivity differences between biomass- and coal-derived chars. *Carbon, 109*, 253-263.

van Vliet, O., Faaij, A., and Turkenburg, W. (2009). Fischer–Tropsch diesel production in a well-to-wheel perspective A carbon, energy flow and cost analysis. *Energy Conversion and Management 50, 50*(4).

Vidal, A., Denk, T., Steinfeld, L., and Zacarias, L. (2010). *Upscaling of a 500 kW Solar Gasification Plan. 18th World Hydrogen Energy Conference*, Essen, Germany.

Wahby, A., Silvestre-Albero, J., Sepúlveda-Escribano, A., and Rodríguez-Reinoso, F. (2012). CO_2 adsorption on carbon molecular sieves. *Microporous and Mesoporous Materials, 164*, 280-287.

Wang, M. J., Roberts, D. G., Kochanek, M. A., Harris, D. J., Chang, L. P., and Li, C. Z. (2014). Raman Spectroscopic Investigations into Links between Intrinsic Reactivity and Char Chemical Structure. *Energy & Fuels, 28*(1), 285-290.

Weiland, F., Nordwaeger, M., Olofsson, I., Wiinikka, H., and Nordin, A. (2014). Entrained flow gasification of torrefied wood residues. *Fuel Processing Technology, 125*, 51-58.

Wood, D. A., Nwaoha, C., and Towler, B. F. (2012). Gas-to-liquids (GTL): A review of an industry offering several routes for monetizing natural gas. *Journal of Natural Gas Science and Engineering, 9*, 196-208.

Xiao, G., Guo, K., Ni, M., Luo, Z., and Cen, K. (2014). Optical and thermal performance of a high-temperature spiral solar particle receiver. *Solar Energy, 109*, 200-213.

Xie, X., Wang, M., and Han, J. (2011). Assessment of Fuel-Cycle Energy Use and Greenhouse Gas Emissions for Fischer−Tropsch Diesel from Coal and Cellulosic Biomass. *Environmental Science & Technology, 45*(7), 3047-3053.

Z'Graggen, A., Haueter, P., Maag, G., Romero, M., and Steinfeld, A. (2008). Hydrogen production by steam-gasification of carbonaceous materials using concentrated solar energy - IV. Reactor experimentation with vacuum residue. *International Journal of Hydrogen Energy, 33*(2), 679-684.

Z'Graggen, A., Haueter, P., Maag, G., Vidal, A., Romero, M., and Steinfeld, A. (2007). Hydrogen production by steam-gasification of petroleum coke using concentrated solar power - III. Reactor experimentation with slurry feeding. *International Journal of Hydrogen Energy, 32*(8), 992-996.

Z'Graggen, A., Haueter, P., Trommer, D., Romero, M., de Jesus, J. C., and Steinfeld, A. (2006). Hydrogen production by steam-gasification of petroleum coke using concentrated solar power - II - Reactor design, testing, and modeling. *International Journal of Hydrogen Energy, 31*(6), 797-811.

Z'Graggen, A., and Steinfeld, A. (2008). Hydrogen production by steam-gasification of carbonaceous materials using concentrated solar energy - V. Reactor modeling,

optimization, and scale-up. *International Journal of Hydrogen Energy, 33*(20), 5484-5492.

Zaida, A., Bar-Ziv, E., Radovic, L. R., and Lee, Y.-J. (2007). Further development of Raman Microprobe spectroscopy for characterization of char reactivity. *Proceedings of the Combustion Institute, 31*(2), 1881-1887.

Zhang, C., Jun, K.-W., Gao, R., Kwak, G., and Kang, S. C. (2016a). Efficient utilization of associated natural gas in a modular gas-to-liquids process: Technical and economic analysis. *Fuel, 176*, 32-39.

Zhang, S. P., Hu, B., Zhang, L., and Xiong, Y. Q. (2016b). Effects of torrefaction on yield and quality of pyrolysis char and its application on preparation of activated carbon. *Journal of Analytical and Applied Pyrolysis, 119*, 217-223.

Zheng, A., Zhao, Z., Chang, S., Huang, Z., Wang, X., He, F., and Li, H. (2013). Effect of torrefaction on structure and fast pyrolysis behavior of corncobs. *Bioresour Technol, 128*, 370-377.

Zhou, H., Yang, S., Xiao, H., Yang, Q., Qian, Y., and Gao, L. (2016). Modeling and techno-economic analysis of shale-to-liquid and coal-to-liquid fuels processes. *Energy, 109*, 201-210.

Zhou, L., Chen, W.-Y., Zhang, X.-L., and Qi, T.-Y. (2013). Simulation and Economic Analysis of Indirect Coal-to-Liquid Technology Coupling Carbon Capture and Storage. *Industrial & Engineering Chemistry Research, 52*(29), 9871-9878.

Zhu, X., and Sheng, C. (2010). Evolution of the Char Structure of Lignite under Heat Treatment and Its Influences on Combustion Reactivity. *Energy & Fuels, 24*(1), 152-159.